Copyright

by

Anthony Michael Garcia

2014

The Thesis Committee for Anthony Michael Garcia
Certifies that this is the approved version of the following thesis:

Durability Testing of Rapid, Cement-based Repair Materials for Transportation Structures

APPROVED BY
SUPERVISING COMMITTEE:

Supervisor: _____
Kevin J. Folliard

Co-Supervisor: _____
Thanos Drimalas

Durability Testing of Rapid, Cement-based Repair Materials for Transportation Structures

by

Anthony Michael Garcia, BSArchE

Thesis

Presented to the Faculty of the Graduate School of

The University of Texas at Austin

in Partial Fulfillment

of the Requirements

for the Degree of

Master of Science in Engineering

The University of Texas at Austin

May 2014

Dedication

To my soon-to-be wife – All I have accomplished has been with your unfailing help and confidence.

Acknowledgements

I would like to thank fiancée, Lyndsey, for her continuous support. Without her help and patience, I would not have made it this far.

I would like to thank Mitchell for the brainstorming sessions, mixes, and (sometimes) stress. It was a pleasure getting to know you. You are one of the best and hardest working people I know, and I could not ask for a better partner.

I would also like to thank Dr. Kevin Folliard for his confidence and the opportunity to work on this project. Your passion for the subject is truly evident and helped fuel my excitement. I would like to thank Dr. Thanos Drimalas for all the help when I had no idea where to go next. Your ability to make the difficult simple was greatly appreciated.

Additionally, I would like to thank Mike Rung for helping make everything practical. Your knowledge helped out in more than one stressful situation. Sherian, thank you for handling the finances and giving me plenty of markers. Also, to all the other students who helped me along the way. Racheal, Fred, Trevor, Nic, Chris, Steve, Sarwar, Saamiya, and Lisa, I appreciate your help and friendship. Last but not least, I would like to thank JC for doing many of the tasks I was unable to do. Your help was invaluable.

Abstract

Durability Testing of Rapid, Cement-based Repair Materials for Transportation Structures

Anthony Michael Garcia, M.S.E.

The University of Texas at Austin, 2014

Supervisors: Kevin J. Folliard, Thanos Drimalas

For repairing concrete transportation infrastructure, such as pavements and bridges, much importance is placed on early-age strength gain as this has a major impact on scheduling and opening to traffic. However, the long-term performance and durability of such repair materials are often not satisfactory, thus resulting in future repairs. This research project focuses on the evaluation of the durability of various rapid-setting cementitious materials. The binders studied in this project include calcium aluminate cement (CAC), calcium sulfoaluminate cement (CSA), Type III portland cement, alkali-activated fly ash (AAFA) , and various prepackaged concrete materials. In addition, selected CAC and CSA mixtures were further modified with the use of a styrene-butadiene latex. The durability aspects studied include freezing-and-thawing damage and the implications of air entrainment in these systems, alkali-silica reaction, sulfate attack, and permeability of the concrete matrix and potential corrosion.

Table of Contents

List of Tables

List of Figures

Chapter 1: Introduction

1.1 Background

With the growth of cities, movement to urban centers, and increased dependency on vehicular traffic, the importance of rapid repair of roadway infrastructure and pavements without interruption of traffic flow cannot be understated. To address these concerns, The Texas Department of Transportation (TxDOT) is researching and developing rapid repair materials for concrete transportation structures to shorten traffic closures. Typical roadway repairs often fail again relatively quickly when compared to the service life of the roadway, essentially requiring repair after repair until the entire roadway is replaced. Often overlooked, durability should be a greater concern when placing and designing repairs.

Although not an exhaustive list, rapid, cement-based repair materials may be composed of calcium aluminate cement concrete, calcium sulfoaluminate cement concrete, accelerated ordinary portland cement concrete, alkali-activated fly ash concrete, or other manufacturer-supplied proprietary concrete blends. Although they all achieve relatively high early strengths, usually near or exceeding 3000 psi (20.7 MPa) compressive strength at 3 hours or 400 psi (2.8 MPa) flexural strength at 4 hours, many of these materials' long-term durability properties have been overlooked. Although the quick gaining of strength minimizes traffic interference, the repair will do little long term good if it must be reinstalled shortly thereafter.

Typical durability issues in concrete include alkali-silica reaction (ASR), freezing-and-thawing and salt scaling damage, sulfate attack, and reinforcement corrosion from chloride intrusion and carbonation. Each of these problems is further exacerbated by the development of cracks, potentially due to the loading from repetitive axel loads on roadways.

The goal of this study is to compare various rapid, cement-based repair materials for their suitability as a long-term repair in transportation infrastructure. To accomplish this, a comprehensive laboratory testing program was performed to address various issues with these materials. The data gathered will allow intelligent selection of the concrete materials to create a durable and economic repair.

1.2 SCOPE AND OBJECTIVES

Conducted by the University of Texas and funded by the Texas Department of Transportation, this research project will provide recommendations on repairs of roadways, bridge decks, and other transportation structures. The research has been broken into two distinct portions as follows:

- Phase I Preliminary Screening presented in Zuniga (2013).
- Phase II and III Comprehensive Lab Screening is divided between this thesis focusing on durability testing and Dornak (2014) thesis focusing on mechanical properties, temperature, and shrinkage.

Preliminary screening yielded a matrix of materials for further testing based on suitable working time, flow, workability, and 3 hour compressive strength. From this data, thirteen mixtures were selected for the majority of testing. Typical cementitious binders included in the Phase I and II screening process includes calcium aluminate cement (CAC), calcium sulfoaluminate cement (CSA), Type III portland cement, variations and combinations of these binders, and proprietary mixtures. In addition, a styrene-butadiene latex polymer was used to modify typical CSA and CAC mixtures.

At a later date, a "final" subset of six materials allowed for more advanced and extensive testing on smaller number of materials. These thirteen Phase II materials, with the final subset of Phase III materials labeled, are shown in Table 1:

Table 1. Phase II & III Material Matrix.

Mix ID*	Phase II	Phase III
P-1	✓	
P-2	✓	✓
P-3	✓	
P-AAFA	✓	✓
CSA-1	✓	✓
CSA-Latex	✓	
CSA-2	✓	
CSA-3	✓	
CAC-1	✓	
CAC-Latex	✓	
CAC-2	✓	✓
CAC-3	✓	✓
PC Type III	✓	✓

**Note: Mix IDs designated characteristic cementitious material. The materials labeled P-x are proprietary materials. Conversely, those labeled CSA-x contain calcium sulfoaluminate cement, CAC-x contain calcium aluminate cement, and PC contain portland cement as their characteristic cementitious material.*

This thesis focuses on the Phase II and III mixtures for the durability testing of this project, with distinction made between Phase II and Phase III mixtures selected after Phase I. The comprehensive durability testing includes laboratory experimentation and interpretation air void analysis and properties under freezing conditions, alkali-silica reaction, sulfate attack, and chloride permeability and potential for corrosion in embedded reinforcing steel. As the durability testing was underway, additional data on mechanical properties, strength gain, and heat development were generated and summarized in Dornak (2014). The research team, with the data presented here, hopes to

determine which field mixture designs developed and screened in Phase I are most suitable for durable transportation structure repair for TxDOT.

The following ASTM standards were followed to quantify the aforementioned durability concerns:

- ASTM C 157 Standard Test Method for Length Change of Hardened Hydraulic-Cement Mortar and Concrete
- ASTM C 231 Standard Test Method for Air Content of Freshly Mixed Concrete by the Pressure Method
- ASTM C 666 Standard Test Method for Resistance of Concrete to Rapid Freezing and Thawing
- ASTM C 672 Standard Test Method for Scaling Resistance of Concrete Surfaces Exposed to Deicing Chemicals
- Modified version of ASTM C 1012 Standard Test Method for Length Change of Hydraulic-Cement Mortars Exposed to a Sulfate Solution
- Modified version of ASTM C 1202 Standard Test Method for Electrical Indication of Concrete's Ability to Resist Chloride Ion Penetration
- ASTM C 1293 Standard Test Method for Determination of Length Change of Concrete Due to Alkali-Silica Reaction
- ASTM C 1556 Standard Test Method for Determining the Apparent Chloride Diffusion Coefficient of Cementitious Mixtures by Bulk Diffusion
- Modified version of ASTM G 109 Standard Test Method for Determining Effects of Chemical Admixtures on Corrosion of Embedded Steel Reinforcement in Concrete Exposed to Chloride Environments

1.3 NOTATIONS

It is common for cement chemists and concrete industry professionals to use a shorthand notation for the phases of cement and concrete. These notations may be used within the thesis and are given as follows:

- C CaO
- S SiO_2
- H H_2O
- A Al_2O_3
- F Fe_2O_3
- $ SO_3

1.4 CONTENT

The remainder of this thesis contains the following chapters, which include:

- Chapter 2 presents the procedures and findings for durability concerns for freeze-thaw damage which includes the following testing: air void analysis tests, including fresh air analysis according to ASTM C 231 and air entrainment, hardened air void analysis, salt scaling testing according to ASTM C 672, and freezing-and-thawing testing according to ASTM C 666.
- Chapter 3 presents procedures and findings for durability concerns for alkali-silica reaction (ASR). ASR tests were conducted according to ASTM C 1293. This chapter includes expansion values of the mixtures and comparisons are made between all thirteen mixtures.
- Chapter 4 presents procedures and findings for durability concerns for external sulfate attack. Sulfate attack tests were conducted according to ASTM C 1012. This chapter includes expansion values and comparisons are made between the thirteen mixtures.

- Chapter 5 presents procedures and findings for permeability and corrosion concerns. Tests associated with these concerns include rapid chloride penetration testing (RCPT) according to a simplified test method, carbonation measurements, 1-d chloride ingression according to ASTM C 1556, and combined fatigue and corrosion testing loosely based on ASTM G 109 and other similar research.
- Chapter 6 will summarize key findings, contrast and compare the repair materials studied within this project, recommend any future testing.

Chapter 2: Freezing-and-Thawing and Salt Scaling Resistance

2.1 Introduction and Background

Although Texas is generally considered a hot weather state, parts of Texas, primarily north of Interstate 20 (IH-20), can be subject to harsh freezing-and-thawing cycles during the winter months. These cycles may cause damage within the concrete's structure as water within the pores changes phase from liquid to solid.

The specific mechanisms relating to individual tests will be discussed later, but a well-distributed matrix of fine air bubbles allows for a relief of the osmotic and hydraulic pressures and helps prevent damage from freezing-and-thawing. To accomplish this, an air entraining admixture must be added to the concrete during mixing in order to produce the desired air-void system.

2.2 Materials and Mixture Proportions

A 4-cubic foot steel drum concrete mixer was used to produce the concrete that was used to measure air in fresh concrete, hardened air, freezing-and-thawing, and salt scaling. It should be noted that the mixing procedure is further described in Zuniga (2013). When making use of proprietary and premanufactured concrete blends, the research team followed the provided manufacturers mixing instructions.

A synthetic air-entraining admixture complying with ASTM C 260 was used in materials CAC-1, CAC-2, CAC-3, and PC Type III. Individual dosage varied between materials due to previous tests performed in Zuniga (2013). During Phase I testing, each material was tested approximately three times with a goal of a stable fresh air content between 5 and 7%. This is a widely accepted percentage to reduce or eliminate the damage from freezing-and-thawing for small sized aggregate due to the relative air

content in the paste. The final dosages of the air-entraining admixture are shown in Table 2.

Table 2. Final dosage of air-entrainment admixture for Phase II and III testing.

Material	AEA (oz/cwt)
P-1	--
P-2	--
P-3	--
P-AAFA	--
CSA-1	--
CSA-2	--
CSA-3	--
CSA-Latex	--
CAC-1	0.25
CAC-2	0.25
CAC-3	1
CAC-Latex	--
PC Type III	0.15

A subset of the Phase II and III materials did not receive any air-entraining admixture due to various constraints. These constraints are listed as follows:

- P-1, P-2, P-3, P-AAFA: These materials are pre-manufactured bags with all required materials. Since the contents of these materials are not completely known, it is assumed that an air-entrainment admixture or other mechanism making it resistant to freezing-and-thawing damage is included.
- CSA-Latex, CAC-Latex: With the addition of styrene-butadiene latex, the manufacturer recommends not using an air-entraining admixture.
- CSA-1, CSA-2, CSA-3, CSA-Latex: It was recommended by the manufacturer that materials comprised of calcium sulfoaluminate cement would not require an

additional air-entraining admixture to maintain resistance to freezing-and-thawing damage.

2.3 AIR VOID ANALYSIS

An air-entrainment admixture (AEA) stabilizes a system of evenly distribute small and stable air bubbles throughout the concrete by introducing surface-acting molecules into the concrete. These molecules have two ends – one hydrophobic and one hydrophilic (Mindess, Young, & Darwin, 2003). The hydrophobic end repels water as the hydrophilic end attracts, creating bubbles as schematically shown in Figure 1.

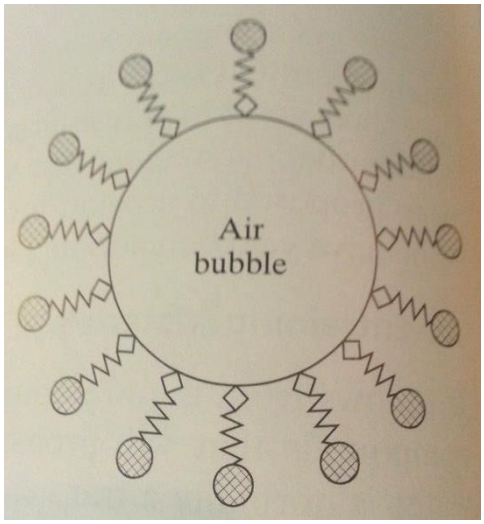

Figure 1. Schematic of air entrained air bubble displaying the admixtures hydrophobic and hydrophilic ends (Mindess, Young, & Darwin, 2003).

It is important to note that air entraining admixtures are specifically formulated to allow a uniform spacing of these bubbles. Various factors can affect the actual amount of entrained air, so each material was tested separately in Phase I, as shown in Zuniga (2013), to determine an appropriate amount of air entrainment admixture.

To quantify the effectiveness of air entraining agents or the entrapped air content of a concrete material, two forms of air void analyses were performed. First, a fresh air analysis was performed using an air chamber and following ASTM C 231. This procedure produces a value for the air present during the fresh state. Although this closely correlates to the hardened air that actually protects from freezing-and-thawing damage, it does not provide any information regarding the size and spacing of bubbles, just the total volume of air.

To analyze the hardened air content, hardware and software for RapidAir 457 was used. This combination allows a statistical analysis of filled air voids to determine not only the air content as a percentage, but also other significant values. These values include, but are not limited to, the specific surface and spacing factor, which, in combination with the air content allow the quality of the air to be more completely determined. This apparatus employs image analysis as a method of evaluating the air-void system.

2.3.1 Experimental Procedure

2.3.1.1 Air Entrainment

The concrete mixing procedure that was followed is outlined in Zuniga (2013). When using an air entraining admixture, it is important to add liquid admixtures as a solution in the mixing water as the water is normally added as suggested in ASTM C 192. This mixing procedure will allow for full engagement of the air entraining agent and distribution of the air matrix throughout the concrete.

2.3.1.2 Fresh Air Analysis

The fresh air analysis was performed along with casting of hardened air samples, salt scaling specimens, and freeze-thaw specimens. The amount of air entrainment was

established during the initial Phase I testing. Fresh air content was measured in accordance to ASTM C 231 using a Type B pressure meter. Despite the rapid-setting nature of the majority of Phase II and III materials, the material was rodded in the pressure chamber (versus vibration) and ASTM C 231 was performed normally.

2.3.1.3 Hardened Air Void Analysis

To perform a hardened air void analysis, 4 inch (102 mm) diameter cylinders were cast simultaneously with fresh concrete used for fresh air analysis. These cylinders were then moist cured for 28 days and then frozen until the hardened air void analysis could be completed.

First, specimens were cut twice along the length using a wet saw, as shown in Figure 2, to approximately 0.5 inch (13 mm) thickness. The sawing must be done carefully to give as uniform a surface as possible and to prevent burrs or other breakage deformities along the edges (Ley, 2007).

Figure 2. Wet saw used for cutting hardened air specimens.

After cutting, specimens were allowed to dry for approximately 24 hours. The following steps were performed in accordance to Appendix B of Ley (2007), with special consideration of the thoroughness of the procedure. Polishing of the specimens was done with the table and nickel plated diamond discs with magnetic backing obtained from ASW Diamond shown in Figure 3 with various grits.

Figure 3. Polishing table and various grit plates for polishing hardened air specimens.

Upon drying, specimens were blackened with the use of permanent rounded-tip Sharpie markers with strokes in one direction and left to dry for another 24 hours. After this time had passed, specimens were blackened in the direction perpendicular to the original strokes to create a more uniform dark appearance. They were then allowed to dry for another 24 hours.

Next, the voids were filled with barium sulfate ($BaSO_a$) powder to create contrast in the specimen. This powder is shown in Figure 4 as follows:

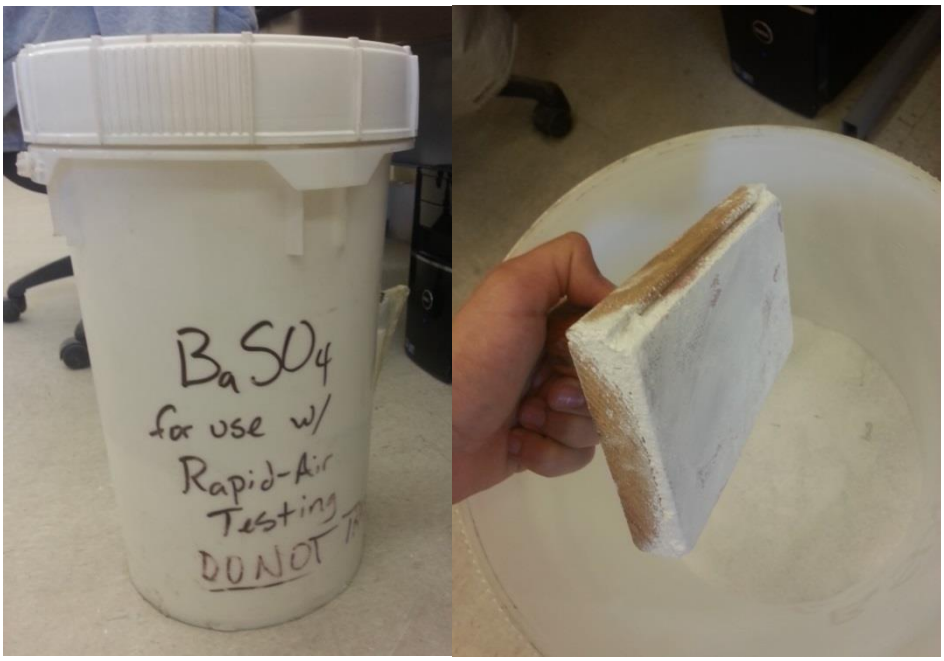

Figure 4. Barium sulfate to fill air voids in colored concrete section.

To apply the powder, it was gathered onto the specimen using a small metal lab spoon. These piles were then pressed into the voids with the use of a large rubber stamp. Next, the specimen was shaken to remove any loose powder and a bare, dry palm passed over the surface to clean any material not trapped in the voids. The process of applying powder and removing excess was then repeated until all voids were filled satisfactorily. The objective is to generate a dark background upon which the white air voids can be easily identified by the image analysis program.

After filling the voids, care must be taken so only voids within the past fraction of the concrete is "read" by the program. To do this, any voids within the coarse aggregate portion of the sample were blackened using Sharpie markers. The final sample, as shown in Figure 5, was ready for analysis.

Figure 5. Example of final concrete specimen ready for use in RapidAir system.

After the sample preparation, the specimens are mounted in the RapidAir hardware shown in Figure 6. The hardware and software allows a computerized version of the modified point count given in ASTM C 457 with each sample only taking a few minutes.

Figure 6. RapidAir system used for performing hardened air void analysis.

2.3.2 Results and Discussion

The hardened air void analysis and comparison of fresh and hardened properties of the various materials yielded the results shown in Table 3.

Table 3. Comparison of fresh & hardened air void analyses for Phase II & III materials.

Material	Additional AE (oz/cwt)	Fresh Air Content (%)	Hardened Air Content (%)	Specific Surface	Spacing Factor
P-1	--	1.5	2.83	1063.0 1/in	0.0053 in
				41.9 1/mm	0.1346 mm
P-2	--	3.9	5.09	466.2 1/in	0.0104 in
				18.4 1/mm	0.26416 mm
P-3	--	3.5	4.5	629.7 1/in	0.009 in
				24.8 1/mm	0.2286 mm
P-AAFA	--	3	2.63	714.1 1/in	0.01 in
				28.1 1/mm	0.2540 mm
CSA-1	--	2.75	10.5	772.6 1/in	0.0043 in
				30.4 1/mm	0.1092 mm
CSA-2	--	10	18.72	571.7 1/in	0.0036 in
				22.5 1/mm	0.0914 mm
CSA-3	--	3.5	3.75	767.3 1/in	0.0076 in
				30.2 1/mm	0.1930 mm
CSA-Latex	--	3.9	5.18	646.4 1/in	0.0079 in
				25.4 1/mm	0.2006 mm
CAC-1	0.25	8	14.1	463.8 1/in	0.0054 in
				18.3 1/mm	0.1372 mm
CAC-2	0.25	7.5	12.66	477.7 1/in	0.0051 in
				18.8 1/mm	0.1295 mm
CAC-3	1	5	5.4	605.8 1/in	0.0085 in
				23.9 1/mm	0.2159 mm
CAC-Latex	--	4.5	3.79	423.7 1/in	0.0136 in
				16.7 1/mm	0.3454 mm
PC Type III	0.15	5	2.395	726.9 1/in	0.0101 in
				28.6 1/mm	0.2565 mm

In most situations, fresh air content is used to determine the appropriateness of concrete for freezing-and-thawing conditions in the field. As previously stated, a fresh air

content of 5 to 7% is appropriate for most conditions. Based on this value, materials except CSA-2, CAC-1, CAC-2, CAC-3, and PC TypeIII were below the lower bound for use when using the ASTM C 231 test. Various materials, including CSA-2 and CAC-2 were above this 7% value, with 10% and 7.5% air respectively.

According to ASTM C 457, the spacing factor is the most important factor in determining theoretical freezing-and-thawing resistance of a particular cement paste matrix. The standard quantifies the maximum spacing factor required to gain a moderate resistance to freezing and thawing as 0.008 inches (0.20 mm). The corresponding specific surface (alpha) is also limited to 1100 inches^{-1} (45 mm^{-1}) for moderate freezing-and-thawing resistance.

Of the 13 Phase II and III materials, four exceeded the maximum spacing factor given in ASTM C 457 for moderate freezing-and-thawing resistance. These materials are P-3, P-AAFA, CAC-3, CAC-Latex, and PC Type III. All materials meet the specific surface value. In later sections, a comparison will be made from these relevant air content values and the specific materials resistance to salt scaling and freezing-and-thawing damage.

2.4 SALT SCALING

Salt scaling is a mechanism of concrete causing deterioration of the finished surface due to cyclical freezing and thawing. This is particularly relevant in flatwork that is the focus of this project due to the importance of the finished surface. The prominence of salt scaling is due to potential deficiencies in the finished surface, loss of air at this location due to finishing, and inadequate curing leading to larger freezable water content and lower strength at the surface (Mindess, Young, & Darwin, 2003).

It is now commonly accepted that salt scaling is due to the glue-spall mechanism (Valenza II & Scherer, 2006). This mechanism includes the propagation of stress concentrations due to salt in water freezing on the surface into the concrete surface. Scaling damage does not increase linearly with salt concentrations in the water, however; at a point of approximately 3 to 4% salt solution, the freezing point of the water drops and virtually never freezes.

2.4.1 Experimental Procedures

Salt scaling susceptibility was testing by closely following ASTM C 672. This test uses a visual rating scale to determine the damage due to salt scaling and is outlined as follows.

Specimens of dimensions 3.5 inches (89 mm) deep and 9 inches (229 mm) square were cast for each material according to the aforementioned standard. The samples were broom-finished, cured with wet burlap for one day, wet cured for 14 days, and then stored at 73°F (23°C) and 50% relative humidity for 14 more days.

A “dam” was then created on each specimen to allow ponding of salt solution. Polyvinyl Chloride (PVC) pipe with 1 inch (25 mm) diameter was attached along the finished edges of specimens and attached and sealed using Liquid Nails construction adhesive. A typical specimen is shown in Figure 7 as follows:

Figure 7. Liquid Nails adhesive and typical specimen used in ASTM C 672 testing.

After the dams were built, a 4% calcium chloride solution was ponded on the surface. The specimens were placed in a chamber which cycles between freezing at 0°F (-17.78°C) and typical lab temperatures of 73°F (23°C) every 16 hours.

The surface is photographed and visually rated after 5, 10, 15, 25, and 50 cycles and rated according to ASTM C 672 using the following scale:

Rating	Condition of Surface
0	no scaling
1	very slight scaling (3 mm [⅛ in.] depth, max, no coarse aggregate visible)
2	slight to moderate scaling
3	moderate scaling (some coarse aggregate visible)
4	moderate to severe scaling
5	severe scaling (coarse aggregate visible over entire surface)

Figure 8. Visual rating of salt scaling specimen surfaces according to ASTM C 672.

It is important to note that visual ratings were performed by the same person whenever possible to eliminate potential discrepancies.

2.4.2 Results and Discussion

After two samples of each material were exposed to 50 cycles according to the procedures of ASTM C 672, the materials displayed various levels of salt scaling damage. Figure 9 through Figure 18 show each slab's surface after 50 cycles. In addition, the slabs at 0, 5, 10, 15, and 25 cycles may be seen in Appendix A. It is important to note that P-1 degraded very early, so pictures are not always presented.

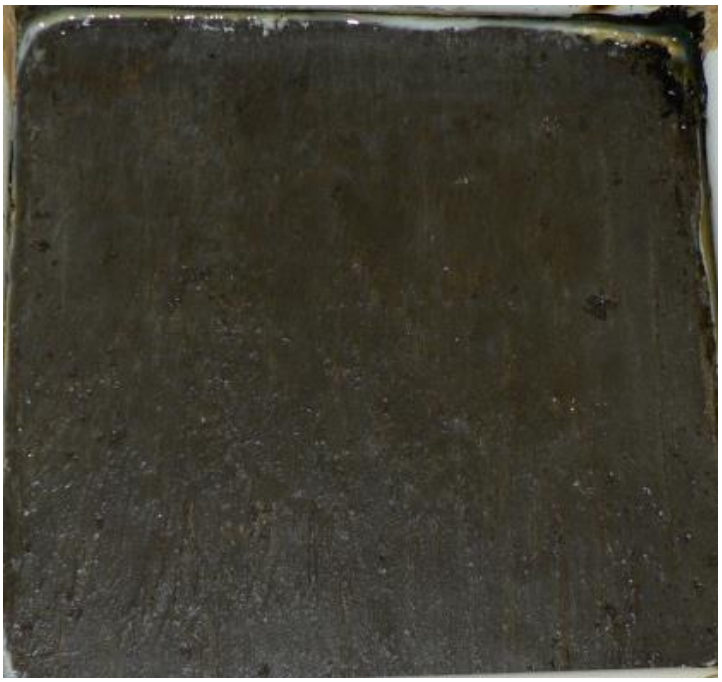

Figure 9. P-2 samples after 50 cycles according to ASTM C 672.

Figure 10. P-3 samples after 50 cycles according to ASTM C 672.

Figure 11. P-AAFA samples after 50 cycles according to ASTM C 672.

Figure 12. CSA-2 samples after 50 cycles according to ASTM C 672.

Figure 13. CAC-1 samples after 50 cycles according to ASTM C 672.

Figure 14. CAC-Latex samples after 50 cycles according to ASTM C 672.

Figure 15. PC Type III samples after 50 cycles according to ASTM C 672.

Figure 16. CSA-3 samples after 50 cycles according to ASTM C 672.

Figure 17. CAC-3 samples after 50 cycles according to ASTM C 672.

Figure 18. CAC-2 samples after 50 cycles according to ASTM C 672.

Figure 19. CSA-1 samples after 25 cycles (50 unavailable) according to ASTM C 672.

Figure 20. CSA-Latex samples after 25 cycles (50 unavailable) according to ASTM C 672.

Based on these samples, each of the specimens from both Phase II and III was visually rated based on the criteria of ASTM C 672. This criteria was carefully evaluated by a single member of the project team and the ratings assigned are presented in Table 4.

Table 4. Visual rating at 50 cycles in accordance with ASTM C 672.

Material	ASTM C672 Visual Rating
P-1	5
P-2	0
P-3	3
P-AAFA	2
CSA-1	5
CSA-2	1
CSA-3	0
CSA-Latex	5
CAC-1	1
CAC-2	0
CAC-3	2
CAC-Latex	2
PC Type III	3

Although the standard does not present any failure criteria for the salt scaling visual rating, the materials P-1, CSA-5, and CSA-Latex were both rated 5 after 50 cycles. No air-entraining admixture was added to these mixtures as the manufacturers of these products claim that none is needed. Although no conclusions may be drawn from the severe rating received by P-1, the rating of CSA-1 and CSA-Latex implies that a calcium sulfoaluminate binder and the accompanying admixture offers little resistance to salt scaling, especially without additional air entrainment. Both materials binders comprise entirely of CSA.

The other materials were each rated 3 or better, concluding, that, in general, they are at least fairly resistant to salt scaling. Among the most resistant include P-2, CSA-3, and CAC-2. Each alternative binder may be resistant to salt scaling if proportioned and used correctly.

2.5 FREEZE-THAW TESTING

Freeze-thaw damage is a prime durability concern in flatwork and structural concrete exposed to freezing and thawing cycles. Through osmotic pressure, water in other locations attempts to dilute the highly-charged ionic solution within pores as water freezes, but if fine pores are not finely spaced, will fail to reach their destination. This causes damage in transit due to high pressures as water travels through the concrete's matrix. In addition, water increases in volume by about 9% when it freezes, which may increase damage caused by osmotic pressure (Mindess, Young, & Darwin, 2003).

2.5.1 Experimental Procedure

To determine the resistance to this freeze-thaw damage, ASTM C 666 was followed. First, specimens of dimensions 4 x 3 x 16 inches (102 x 76 x 406 mm) were cast using the aforementioned air entrained mix when applicable. These specimens were then wet cured for 14 days, frozen to a temperature less than 4°F (2°C), and the initial resonant frequency is measured as shown in Figure 21.

Figure 21. Equipment for testing the fundamental transverse frequency of concrete samples according to ASTM C 666.

Freeze-thaw testing proceeded by placing specimens in metal containers, surrounding them with water and subjecting the specimens to repeated freezing-and-thawing cycles. The fundamental frequency is measured during the thawing phase every 36 cycles. It is important to note that fundamental frequency was measured by the same technician as often as possible to eliminate user error and differences in judgment. In addition, each specimen is weighed during this period to further characterize damage done by repetitive freezing-and-thawing. After measurement, specimens are returned to random locations within the freezing-and-thawing chamber, as shown in Figure 22.

Figure 22. Specimens for ASTM C 666 in the freezing-and-thawing chamber.

The individual cells are then filled with water, and freezing-and-thawing cycles continued. Each specimen was subjected to at least 300 freezing-and-thawing cycles or until the relative dynamic modulus of elasticity reaches 60% of the original modulus. The relative dynamic modulus of elasticity can be calculated for each specimen according to ASTM C 666 as follows:

$$P_c = (n_1^2/n^2) \times 100 \qquad \text{Eq. 1 } \textit{(ASTM C 666, 2008)}$$

where:

P_c = relative dynamic modulus of elasticity, after c cycles of freezing and thawing, percent,

n = fundamental transverse frequency at 0 cycles of freezing and thawing, and

n_1 = fundamental transverse frequency after c cycles of freezing and thawing.

When the test has ended due to the above criteria, the durability factor (DF) may be calculated to further characterize the material's resistance to freezing-and-thawing damage. This durability factor is given at the point of tests termination, and may be calculated according to ASTM C 666 as follows:

$$DF = PN/M \qquad \text{Eq. 2 } \textit{(ASTM C 666, 2008)}$$

where:

DF = durability factor of the test specimen,
P = relative dynamic modulus of elasticity at N cycles, %,
N = number of cycles at which P reaches the specified minimum value for discontinuing the test or the specified number of cycles at which the exposure is to be terminated, whichever is less, and
M = specified number of cycles at which the exposure is to be terminated.

2.5.2 Results and Discussion

In general, calculating the durability factor and comparing it to time is a strong indicator of a materials resistance to freezing-and-thawing damage, at least in a manner relative to the other materials. The rate of degradation due to freezing-and-thawing damage and, thus, drop in this modulus is relatively slow in most materials. As shown in Figure 23 and Figure 24, the majority of both Phase II and III materials held relatively high dynamic moduli through approximately 300 cycles.

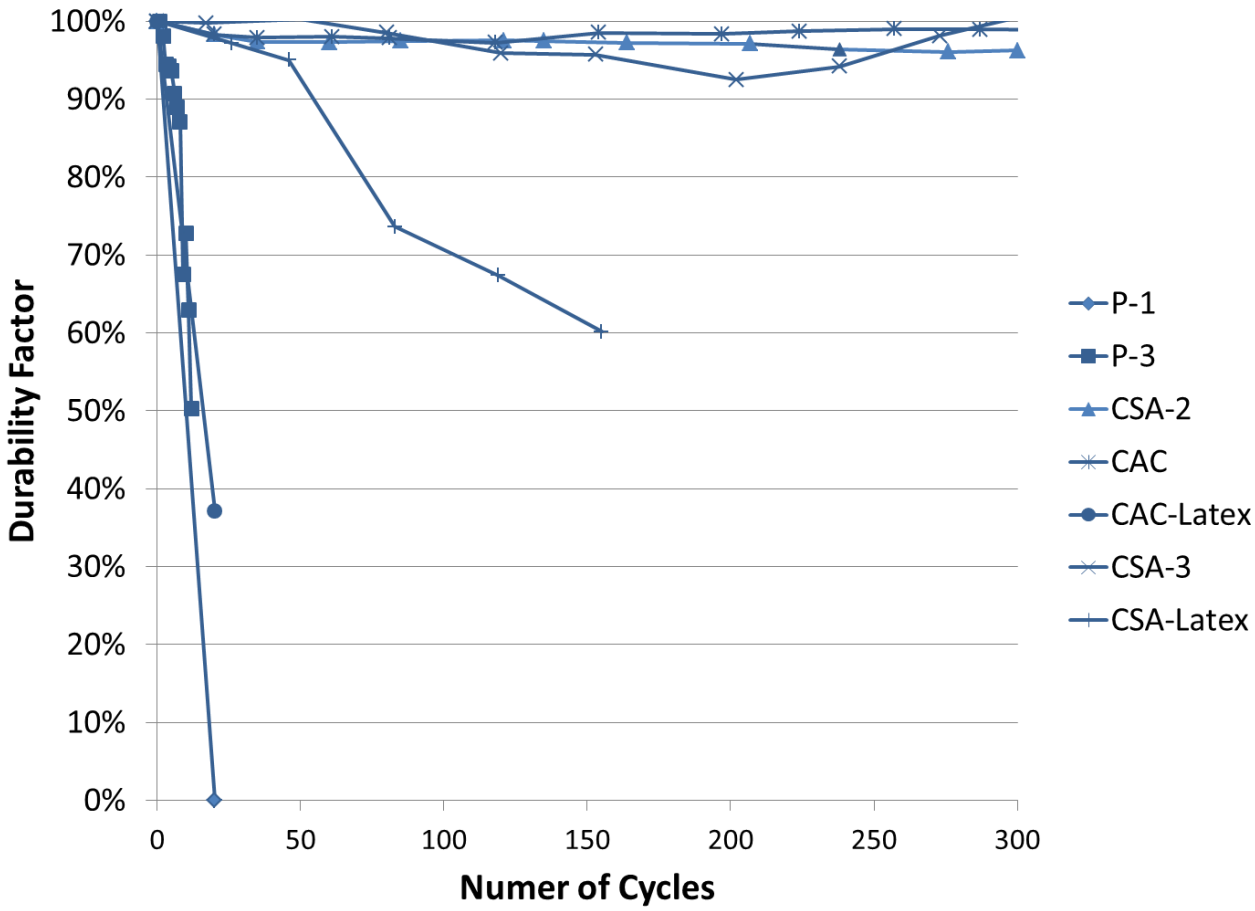

Figure 23. Relative dynamic modulus of elasticity of Phase II materials.

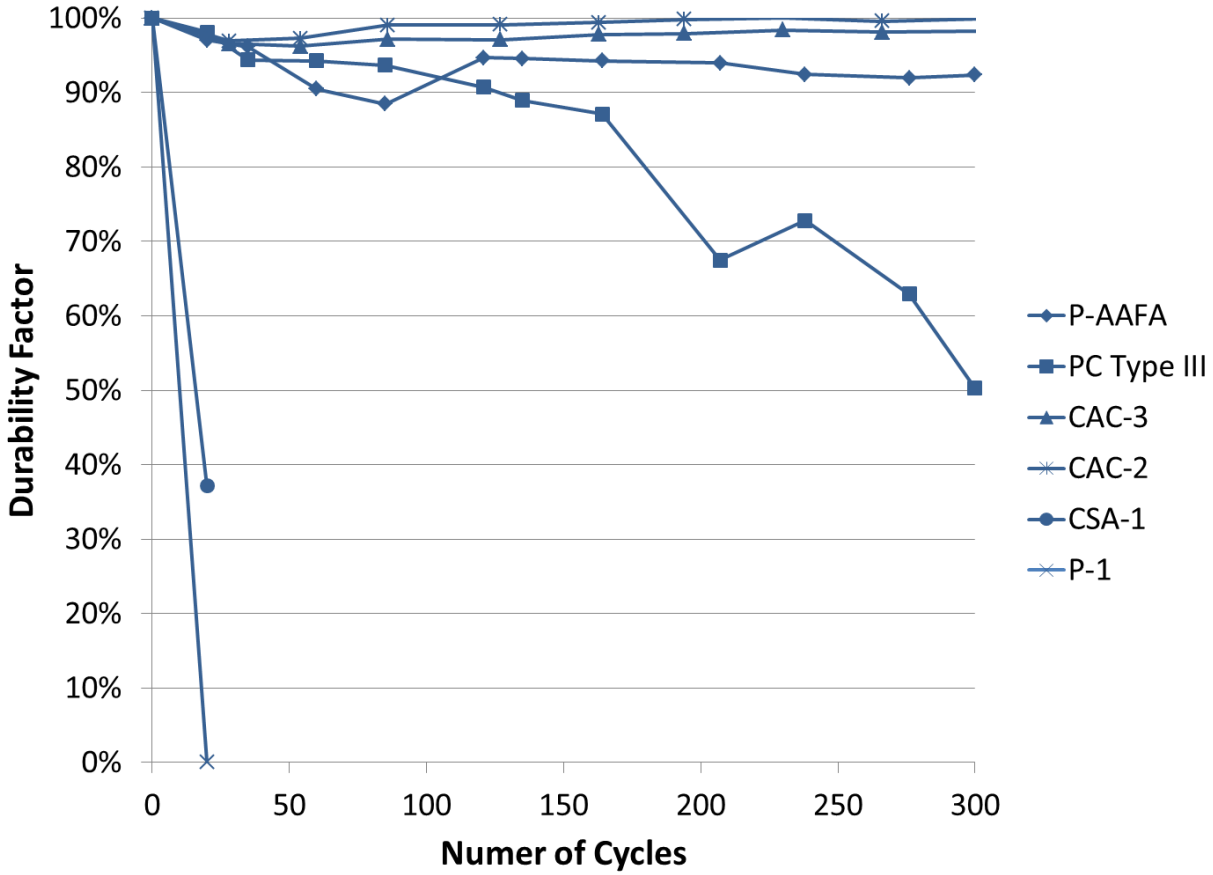

Figure 24, Relative dynamic modulus of elasticity of Phase III materials

Only 4 of the total 13 materials displayed a drop in the relative dynamic modulus of elasticity to below 60% before the 300 cycle limit. These materials included P-1, CSA-1, CSA-Latex, and PC Type III, covering all binder types relevant to this project besides calcium aluminate cement. The final durability factor and the materials final compliance with ASTM C 666 is shown in Table 5. Compliance was determined based on the number of cycles equaling or exceeding 300 (also shown) and a dynamic modulus of elasticity.

Table 5. Relevant values and compliance with ASTM C 666 criteria.

Material	Durability Factor	ASTM C666 Compliance	No. of Cycles	L > 0.008 inches (0.20 mm)?
P-1	0	Fail	20	No
P-2	92.5	Pass	300	No
P-3	93.25	Pass	300	Yes
P-AAFA	92.25	Pass	300	Yes
CSA-1	2.5	Fail	20	No
CSA-2	96	Pass	300	No
CSA-3	100.75	Pass	300	No
CSA-Latex	31	Fail	155	No
CAC-1	108	Pass	327	No
CAC-2	100.5	Pass	302	No
CAC-3	99	Pass	302	Yes
CAC-Latex	93.75	Pass	300	Yes
PC Type III	50.5	Fail	300	Yes

When performing a typical ASTM C 666, there seems to little correlation between the alternative concrete systems used and the spacing factor of 0.008 inches (0.20 mm) recommended by ASTM. Of the four materials with spacing factors over this value found by the hardened air void analysis, only one, PC Type III, the only full ordinary portland cement (OPC) materials of the group, failed to comply with ASTM C 666 and produced a high spacing factor. With the other materials, there was no correlation, possibly due to the individual differences between the materials relative to OPC concrete. It is possible that different binders have different critical spacing factors, owing to the differences in the materials and resultant microstructure. More work is needed to determine if this is in fact the case, but is an interesting finding that deserves further attention. Given these results, it suggests that performance testing using ASTM C 666 is likely a better evaluation method for assessing alternative binders, rather than applying the 0.008 inch

(0.20 mm) spacing factor that is typically applied only to portland cement concrete mixtures.

The ordinary portland cement, PC Type III, outperformed 3 other materials, but upon reaching the 300th freezing-and-thawing cycle, it was determined that it had dropped below the dynamic modulus limit of 60% between 276th and 300th cycle.

2.6 SUMMARY AND CONCLUSIONS

The summary and conclusions of the air content and freeze-thaw performance of the materials are as follows:

- Although both fresh and hardened air content generally correspond, greater than 5% fresh air content does not necessarily correspond to an adequate spacing factor for moderate frost resistance according to ASTM 1556.
- The ASTM C 672 salt scaling test yielded three materials with the worst visual rating of 5. Each of these materials was found to have an adequate spacing factor.
- ASTM C 672 and C 666 closely correspond. All materials with a visual rating of 5 also failed to comply with the freeze-thaw requirements. Only PC Type III failed the ASTM C 666 compliance with a visual rating of less than 5. It was rated 3.
- Materials P-3, P-AAFA, and CAC-3 maintained a good visual rating and ASTM C 666 compliance despite failing both the 5% fresh air limit and spacing factor requirements. This is likely due to the inclusion of fibers in P-AAFA. P-3 and CAC-3 may gain the resistance due to the combination of cements in the mix.
- Materials other than OPC concrete do not abide by typical rules of critical spacing factor, possibly due to difference in microstructure. Additional investigation will be

required. Until this time, performance testing such as ASTM C 666 or ASTM C 672 should be used with materials containing alternative binders.

Chapter 3: Alkali-Silica Reaction

3.1 Introduction and Background

Alkali-silica reaction (ASR) occurs in portland cement concrete when silica within aggregates dissolves in the high-pH pore solution in concrete. The attack is triggered initially by hydroxyl ions in the pore solution and then by the alkalies in the pore solution, creating an expansive gel. This expansive alkali-silica gel in ordinary portland cement concrete and other conventional concrete materials and "may cause abnormal expansion and cracking of concrete in service" (Farzam, et al., 2005). It requires water to proceed, and, thus, is only a concern in potentially moist environments. This cracking can lead to other durability problems such as corrosion of reinforcing steel. It allows for moisture and/or chlorides to penetrate into the concrete, potentially increasing the potential for freeze-thaw distress and/or corrosion of reinforcing steel. In addition, the cracking may lead to loss of strength in structural applications..

ASR is readily prevented by may be limiting the pH of the pore solution, the control of alkali concentrations, controlling active silica within the aggregates, reducing the moisture that the concrete may be exposed to, and the alteration of the gel to a unexpansive product (Mindess, Young, & Darwin, 2003). After ASR has been initiated in the field, it is very difficult to control. It is much easier to reduce the likelihood of ASR by selecting materials and mixture proportions using available prescriptive specifications or by using performance tests, with ASTM C 1293 (concrete prism test) being the most reliable test.

3.2 Materials and Mixture Proportions

To accelerate ASR for lab testing, the use of a reactive aggregate is needed. In addition, ASTM C 1293 provides for the evaluation of either the reactivity of either fine

or coarse aggregates by using known nonreactive aggregate in place of one. In this testing, a highly reactive fine aggregate was used in combination with a non-reactive coarse aggregate. The gradation of the coarse aggregate, a limestone, is provided in Table 6. The specific gravity of this limestone was 2.75 with an absorption capacity of 2.75%. The coarse aggregate was used in the as-received gradation.

Table 6. ASTM C 33 Gr. 57 Limestone Coarse Aggregate Sieve Analysis.

Sieve Size	Percent Passing
1.5 in (38.1 mm)	100
1 in (25.4 mm)	100
3/4 in (19.05 mm)	85
1/2 in (12.7 mm)	44
3/8 in (9.53 mm)	19
No. 4	6
No. 8	2

In contrast, the fine aggregate is a siliceous sand from El Paso, Texas. The sand contains large amounts of quarts (64%), chert (17.1%), and feldspar (11.5%). In addition, the aggregate meets the gradation requirements of ASTM C33 for fine aggregate. It is important to note that mixing procedures did not allow aggregate modification in any of the "all-in-one" mixes, including P-1, P-2, P-3, and P-AAFA as these mixtures already contain aggregates. Lastly, because the intention of this project was to evaluate specific

rapid repair mixtures and most of these contained binders other than portland cement, NaOH was not added to the mixing water as is the case in ASTM C 1293, where the boosted alkalies are added to increase the alkali content to 1.25% Na_2O_e. Although the materials studied in this project do not necessarily meet the intended cement or aggregate composition used in ASTM C 1293, by combining selected binders with a highly-reactive aggregate or by testing the as-received bag materials in ASTM C 1293 testing conditions (above water at 100 °F (38 °C), one can still evaluate the relative susceptibility of these materials and mixtures to ASR.

3.3 Experimental Procedures

3.3.1 ASTM C 1293

Experimental procedures for quantifying alkali-silica reactivity in the rapid, cement-based repair materials studied in this project generally followed ASTM C 1293 characterized the expansion do to ASR due to the aggregate, alkaline pore solution, and ingress of moisture into the system. Although this expansion will likely greatly differ from field conditions, it allows for a general assessment of reactivity, especially when compared to other materials as was done in this project.

To perform these tests, four 3 x 3 x 11.25 inch (750 x 750 x 2850 mm) concrete prisms were cast in steel molds with steel gauge pins cast into each end. These prisms were then left to cure in the temperature controlled mixing room and demolded at 24 hours. Next, each prism was stored in a typical five gallon bucket, as shown in Figure 21. Each bucket was lined with felt and 0.80 inches (20 mm) of water placed in the bottom to maintain a high relative humidity within the system.

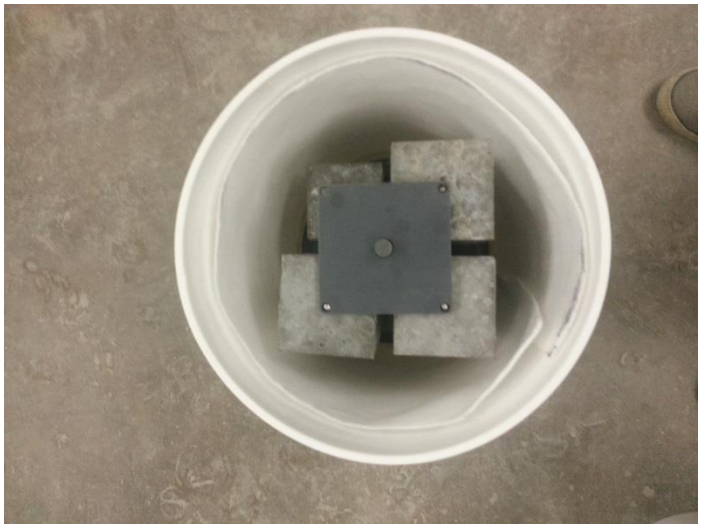

Figure 25. Container for moisture and orientation control of prisms for ASTM C 1293 testing.

It is important to note that a high relative humidity was maintained without actively saturating the prisms. The prisms were placed on a plastic rack to raise them above the water level. The buckets were then sealed and stored in a 100 degree Fahrenheit (38 degrees Celsius) chamber, as shown in Figure 26, throughout the life of the test.

Figure 26. Temperature and humidity controlled room for ASTM C 1293 testing.

This high temperature specified in ASTM C 1293 accelerates the test for experimental use. Each specimen was measured at 7 days from casting, but removed twenty-four hours before measuring to acclimate to a consistent “room temperature” of 73 °F (23 °C). Measurements were performed using a comparator, and each specimen was weighed for consistency.

After each measurement, the specimens were “flipped top to bottom” relative to their original position and returned to the five gallon buckets. The water level was then checked, and the bucket returned to the high temperature room.

ASTM C 1293 specifies for measurements to be taken at days 7, 28, and 56 and months 3, 6, 9, and 12 months. The aforementioned procedure was repeated for each measurement.

3.3.2 Pore Press

Because alkali-silica reaction is driven by aggregates being exposed to a high pH pore solution, characterizing pore solution composition at various points of maturity for the material may be important in alkali-silica reactivity. This characterization was especially desired for P-AAFA because an alkali activator is used in the cement, and it is of technical interest to quantify the effects of alkali activator addition on pore solution composition. To access the pore solution, the pore press, as shown in Figure 27, was used.

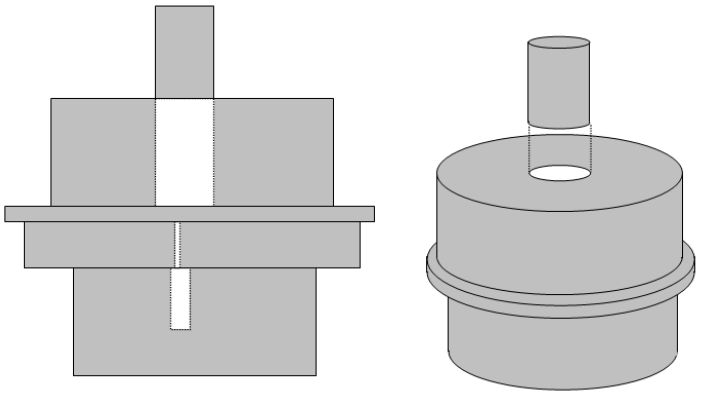

Figure 27. Schematic diagram of pore press used in extracting concrete pore solution.

First, the concretes sample was crushed into pieces less than 0.375 inches (10 mm) in size. Approximately 250 grams of these pieces are used in the pore press and this value recorded.

Next, the equipment was set up. To do this, the base was set on the lower bearing block of the compression testing machine. The sample vile weight was recorded and then the container placed into the pore press base. Next, Part B of the base was set on the lower piece. The O-ring was then greased and seated properly. The area of Part B where the sample rests was lubricated with Teflon lubricant and place the positioning ring on

Part B. The interior cavity of Part A was lubricated with Teflon lubricant. Finally, Part A was centered over and lowered onto Part B. Careful attention was paid to not move Part A after it was set in place so the O-ring was not disturbed.

Now, approximately 1/3rd of the 250 grams of sample was poured into the cavity of Part A using a modified funnel and compacted using a small pestle. This process was repeated for two more lifts and level at approximately 0.5 inch (13 mm) from the cavity's top. A 0.1875 inch (4.8 mm) Teflon disc was placed on top of the sample.

Next, the surface of the piston was lubricated with the aforementioned lubricant and inserted into the cavity on top of the Teflon disc. The piston was checked to ensure it was perpendicular to the pore press setup. The protective disc was centered on top of the piston and stacked with bearing plates to allow the compression testing machine to make contact and continue through the entire stroke of the equipment.

To extract the pore solution, a load of approximately 5000 lbs (22 kN) was applied with the compression machine shown in Figure 28 and was then released. The piston was checked to guarantee it was turning freely. Next, a load of approximately 500,000 lbs (2,220 kN) was applied at a load rate of 30,000 to 40,000 lbs per minute (133 to 178 kN per minute). The maximum load was held for about 1 minute. The piston was then unloaded.

Figure 28. Forney FX700 compressive testing machine.

The pore press was then dismantled and the sample removed. The concrete specimens were removed and examined, with their appearance similar to Figure 29.

Figure 29. P-AAFA samples after attempting pore solution extraction via pore press.

3.4 Results and Discussion

In general, the material in this study performed well based on a single year expansion limit of 0.04% cited in Appendix X1.2 of ASTM C 1293. The mixtures that exceeded this expansion limit at one year or less include P-AAFA, CAC-3, P-1, and CAC-Latex. It is important to note that the pore press yielded no pore solution for material P-AAFA despite the relatively high load. The pore solution composition for this material is currently unknown and will not be speculated at this time.

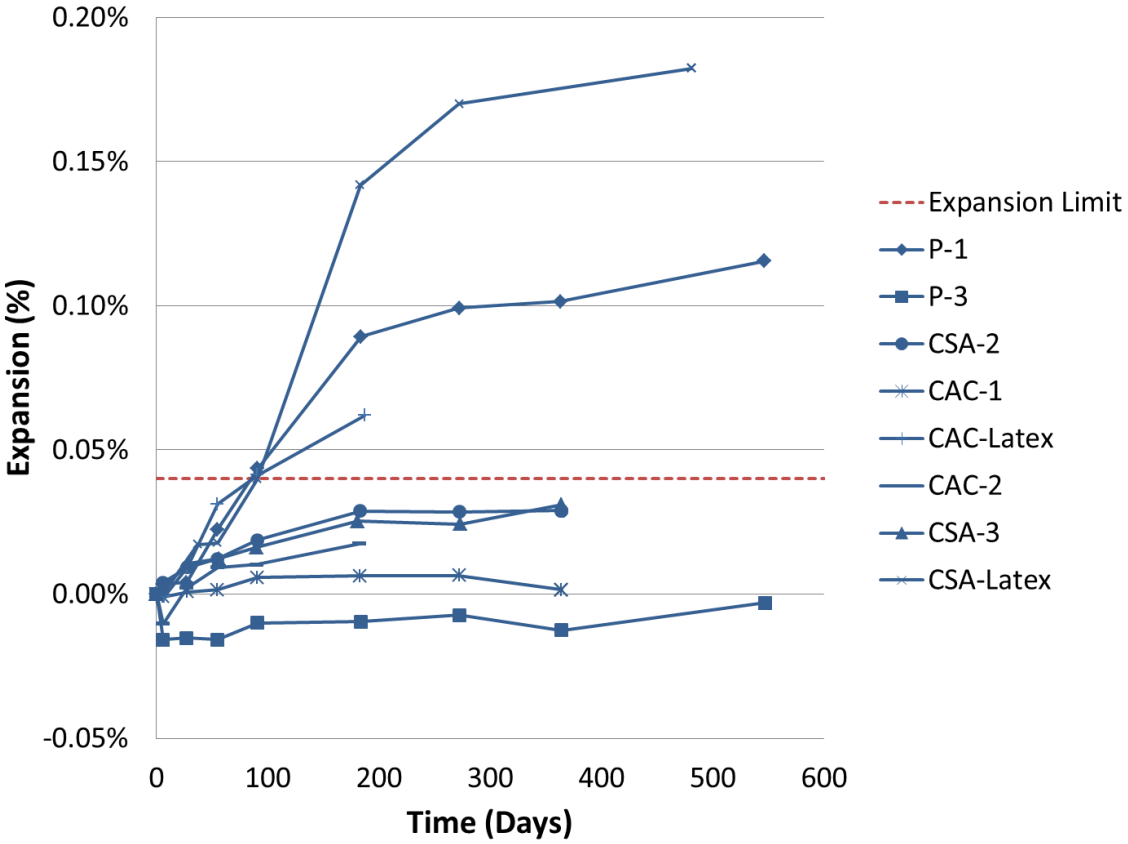

Figure 30. Expansion of Phase II materials via ASTM C 1293.

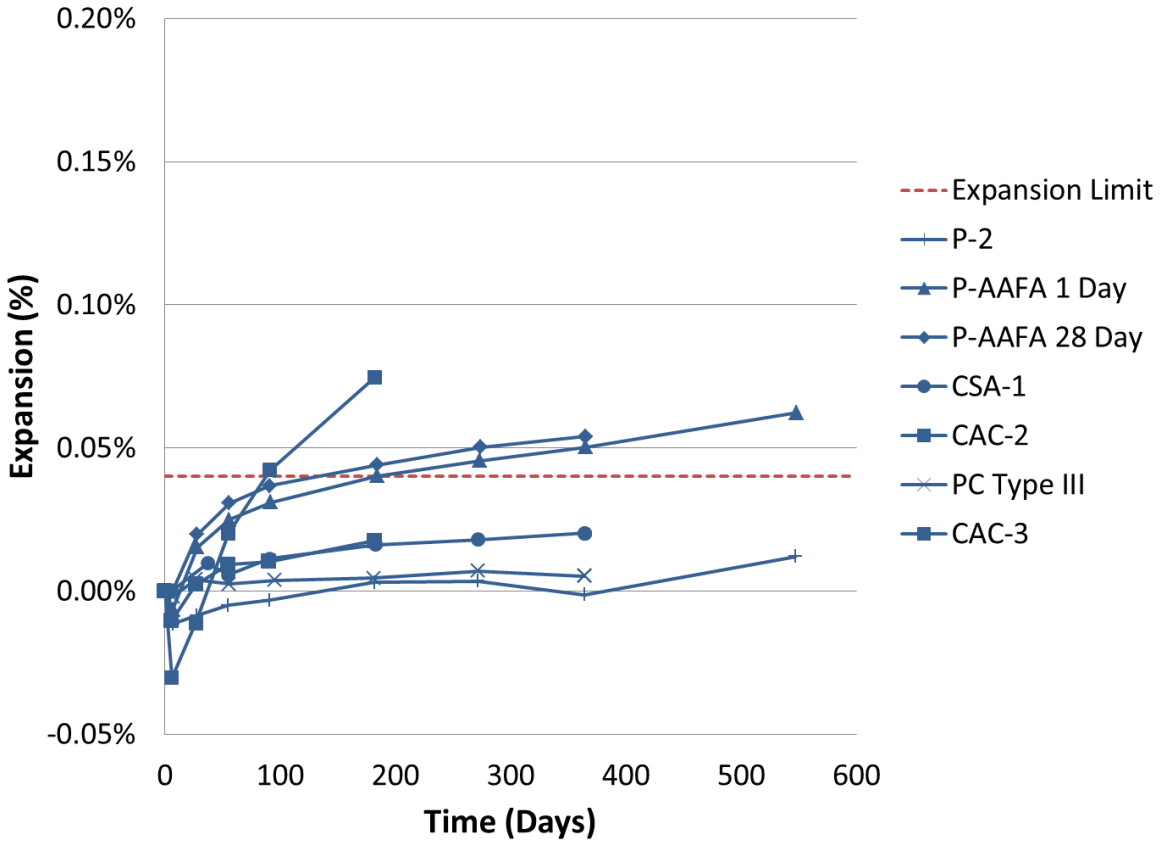

Figure 31. Expansion of Phase III materials via ASTM C 1293.

Because alkali-silica reaction is created by a combination of siliceous aggregate and pore solution alkali content, it appears logical that all pre-packaged, all-in-one products other than P-2 succumbed to this reaction. For materials P-1, P-2, and P-AAFAA, it is likely that the pore solution is high in alkalinity and that the aggregate is reactive, or alternately, another reaction may have caused the expansion. Of these, it is known that P-AAFA has a highly alkaline pore solution due to its nature as a alkali-activated fly ash product. The other pre-packaged materials all remained below the 0.04% expansion limit given in ASTM C 123, suggesting that either the aggregates were non-reactive or the pore solution pH was too low to dissolve the reactive aggregates. It is also possible that some binder systems lacked sufficient calcium to generate expansive ASR

gel. More generally, the other materials (not all-in-one) performed well when tested for ASR. All materials outside of those mentioned were below the expansion limit.

3.5 SUMMARY AND CONCLUSIONS

The summary and conclusions of the alkali-silica reaction performance of the materials are as follows:

- Only four materials failed the ASTM C 1293 expansion limit of 0.04% at two years. One of these materials is P-AAFA, an alkali-activated fly ash material, which is expected to have a very highly alkaline pore solution.
- Styrene-butadiene latex increase the expansion of calcium aluminate cement (CAC-1 to CAC-Latex) and calcium sulfoaluminate cement (CSA-1 to CAC-Latex) significantly. More work is needed to understand the underlying mechanism for this behavior.
- Besides latex modified materials and P-AAFA, the only materials to exceed the 0.04% expansion limit were P-1 and CAC-3. The content of the aggregate was not analyzed for material P-1.

Chapter 4: Sulfate Attack

4.1 Introduction and Background

One form of distress observed in concrete structures worldwide is external sulfate attack. The sulfates which cause this reaction are often present in soils and groundwater. External chemical sulfate attack leads to deleterious expansion in concrete due to the degradation of C_3A, then the formation of gypsum, and finally the formation of ettringite. In addition, transportation structures are susceptible due to the presence of sulfates in soils, water, and pollution (Mindess, Young, & Darwin, 2003).

In general, cements with lower C_3A content are more resistant to external chemical sulfate attack than cements with higher C_3A contents. In addition, a less permeable microstructure and the consumption of $Ca(OH)_2$, both typically helped by supplementary cementing materials (SCMs), are also known to help prevent sulfate attack.

4.2 Materials and Mixture Proportions

Prisms for sulfate attack follow the typical mixing procedures and materials outlined in Zuniga (2013). ASTM C 1012 is the most commonly used sulfate attack test in the United States, but it relies on the testing of small mortar bars. Although ASTM C 1012 specifies suggested properties and proportions, this specification was modified to allow the use of concrete prisms of the typical material proportions developed in Phase I or provided by the material manufacturer. The modifications are as follows:

- ASTM C 1012 specifies an aggregate-to-cementitious material ratio of 2.75 and a water-to-cement ratio of 0.485. For this project, both proportion requirements were ignored so typical rapid setting material proportions could be used. This also includes

the use of 2-inch (50 mm) concrete prisms of 10-inches (250 mm) length instead of the typical 1-inch (50 mm) mortar bars.

- The test was also modified to use the same fine aggregate proposed in (Zuniga, 2013). This differs from the standard.

For each material, at least three 2 x 2 x 11.25 inches (500 x 500 x 2850 mm) prisms were cast to develop average properties of the specimens under sulfate attack.

4.3 Experimental Procedures

Experimental procedures for quantifying susceptibility to external chemical sulfate attack in concrete can be quantified using ASTM C 1012. Although the specification calls for curing of specimens until a compressive strength of 2850 psi (20 MPa), most specimens were instead cured for 1 day, 28 days, or both to compare the materials at similar ages. Each concrete prism was cast in steel molds with typical comparator pins at each end.

After the designated curing periods, each concrete prism was placed in sealed container filled with 5% sodium sulfate solution. At 1 day, the prisms are measured using a comparator as shown in Figure 32:

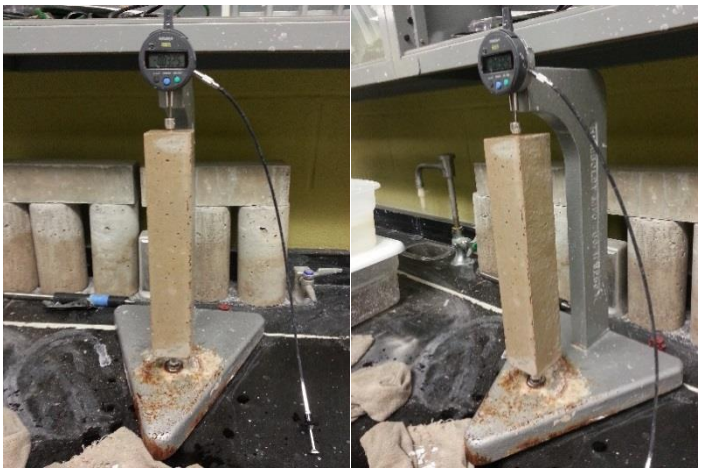

Figure 32. Comparitor for mesuring length change in concrete.

The sulfate solution in the containers was replaced after each measurement. Subsequent measurements are taken at 2, 3, 4, 8, 13, and 15 weeks and after 4, 6, 9, 12, 15, and 18 months.

4.4 Results and Discussion

The expansion values for Phase II and III materials using both 1 and 28 day cures were recorded at the aforementioned times through 18 months. After this time period, the test was stopped. The results are shown in Figure 33. Please note that some Phase II and III materials have not yet reached 18 months under testing at the time of this report. The data will be recorded and reported at a later date.

Because there are no standard limits for the expansion of concrete exposed to external sulfates, an expansion of 0.04 percent is used herein as it represents the level of expansion that typically causes concrete to crack. This value is also consistent with concrete expansion limits used for ASR, both in ASTM C 1293 and for outdoor exposure blocks stored on the UT exposure site at the J.J. Pickle Research Campus.

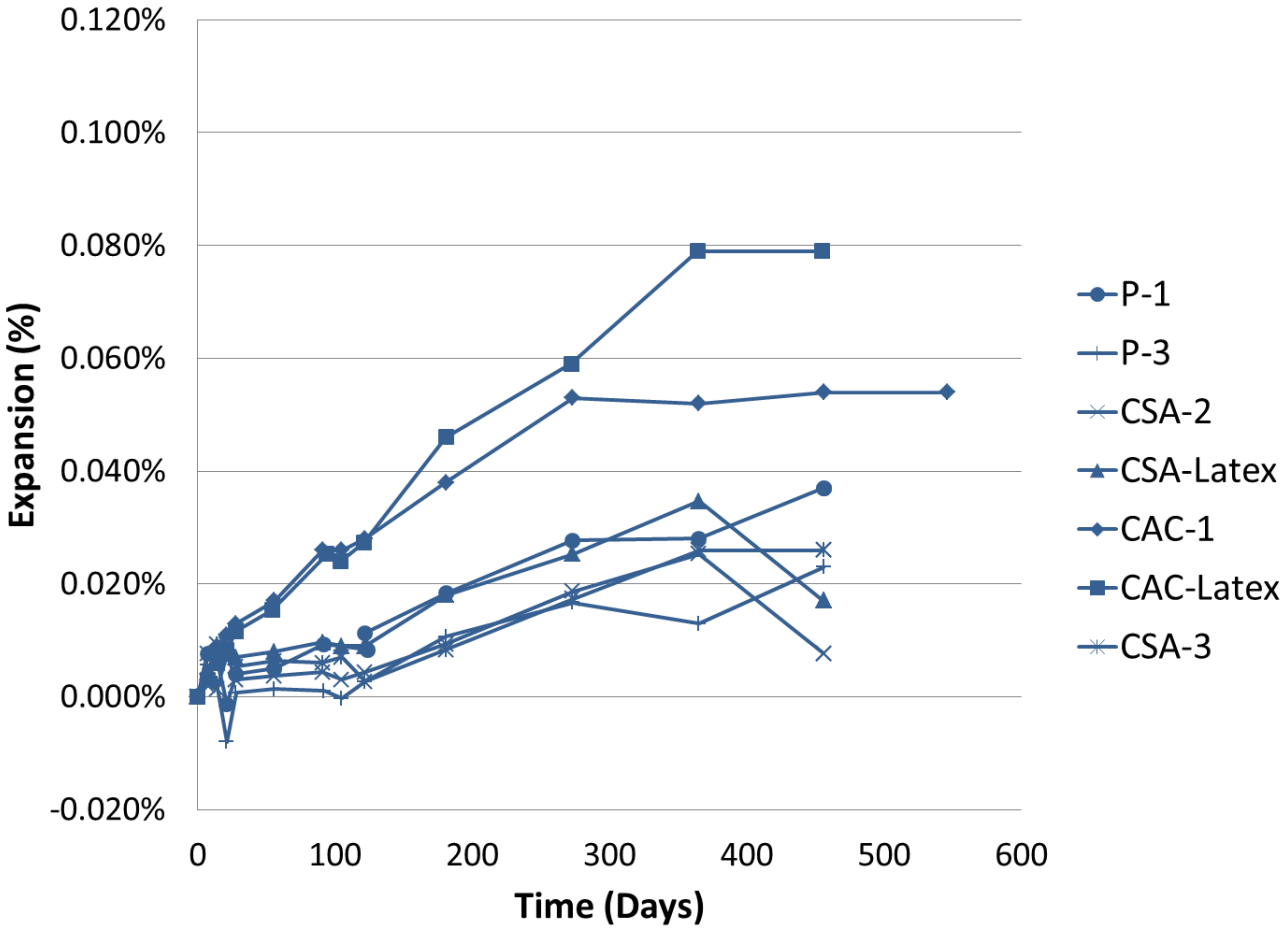

Figure 33. ASTM C 1012 expansion of Phase II materials after 1 day cure.

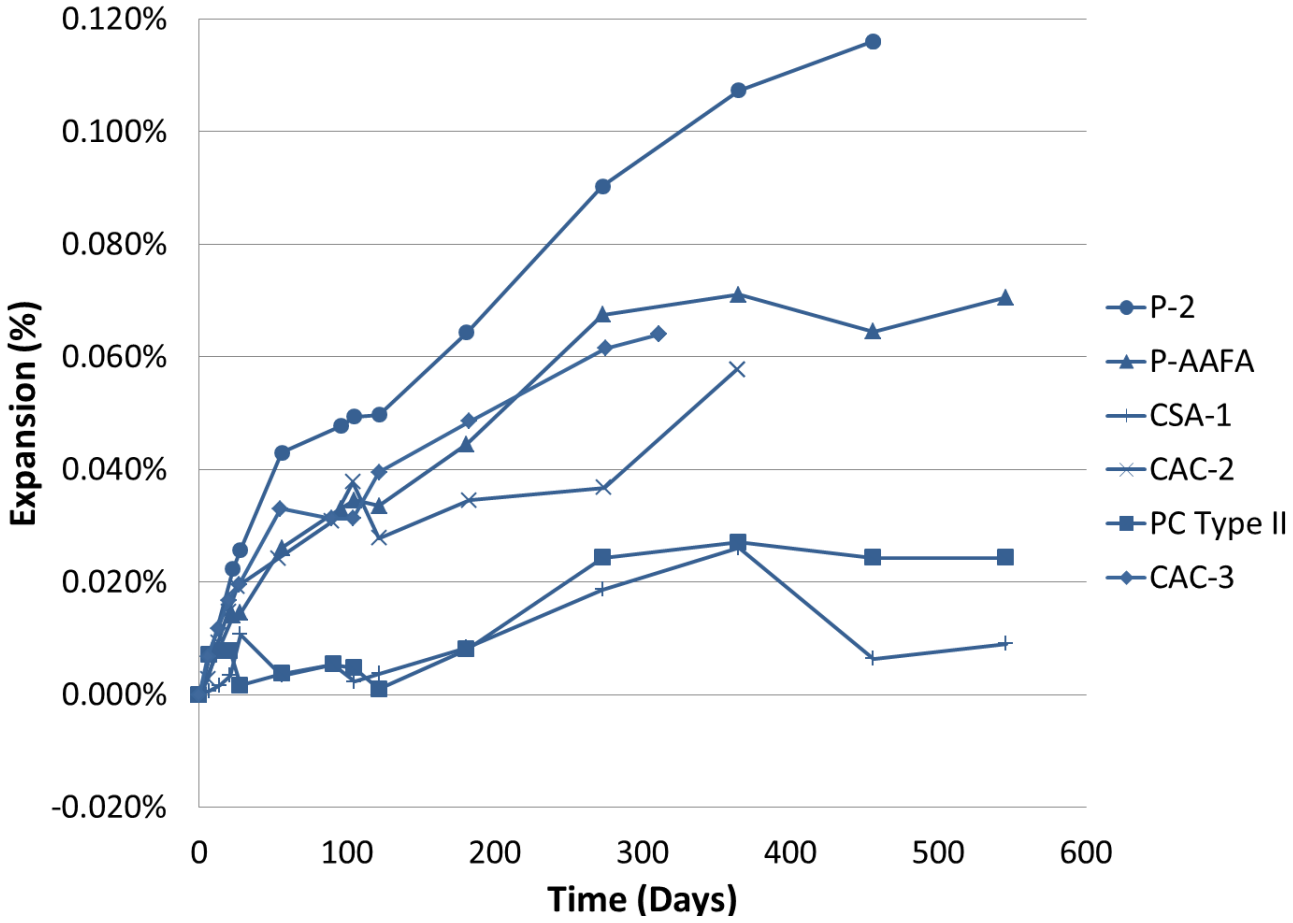

Figure 34. ASTM C 1012 expansion of Phase III Materials after 1 day cure.

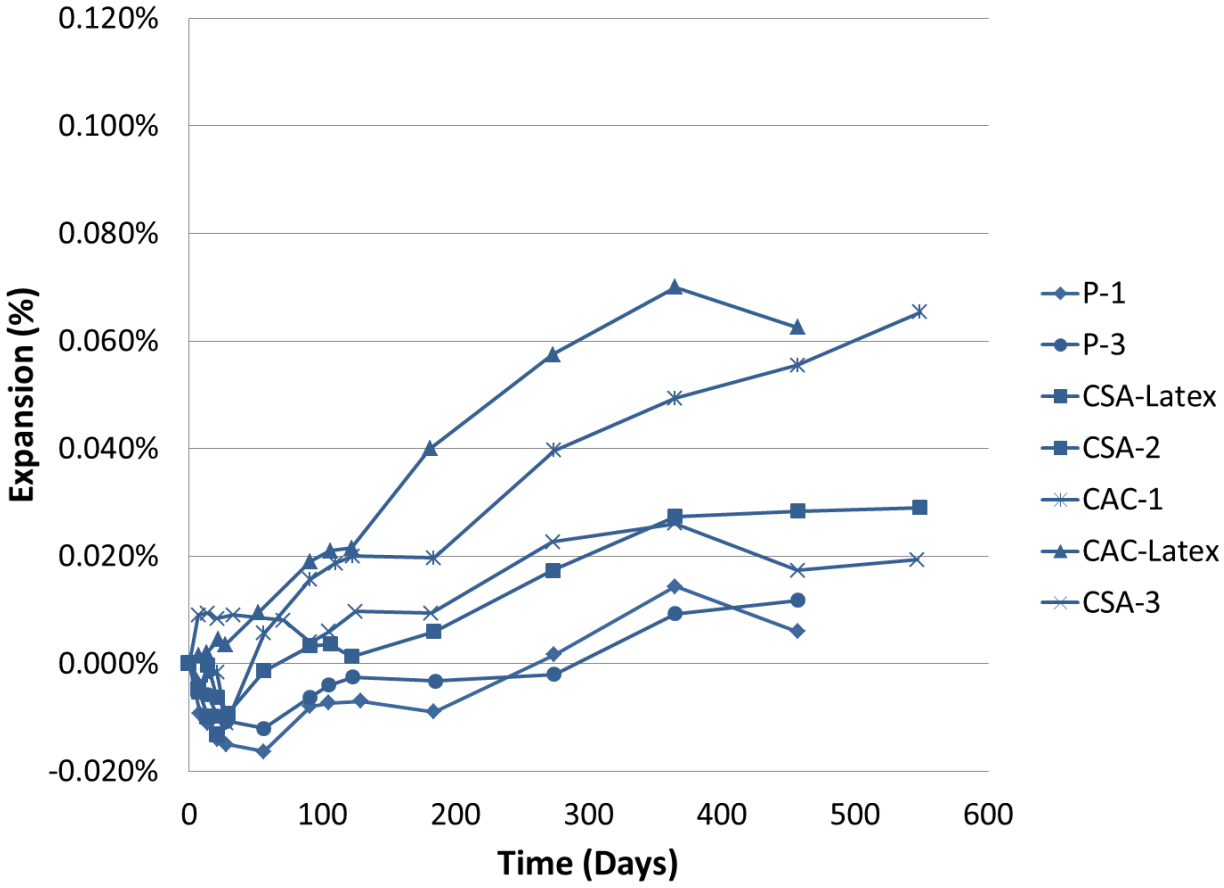

Figure 35. ASTM C 1012 expansion of Phase II Materials after 28 day cure.

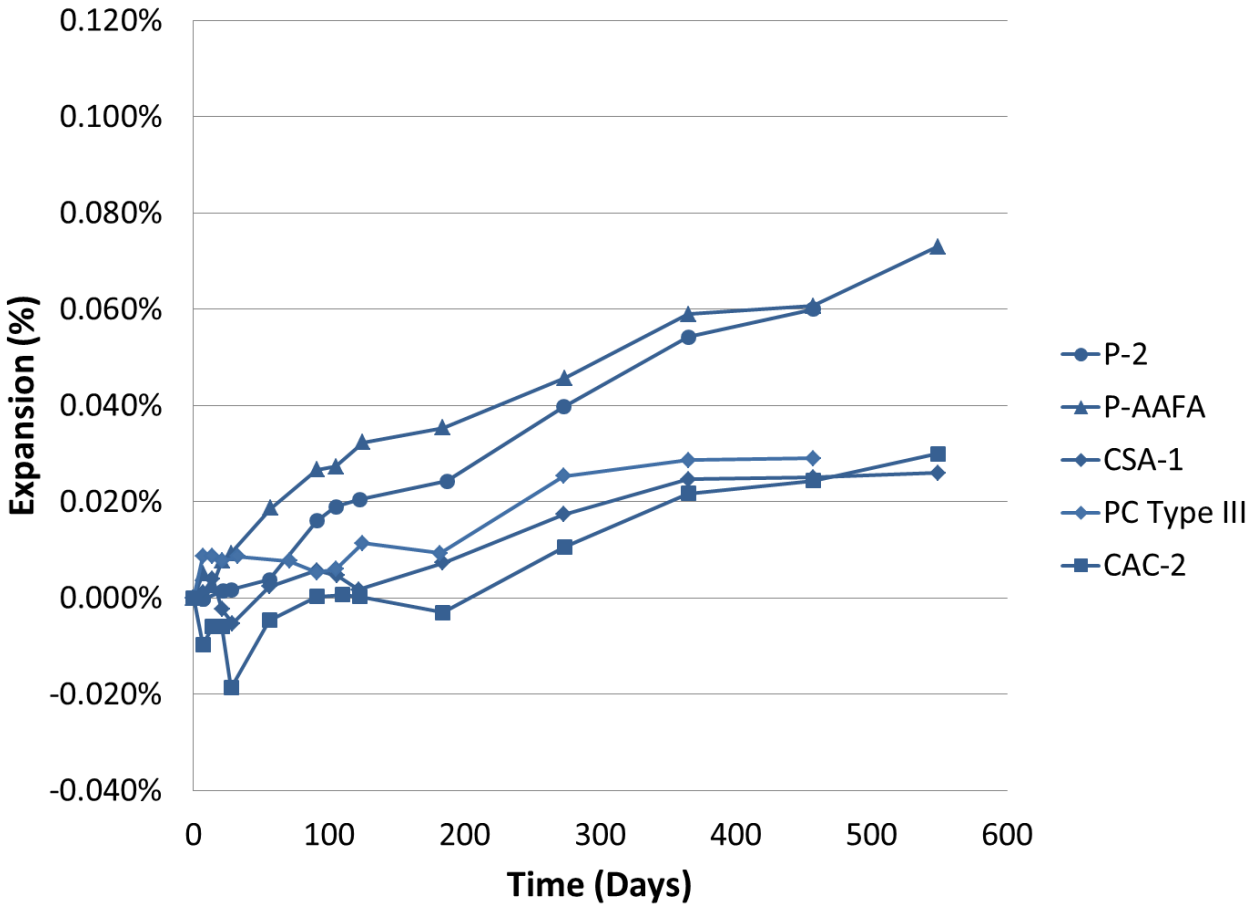

Figure 36. ASTM C 1012 expansion of Phase III Materials after 28 day cure.

Materials P-2 and P-AAFA exhibited the most expansion with maximum values of 0.126% and .071% under 1 day curing conditions and 0.054% and 0.059% under 28 day curing conditions, respectively. Despite this, P-2 and P-AAFA expanded less than the limit of 0.4%.

Another unexpected outcome of the ASTM C 1012 testing performed for this project was the effect of the styrene-butadiene latex modifying of both materials, CAC and CSA. The effect of sulfate attack on both specimens was more pronounced then when not modified by the latex. General knowledge of latex modifying anticipates a more

dense pore structure and higher resistance to sulfate attack when modified with styrene-butadiene latex (Shaker, El-Dieb, & Reda, 1997).

4.5 SUMMARY AND CONCLUSIONS

The summary and conclusions of the performance in a sulfate environment of the materials are as follows:

- In all materials, increasing curing time form 1 day to 28 days improved resistance to sulfate attack.
- The addition of styrene-butadiene latex (CAC-1 to CAC-Latex and CSA-1 to CSA-Latex) worsened the sulfate resistance in both instances.
- Calcium aluminate cement was not resistant to sulfate attack in our tests. This is contrary to common knowledge of CAC.
- Nearly half of the materials (6 of 13) failed when only subjected to a single day of curing.

Chapter 5: Permeability and Corrosion

5.1 Introduction and Background

Transportation structures are particularly susceptible to corrosion due to deicing salts and other salt solutions. A truly durable structure would not allow the corrosive solutions to reach reinforcing steel and degrade the structural performance.

There are two primary sources of corrosion of reinforcing steel in concrete – chlorides and carbonation. Chloride penetration was tested in three manners in this project. A simplified version of ASTM C 1202 for Rapid Chloride Penetration Testing (RCPT) published by Riding, Poole, Schindler, Juenger, & Folliard (2008) was used, the apparent chloride diffusivity of concrete was measured using ASTM C 1556, and the impact of chloride ingress into repaired, reinforced concrete beams was evaluated using a modified ASTM G 109. Carbonation was tracked over the course of 11 months as detailed in CEN/TS 12390-10:2007.

5.2 Materials and Mixture Proportions

Each test used the typical materials and mixture proportions and procedures described in Zuniga (2013). In the simulated bridge deck for fatigue corrosion testing, the materials and mixture proportions as follows:

- Fine aggregate: River sand from the Colorado River in Austin, Texas. The aggregate has a fineness modulus of 2.71, with percent passing gradation as shown in Figure 37.
- Coarse aggregate: Grade 57 river gravel with an absorption capacity of 1.29% and a specific gravity of 2.60. This aggregate is further described in Table 7.

- Volumetric mix design: The following mix design, as shown in Table 8, was used in Pesek (2011) with the cubic feet of each constituent expressed per cubic yard of concrete.
- The mixtures were deemed both small and workable enough to go without any admixtures when mixed with the aid of a vibrating table.

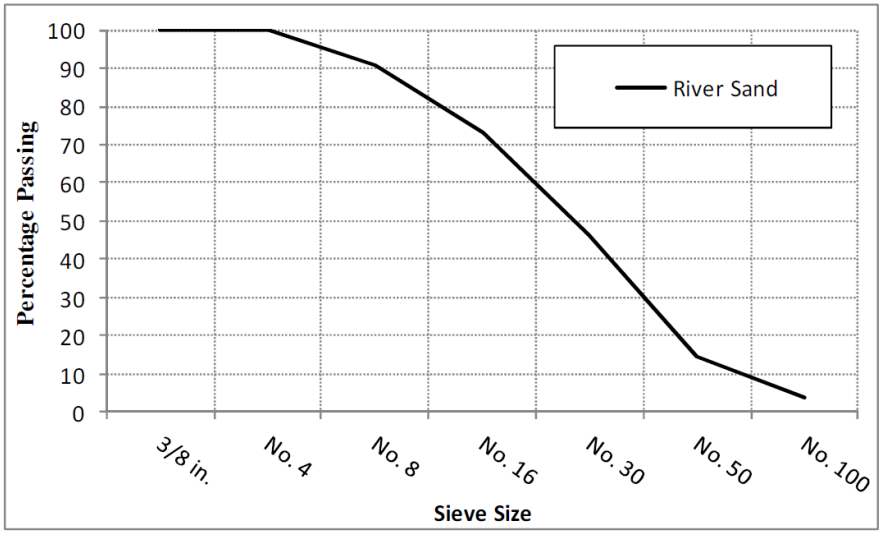

Figure 37. Gradation analysis of fine aggregate (Pesek, 2011).

Table 7. Gradation analysis of Gr. 57 River Gravel for bridge deck mix.

Sieve Size	Percent Passing
1.5 in (38.1 mm)	100
1 in (25.4 mm)	100
3/4 in (19.05 mm)	79
1/2 in (12.7 mm)	58
3/8 in (9.53 mm)	41
No. 4	7
No. 8	1

Table 8. Volumetric mixture design of bridge deck mix.

Cement (ft^3/yd^3)	Water (ft^3/yd^3)	Paste Volume (ft^3/yd^3)	Coarse Aggregate (ft^3/yd^3)	Fine Aggregate (ft^3/yd^3)	Total Aggregate (ft^3/yd^3)
2.58	3.66	6.25	12.08	8.53	20.61

It is important to note that a top portion of the bridge deck was mixed with 0.5 percent calcium chloride per pound of cement to increase the rate of corrosion for testing. This procedure was suggested by Dr. Michael D. A. Thomas, P.Eng. of the University of New Brunswick. It will be further described in Section 5.6.1.

5.3 Rapid Chloride Penetration Testing

Rapid Chloride Penetration Testing (RCPT) was performed in accordance to the Simplified Concrete Resistivity and rapid Chloride Permeability Test Method developed by Riding, Poole, Schindler, Juenger, & Folliard (2007). This method greatly simplifies the typical Rapid Chloride permeability Test, ASTM C 1202, by "avoid[ing] cutting samples, dessication, test duration, and sample heating." (Riding, Poole, Schindler, Juenger, & Folliard, 2008). It also produces better results when supplementary cemenititious materials (SCMs) are used or when certain admixtures are present. Since the composition of some of the repair materials presented in this project are at least partially unknown, the rapid method was greatly preferred.

5.3.1 Experimental Procedures

To perform the aforementioned simplified test, two 4 x 8 inch (100 x 200 mm) cylinders were cast for each mixture according to the mixing guidelines. Each mixture was proportioned as typical and outlined in Zuniga (2013). From each material, one sample was moist-cured for 28 days and the other moist cured for 56 days.

After moist curing, the specimen is covered with a 7.4 inch (188 mm) long acrylic sleeve instead of the sleeve specified in the original test. The specimen is then inserted between each half of the test cell and the two halves are clamped onto the specimen with long bolts. A seal is created between the sleeve and the halves of the test cells.

Next, the cell at the top surface of the concrete cylinder specimen is filled with 3.0% NaCl solution. The other cell is then filled with 0.3 N NaOH solution. The cell at the top surface is connected to the negative terminal and the opposite side to the positive. After connection, the terminal was turned on and set to 60 volts. At this time, the initial current is read and recorded. After 5 minutes, according to Riding, Poole, Schindler, Juenger, & Folliard (2008), the voltage is once again recorded and the test may be

stopped. The total charge passed through the sample, which is required by ASTM C 1202, was ignored.

5.3.2 Results and Discussion

In general, the materials presented in both Phases II and III performed well when subjected to the simplified rapid chloride permeability test. All but a single material showed noticeable improvement when cured at approximately 56 days versus 28 days as curing is typically prescribed. The results are shown in Figure 38 and Figure 39.

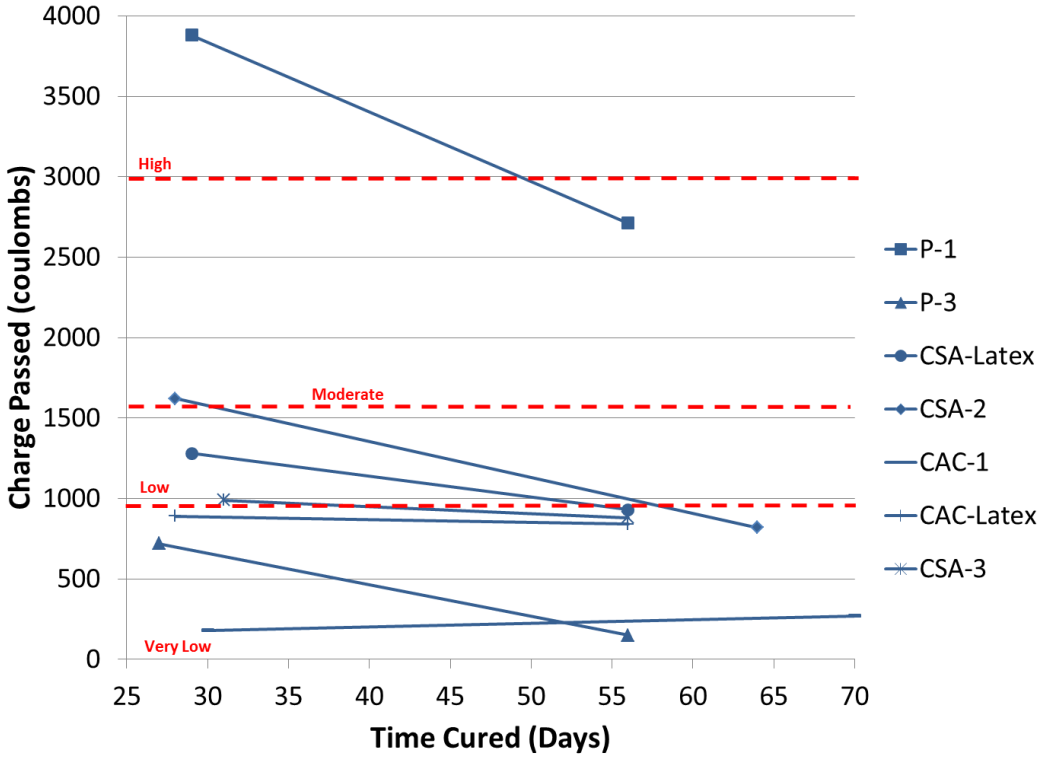

Figure 38. Results of simplified Rapid Chloride Permeability Test for Phase II materials.

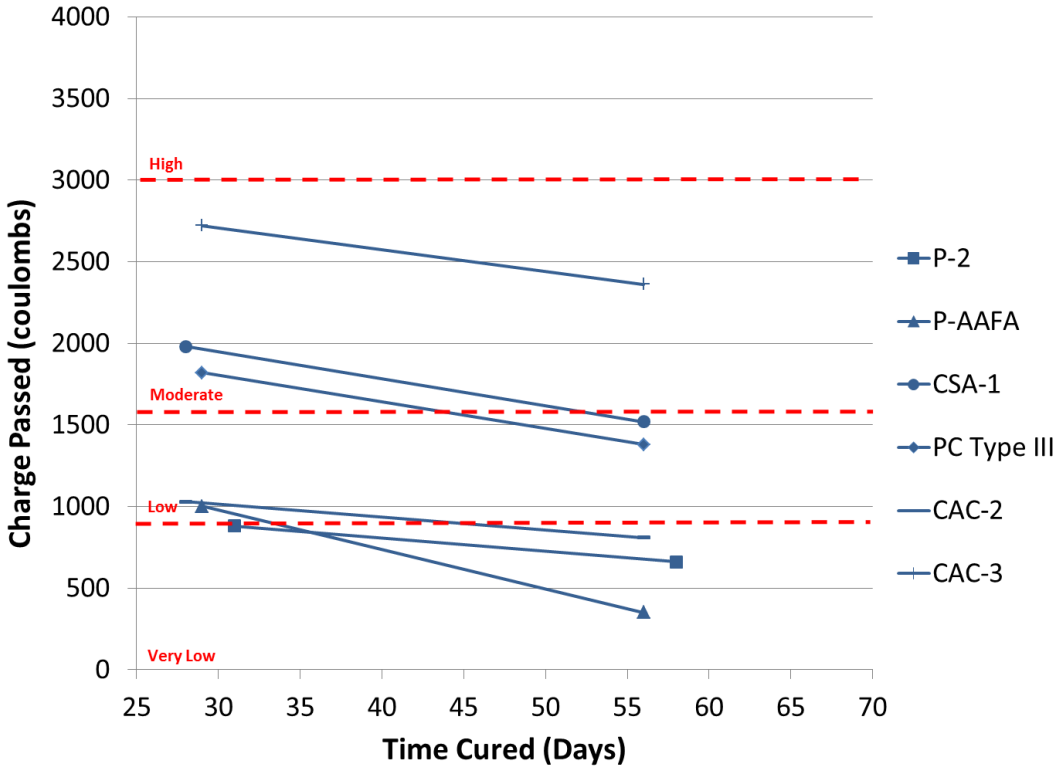

Figure 39. Results of simplified Rapid Chloride Permeability Test for Phase III materials.

As shown Figure 38, only P-1 could be classified as having high permeability according to the method. It should also be noted that if this material is cured for 58 days instead of 28 days, it is no longer above the 3000 coulomb limit for high permeability concrete.

Also, only three materials may be classified as having moderate permeability within the range of 1600 and 3000 coulombs. These materials are CSA-1 and PC Type III of Phase II and CSA-2 of Phase III, although each passes into the low permeability category of cured for 58 days.

Although curing for extended periods of time in an instance that calls for rapid, cement-based repair materials in transportation is unlikely, this study highlights the benefit of curing time. In general, even minimal curing can have a remarked effect on the

ability of a material to resist intrusion by creating a more torturous pore structure. Curing should be implemented whenever possible and for as long as possible.

5.4 CARBONATION

Carbonation is the absorption of carbon dioxide gas into the concrete structure and the eventual conversion of calcium hydroxide and other hydration products to carbonates by atmospheric carbon dioxide. This conversion causes a change in the concrete's pH to below the corrosion threshold of about 11.5. This drop in pH will initiate corrosion in the reinforcing steel if it reaches the appropriate depth, so the rate and penetration of carbonation is important to maintain the durability of concrete structures. Carbonation depths in well cured concrete with a low water-to-cement ratio seldom exceed 1 inch (25 mm) in depth, but it is important to test the alternative rapid-repair materials used in this project for differences (Mindess, Young, & Darwin, 2003).

5.4.1 Experimental Procedures

Carbonation was measured over a period of 11 months following procedures detailed in CEN/TS 12390-10:2007. Prisms of dimensions 4 x 4 x 16 inches (100 x 100 x 400 mm) were cast and placed outside. For each material to be studied, a single sample was placed both inside an enclosure and outside, as shown in Figure 40.

Figure 40. Test location of carbonation prisms.

At intervals of 6 months and 11 months, carbonation depths were measured through the use of a Phenolphthalein pH indicator. The samples were broken perpendicular to the long faces and sprayed with indicator. Since carbonation lowers the pH of concrete to below 11.5, the indicator only "colors" the uncarbonated portions of concrete. This depth was then measured using a ruler as shown in Figure 41.

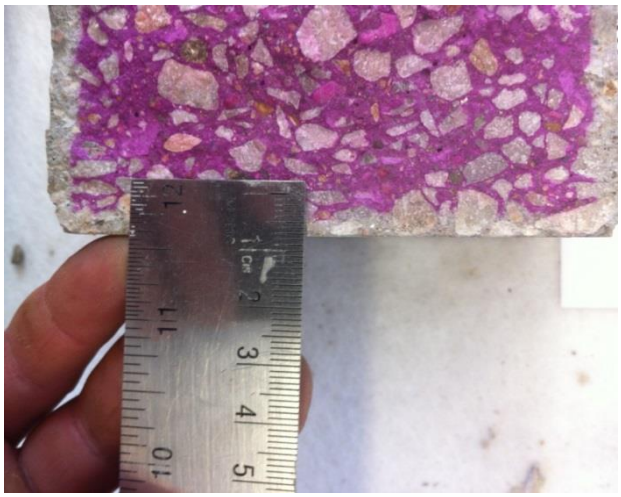

Figure 41. Action of Phenolphthalein pH indicator and measurement of carbonation depth.

After the depths for each material are measured, pictures of each specimen are taken. Also, Sikagard 550W Elastocolor white base is applied onto the broken plane to prevent carbonation from the ends of the specimen. The prisms are then placed outside in their previous location and facing the previous direction.

5.4.2 Results and Discussion

In general, every material performed worse than the Type III ordinary portland cement. This result, as shown in Table 9, is likely due to the ill effects of most common secondary cementitious materials (SCMs) on the ingress of carbonation.

Figure 42. P-AAFA sample displaying carbonation depth at 11 months using Phenolphthalein PH indicator.

Figure 43. CSA-1 sample displaying carbonation depth at 11 months using Phenolphthalein PH indicator.

Figure 44. CAC-3 sample displaying carbonation depth at 11 months using Phenolphthalein PH indicator.

Figure 45. P-2 sample displaying carbonation depth at 11 months using Phenolphthalein PH indicator.

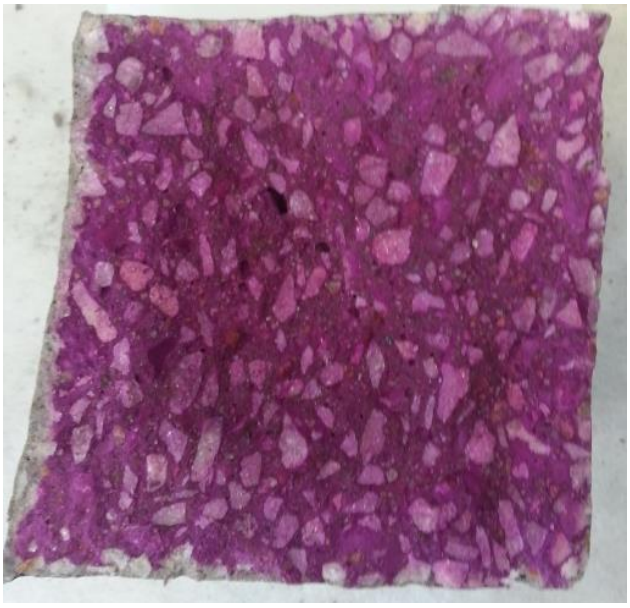

Figure 46. PC Type III sample displaying carbonation depth at 11 months using Phenolphthalein PH indicator.

Figure 47. CAC-1 sample displaying carbonation depth at 11 months using Phenolphthalein PH indicator.

Table 9. Carbonation depths for Phase III materials at 6 and 11 months.

Material	6 Months		11 Months	
	Inside	Outside	Inside	Outside
P-2	0.15 in	0.05 in	0.11 in	0.04 in
	0.75 mm	1.2 mm	2.8 mm	0.98 mm
PC Type III	0.00 in	0.00 in	0.05 in	0.00 in
	0.02 mm	0.02 mm	1.28 mm	0.13 mm
CAC-3	0.02 in	0.01 in	0.25 in	0.13 in
	0.51 mm	0.30 mm	6.29 mm	3.30 mm
CAC-2	0.01 in	0.01 in	0.14 in	0.12 in
	0.24 mm	0.30 mm	3.48 mm	3.13 mm
P-AAFA	0.02 in	0.01 in	0.29 in	0.17 in
	0.56 mm	0.30 mm	7.28 mm	4.28 mm
CSA-1	0.03 in	0.01 in	0.34 in	0.14 in
	0.65 mm	0.30 mm	8.68 mm	3.48 mm

In addition, each specimen showed more carbonation when placed inside an enclosure. The standard supports this data by stating that the Stevenson screen allows the

movement of atmosphereic conditions yet prevents the exposure of specimens to precipitation and solar radiation (CEN, 2007).

As anticipated, all materials performed worse than PC Type III. Typically, secondary cementitious materials or other alternative binders create an environment more conducive to carbonation.

Of the Phase III materials, CSA-1 and P-AAFA allowed the most carbonation to take place with a value greater than 0.25 inch (6.4 mm) when inside the carbonation enclosure. Although well below the minimum cover requirement of 0.75 inch (19 mm) called for in ACI 318, the carbonation depth may become more of an issue over the full life of a structure or roadway.

5.5 CHLORIDE DIFFUSION

The ingression of chlorides into concrete and the rate this occurs can cause corrosion of the reinforcing steel when deicing salts or other chloride solutions are ponded on or applied to concrete.

It is important to understand the diffusion of chlorides into the concrete's matrix to allow for an indirect correlation to overall permeability and corrosion resistance of a concrete material.

5.5.1 Experimental Procedures

Following the procedure given in ASTM C 1556, the apparent chloride diffusion coefficient can be found. First, cast 4 inch (100 mm) x 8 inch (200 mm) cylinders of the Phase III materials were cast according to standard mixture proportions. The cylinders were cured for 28 days. After curing, the specimens were cut using a wet saw in accordance to ASTM C 1556 as shown in Figure 48 and frozen until further use.

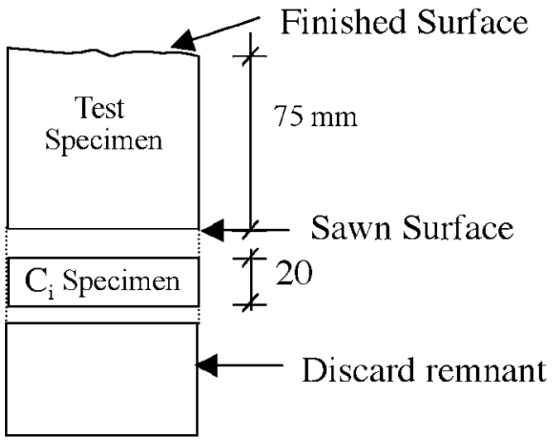

Figure 48. Preparation of test specimens for chloride diffusion test (ASTM 1556).

After all specimens were cast and cut, the test specimens were removed from the freezer and Sikadur Injection Gel was applied to all sides besides the finished surface. The specimens were left to cure at standard temperature and 50% relative humidity for 24 hours. When the epoxy set, each specimen is weighed and then submerged in a saturated calcium hydroxide water bath. After 24 hours, the surface is lightly dried and mass weighed. The specimen is then submerged again and reweighed at 24 hours intervals until the mass does not change by more than 0.1% over this time period.

After the mass remains stable, they are rinsed with water and submerged in in an exposure liquid, "[a]n aqueous NaCl solution prepared with a concentration of 165 ± 1 g NaCl per L of solution" (ASTM C 1556, 2011a) for 35 days. After 35 days, the specimens are frozen until profile grinding may begin.

Profile grinding is performed at depths of 1 or 2 mm at a time. These depths, from the finished face, are listed as follows: 1 mm, 2 mm, 3 mm, 4 mm, 6 mm, 8 mm, 10 mm, and 12 mm. Each sample was ground at these depths despite differing water-to-cement ratios and pozzolan and slag contents. It was more relevant to the project that each material be compared in the same manner than follow the specification in this instance.

To perform profile grinding, each test specimen was clamped to a table and slowly and carefully grinded using a profile grinder commonly used for this test. The concrete powder from each layer was carefully gathered in a plastic bag, labeled, and stored for later use. After each layer was collected, the C_i Specimen was ground to develop a baseline sample to be tested.

Finally, the collected concrete powder can be tested for chloride content. Each layer is analyzed using James Instruments, Inc. CL-2020 chlorimeter according to modified SHRP Product 2030: Standard Test Method for Chloride Content in Concrete (2004). The following solutions were mixed according to this document to aid in the measurement of chloride ions in the powdered concrete:

- A digestion solution used for extracting chloride ions. It is made up of a ratio of 60 grams glacial acetic acid, 50 g isopropyl alcohol, and distilled water up to 1 liter.
- Calibration solutions purchased from James Instruments, Inc. of with a wide range of chloride concentrations.
- Stabilizing solution made up of "a dilute NaCl solution containing 3.75 ppm chloride" which "helps in controlling the temperature of the extraction solution" (Islam, 2004).

After calibration using the solutions and onscreen prompts, the chloride content was measured. 3 grams of powder was mixed with the 20 mL digestion solution, the lid to the container was closed, and the container was shaken by hand for 30 seconds. After shaking, the solution is left to stand for 2.5 minutes and then 80 mL of stabilizing solution is added. Finally, the chloride content is measured with the CL-

2020 as shown in Figure 49. The chloride content for each depth is recorded. This procedure is then repeated for every sample.

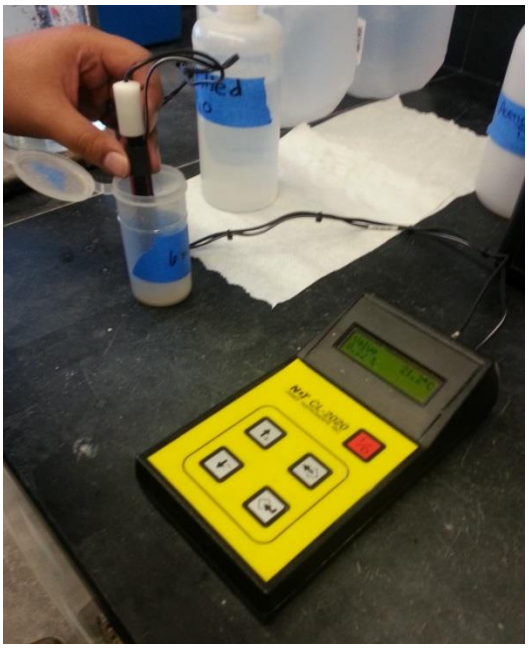

Figure 49. Measuring chloride content using James Instruments, Inc. CL-2020 chlorimeter.

5.5.2 Results and Discussion

Diffusion of chloride ions may cause corrosion of the reinforcing steel, so it is important to know both the innate chloride content of a particular concrete and the ability for ponded chlorides to penetrate. During the conducting of ASTM C 1556, the initial chloride content of each of the Phase III materials was calculated. These values are shown in Table 10.

Table 10. Initial chloride content of each Phase III materials.

Material	Initial Chloride Content
PC Type III	0.01150%
CAC-2	0.00605%
CAC-3	0.02800%
P-2	0.03735%
CSA-1	0.00810%
P-AAFA	0.00565%

As shown, PC Type III has an initial chloride content of 0.115%, more than 3 times that of the next highest, P-2. Also, as expected, this material allowed the penetration of a relatively large amount of chloride ions, at least within the first few millimeters. The PC Type III binder is made up of Type III portland cement and lacks alternative binders such as silica fume that could make a less permeable pore structure.

Generally speaking, CSA-1 allowed the most penetration of chloride solution during the ASTM C 1556 testing. In contrast, P-2, one of the premanufactured concrete all-in-one products, allowed the least penetration by chloride solution. This product likely performed well because of an optimized blend of cements, allowing for a more torturous pore structure both due to the development of cementitious products and physical packing of the cement particles (Mindess, Young, & Darwin, 2003).

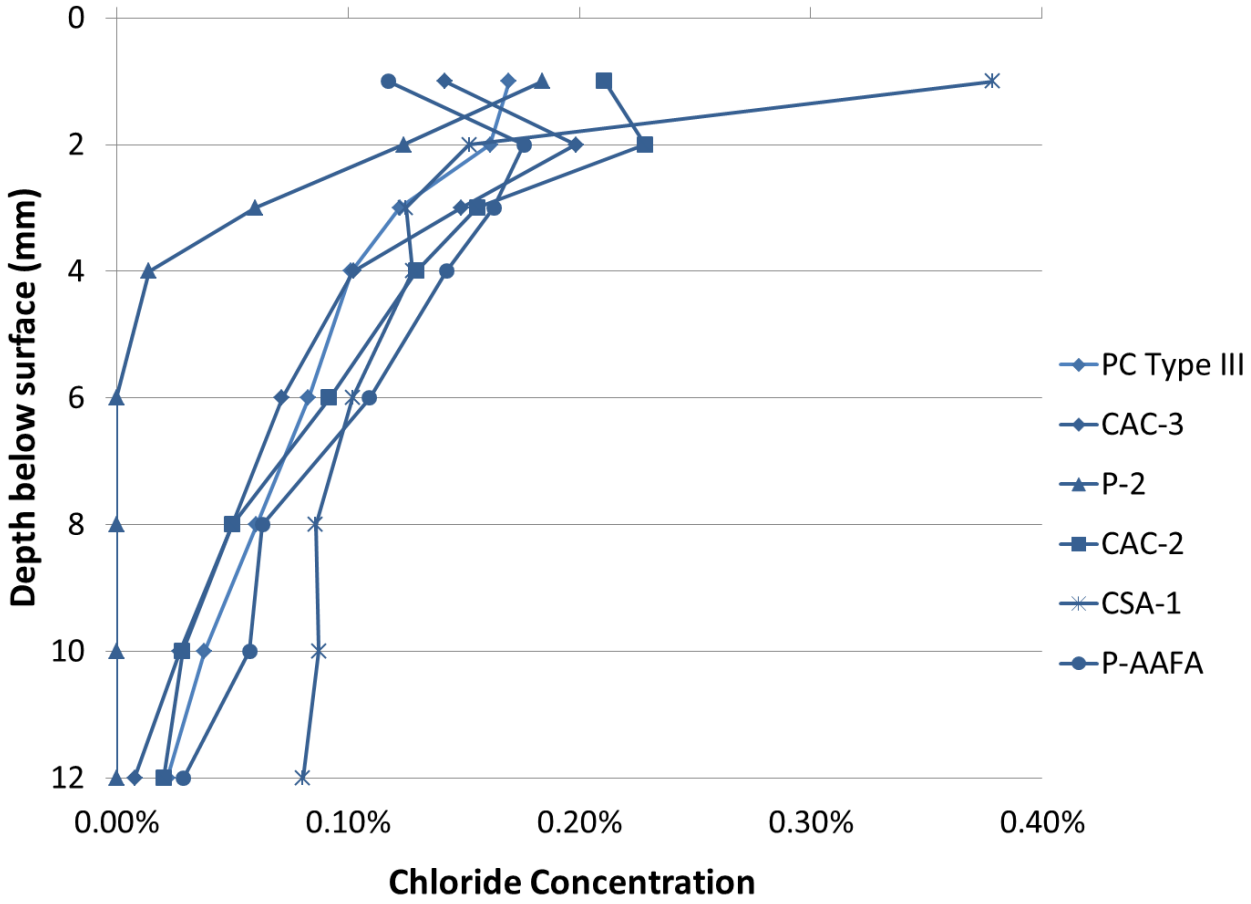

Figure 50. Diffusion of chloride ions into Phase III materials.

5.6 Combined Fatigue and Corrosion Testing

Pavements and transportation structures are subject to repetitive axel loading as vehicles pass. These loads only stress the structures to a fraction of their theoretical strength, and, because repetitive, may be considered fatigue loads.

When a damaged section is repaired and the aforementioned loads are repetitively applied, debonding of the repair is a concern. Bond strength in a more general sense is given in (Dornak, 2014). As requested by the Texas Department of Transportation, this project intended to develop a correlation between the fracturing of repair bonds under

fatigue loading and the potential ingress of chlorides through this "gap" reaching the reinforcing steel and causing corrosion.

5.6.1 Experimental Procedures

At the request of TxDOT, a more thorough approach representative of an actual in-place bridge deck pavement was requested. With assistance from Dr. Harovel Wheat of the Department of Mechanical Engineering at the University of Texas at Austin and Dr. Michael D. A. Thomas, P.Eng. of the University of New Brunswick, a highly modified version of ASTM G 109 was developed.

First, small "beams" with 6 x 6 x 21 inches (152 x 152 x 533 mm) dimensions and a nominal portion of 3-inches by 6-inches by 6-inches (76 x 76 x 262 mm) "removed" from the center. In these prisms, four no. 3 bars were cast with a cover of 0.75 inches (19 mm) at the top and bottom and 0.5 inches (13 mm) on each side. Typical dimensions of these beams are shown in Figure 51 with molds and reinforcing steel shown in Figure 52 as follows:

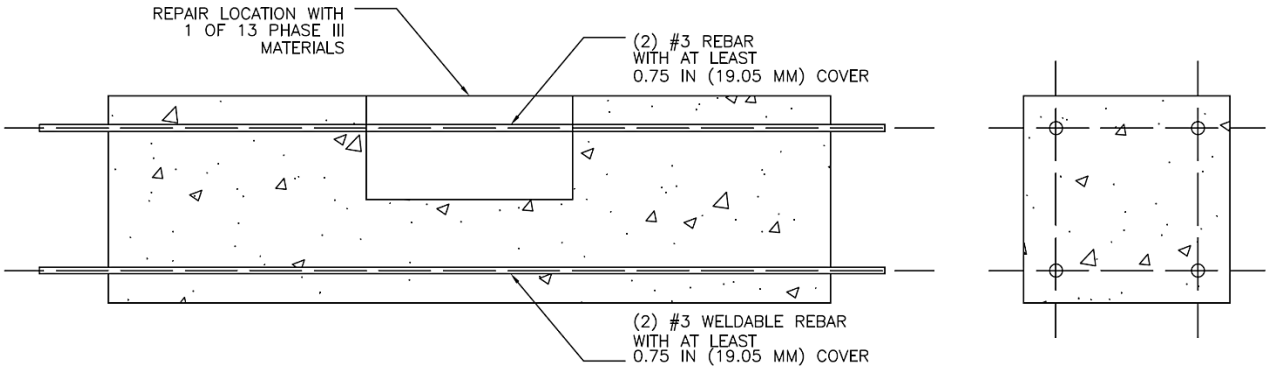

Figure 51. Design drawings of fatigue-corrosion beams.

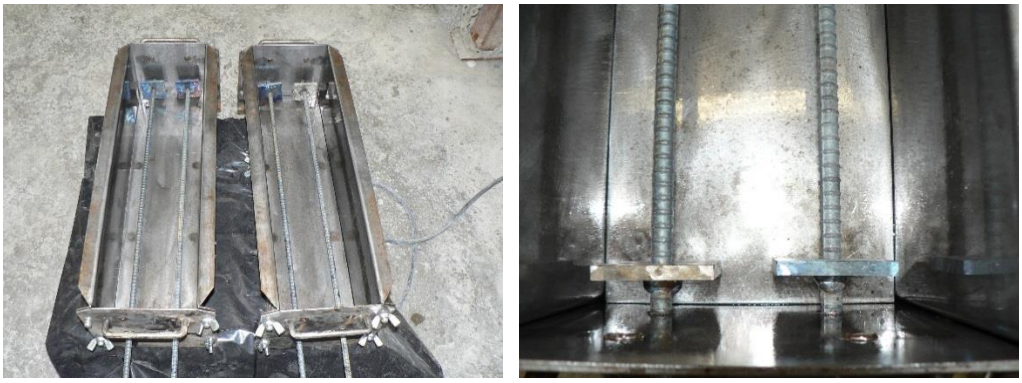

Figure 52. Molds for fatigue corrosion specimens displaying reinforcing steel and welded plates for development.

It is important to note that each of two 7.5 x 6 x 3 inch (190 x 152 x 152 mm) portion of the top layer also contained 3% calcium chloride to help induce corrosion. The bottom layer was cast according to the mix procedure outlined by Zuniga (2013) and shown in Figure 53.

Figure 53. Casting the bottom layer of fatigue-corrosion beams.

Then a foam insert was used as the second layer containing calcium chloride was cast. Both layers were consolidated with a vibrating table to prevent honeycombing

around the reinforcing steel. The top layer casting, reinforcing steel, and foam inserts are shown in Figure 54.

Figure 54. Casting top layer of fatigue-corrosion beams and displaying foam inserts for eventual repair material casting.

The beams were then placed in a 100-percent humidity moist room to cure for 7 days. On the 7th day, the base was moved to a standard drying shrinkage room for 20 additional days. After 27 days from original casting, a repair of one of the final subset of six materials was cast in “removed” center portion. Once again, this portion was consolidating with a vibrating table to prevent honeycombing despite the rapid time of set. This repair was cured with wet burlap for a single day. An example of the final specimen is shown in Figure 55.

Figure 55. Example of final fatigue-corrosion beam and inset repair material.

After 24 hours, the half-depth repaired specimens were placed in the MTS fatigue loading machine. This machine allows repetitive application of low loads in a cyclic manner for fatigue testing. The specimens were simply supported as shown in Figure 56 and point-loaded at the center of the repair. Loads cycled between 2300 and 8000 force-pounds (10.2 to 35.6 kN) for 1 million cycles.

Figure 56. Loading fatigue-corrosion beams under repetitive loads using MTS loading machine.

At the conclusion of the cyclical fatigue loading, sample beams were removed from the loading apparatus and a rectangular plastic dam with base dimensions 6 inches (152 mm) by 12 inches (305 mm) was attached around the repair and surrounding concrete with Liquid Nails construction adhesive. Next, the specimen coated with Sikadur Injection Gel structural epoxy excluding the dammed portion and bottom. The reinforcing steel penetrating from the ends of the specimen were also carefully avoided when applying the structural epoxy. The coat was allowed to cure for one week in standard temperatures.

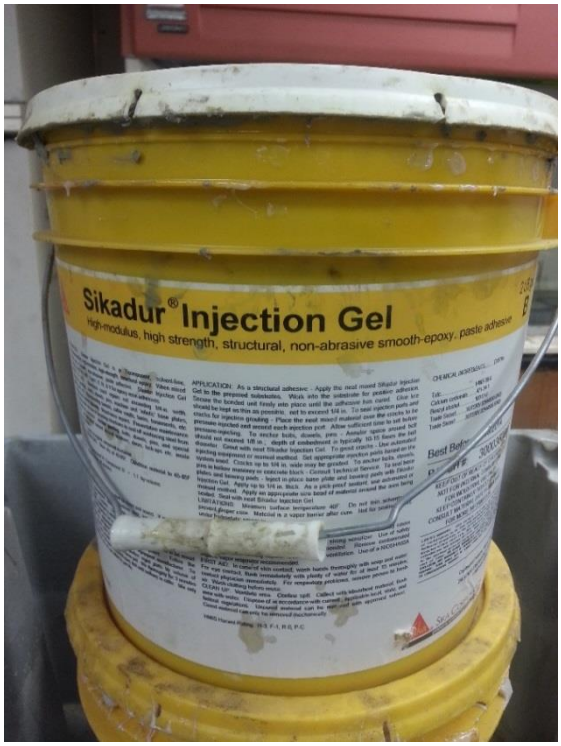

Figure 57. Sikadur Injection Gel used for sealing fatigue-corrosion beams.

After one week of curing, provisions for measuring both half-cell potential and macrocell corrosion were applied to the reinforcing steel at one end. Brass grounding

claps with attached copper wire were mounted to each bar. In addition, a 100 ohm resistor was attached between the two lower bars and a single upper bar.

After one week I this configuration, 3% calcium chloride solution was ponded in the dam 1.5 inches (40 mm) above the concrete's surface. At this point, macrocell corrosion was measured in a manner similar to Maruya et al. The voltmeter was attached to a reference electrode with the ground and a single reinforcing bar with the other connection. Voltage readings were recorded for each bar by placing the reference electrode in the salt solution as shown in Figure 58. One week later, the calcium chloride solution was removed from the damn, and the cycle repeated.

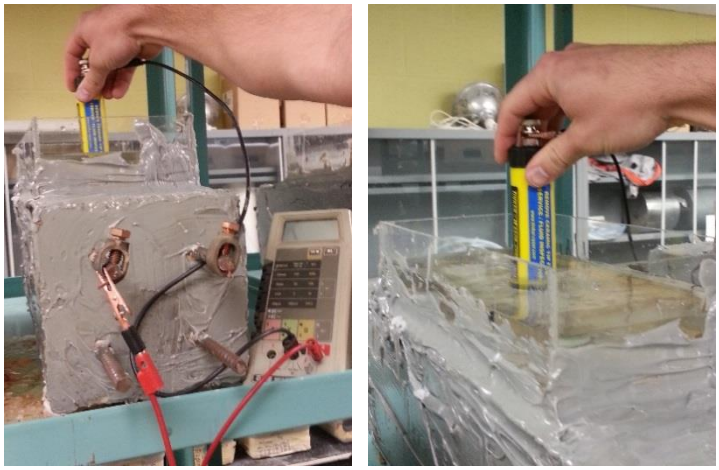

Figure 58. Measuring macrocell voltage of reinforcing steel using voltmeter and reference electrode .

5.6.2 Results and Discussion

To show corrosion has initiated, a "remarkable decrease" (Maruya, Takeda, Horiguchi, Koyama, & Hsu, 2007) must be shown in the voltage measurements using the reference electrode and performing half cell potential. At approximately 14 weeks (98 days) from the initial ponding, this remarkable decrease in potential has not occurred in

any of the 6 Phase III materials as shown in Figure 59 through Figure 65. In each chart, solid lines represent the measurements for the top reinforicng bars and dashed lines represent bottom reinforcing bars. Circular markers are the fatigue-loaded specimens and triangular markers are unloaded.

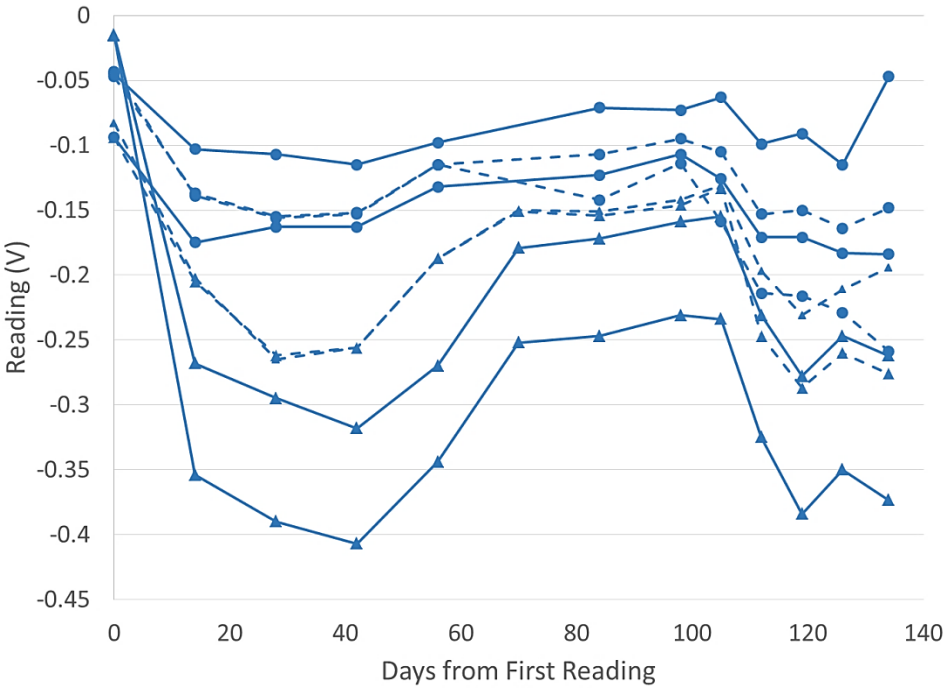

Figure 59. Macrocell potential measurement for PC Type III.

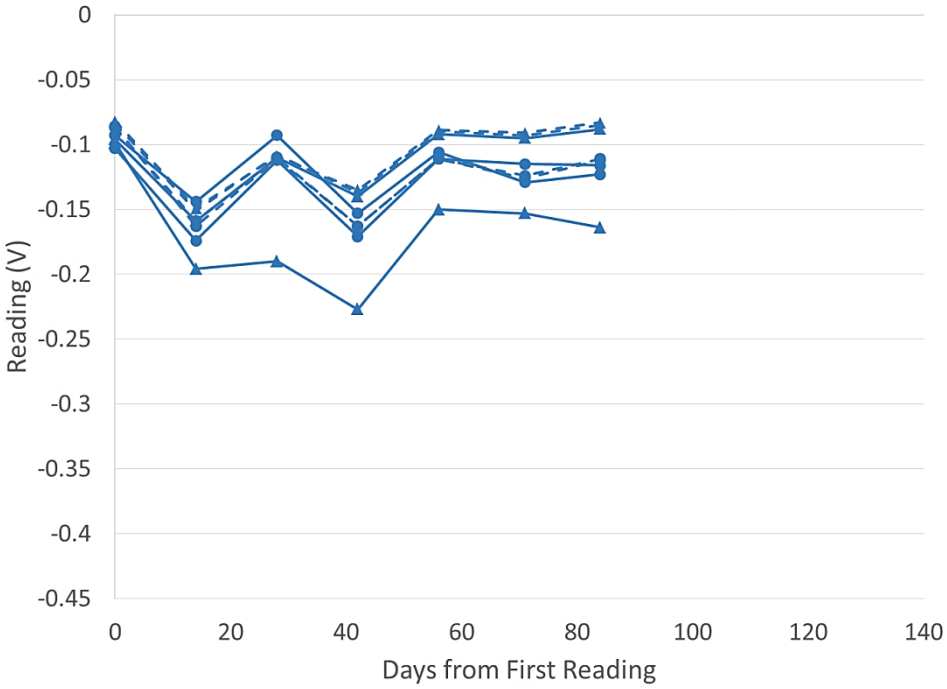

Figure 60. Macrocell potential measurement for CSA-1.

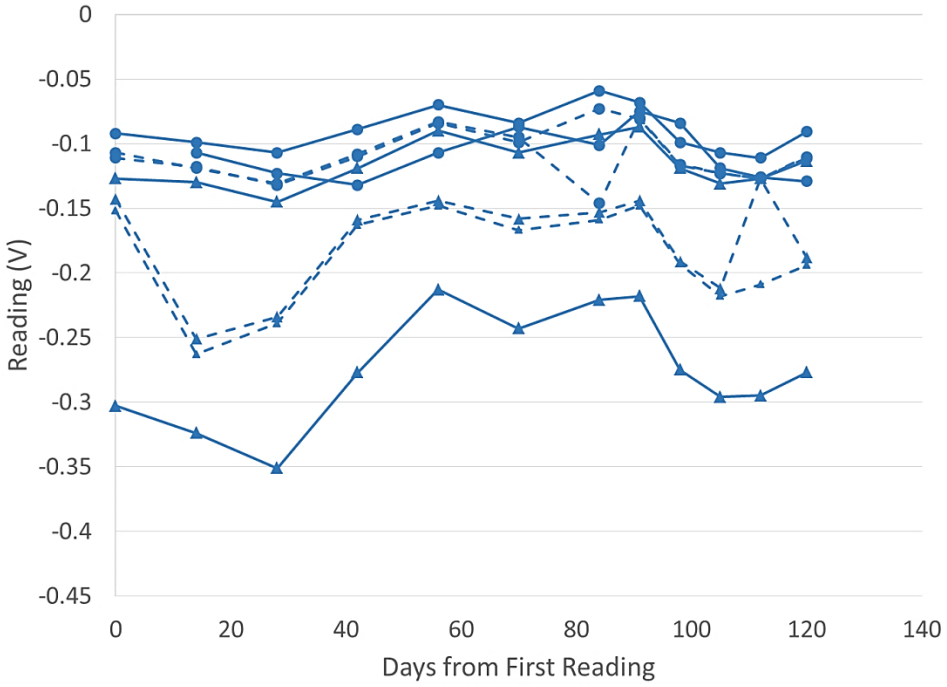

Figure 61. Macrocell potential measurement for CAC-2.

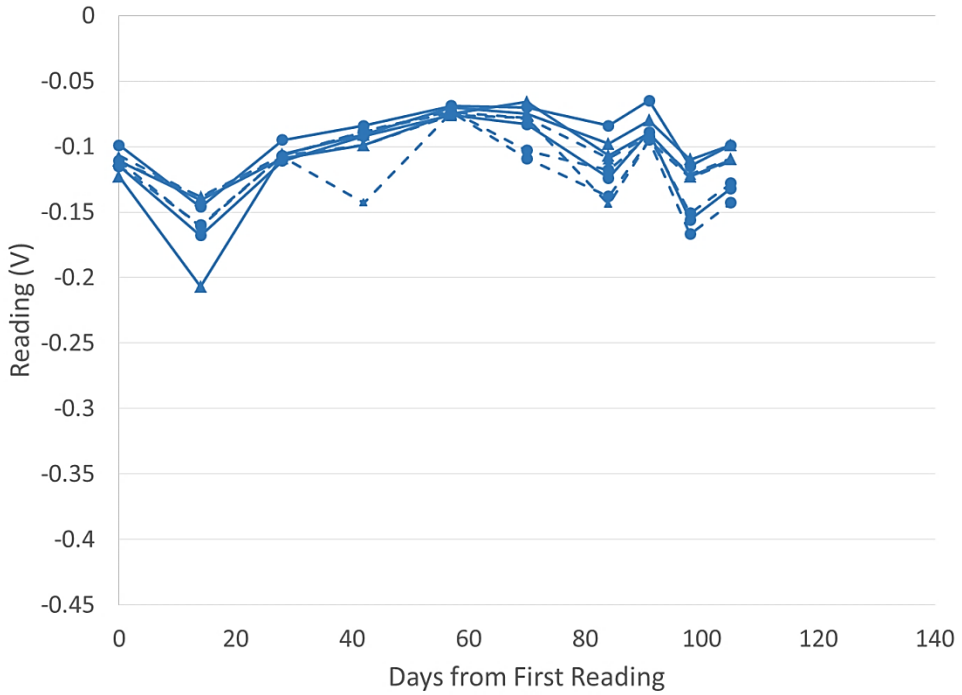

Figure 62. Macrocell potential measurement for CAC-3.

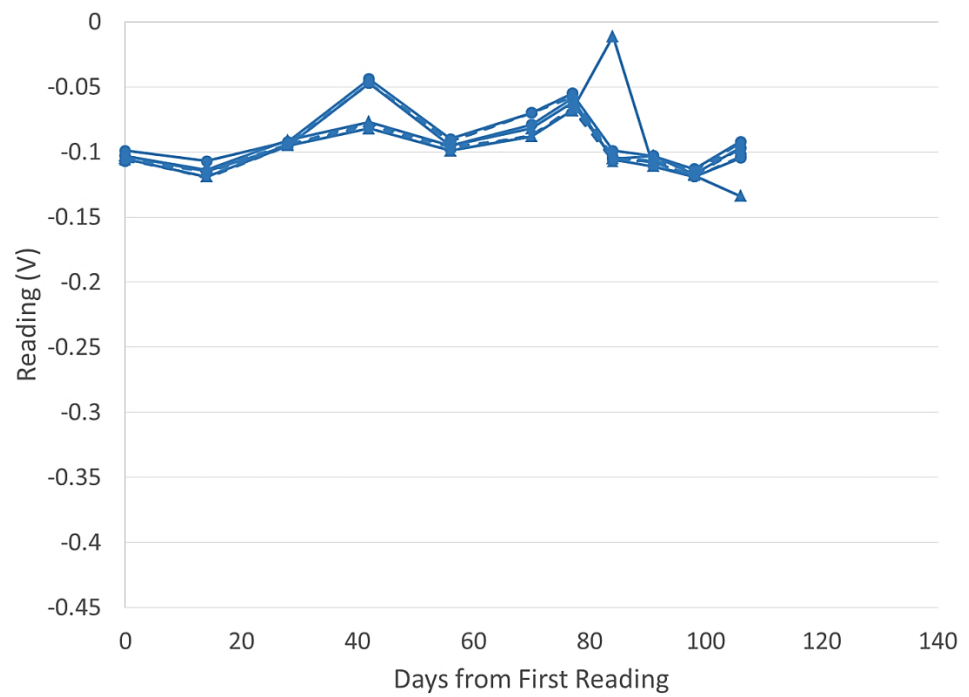

Figure 63. Macrocell potential measurement for P-2.

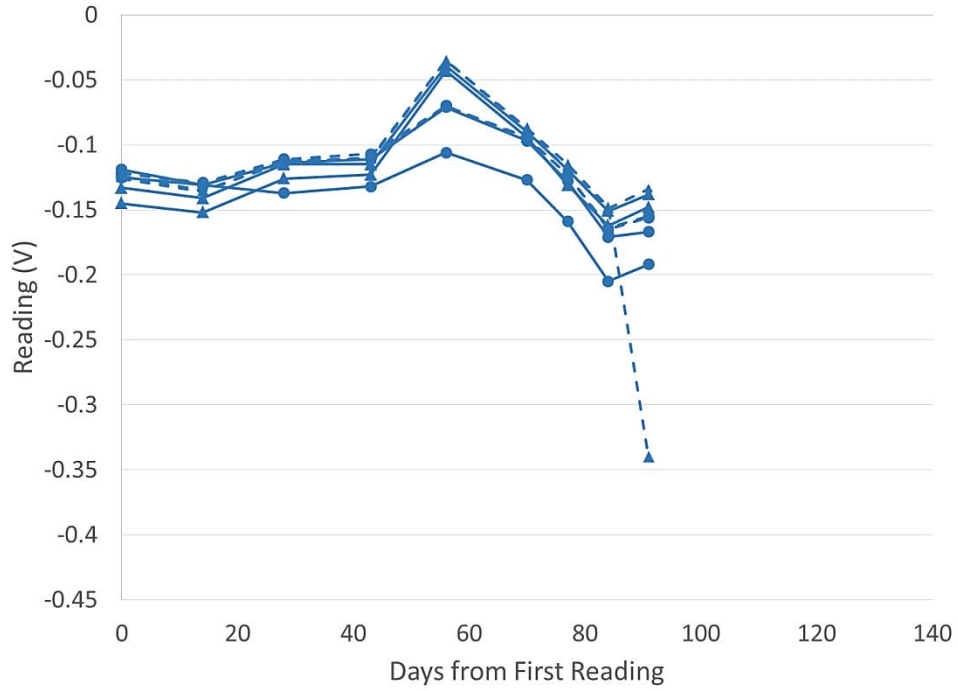

Figure 64. Macrocell potential measurement for P-AAFA.

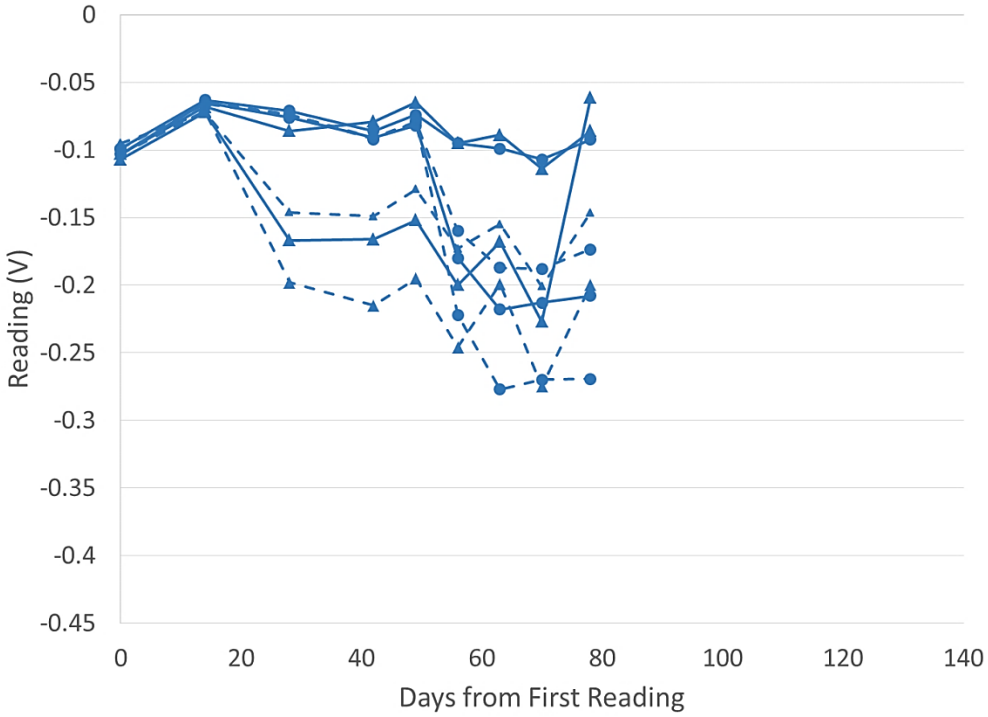

Figure 65. Macrocell potential measurement for control mix.

For most materials, each of the reinforcing bars have performed similarly. It is to be expected that at corrosion initiation, likely occurring in the top bars, the voltage for those bars will drop significantly from those shown in the aforementioned figured. With the chlorides mixed into the top layer of concrete and the frequent wetting-and-drying cycles (weekly), corrosion is expected to initiate sooner than similar studies. Despite this, there is little way to predict the onset of this corrosion, and it could still take significant time until it begins. These specimens will remain under testing well beyond the completion of this project.

5.7 SUMMARY AND CONCLUSIONS

The summary and conclusions of the permeability and corrosion performance of the materials are as follows:

- All materials performed well according to the simplified Rapid Chloride Permeability Test when cured for 28 days. P-1 and CAC-3 displayed moderate permeability, with every other materials displaying low permeability or better.
- The materials generally performed well according to the simplified Rapid Chloride Permeability Test when cured only for 1 day. Only P-1 displayed high permeability, with every other material displaying moderate or better permeability.
- In all instances, additional curing improved permeability according to the simplified Rapid Chloride Permeability Test.
- For all mixtures, carbonation depths increased between 6 and 11 months, with the exception of P-2. Although a slight reduction in carbonation was measured in this material, it can be assumed that discrepancies along the prism's length caused this difference. Carbonation cannot actually be reduced.

- In all instances, prisms within the Stevenson screen displayed increased carbonation depths when compared to those outside. Concrete not exposed to weather is expected to display increase carbonation depth.
- Carbonation at 11 months reaches depth that may cause concern if reinforcement cover in structural concrete is low.
- Simplified Rapid Chloride Permeability Test and chloride permeability due to the modified ASTM C 1556 generally correspond. The least permeable material according to the ponding test was P-2, which displayed very low permeability for both 1 day and 28 day curing conditions according to RCPT. CSA-1, the worst performing material according to the ponding test, was 1 of 2 materials displaying moderate permeability with a 1 day curing period.
- Although the time each fatigue and corrosion beam was tested varies, no material displayed corrosion during the test period. The test will be continued into the indefinite future.

Chapter 6: Conclusions

The durability of rapid repair materials is often overlooked when compared to their strength development. Despite this, a durable repair material will allow the repair to be replaced less often in transportation structures.

After extensive testing of the Phase II and III materials, their durability properties are tabulated in Table 11. This table should allow a general comparison of the materials and their overall resistance to freezing-and-thawing damage, alkali-silica reaction, sulfate attack, and corrosion.

Table 11. Durability comparison table.

Mix ID	Compliance or Relevant Value										
	>5% Fresh Air	Spacing Factor	ASTM C 672 Rating	ASTM C 666 Compliance	ASTM C 1012 Compliance		ASTM C 1293, <0.04% Exp.	RCPT Concrete Permeability		11 Month Carbonation Depth	Chloride Penetration (rank)
					1 Day	28 Day		1 Day	28 Day		
P-1		✓	5		✓	✓		High	Mod.	--	--
P-2*		✓	0	✓			✓	V. Low	V. Low	0.030 in (0.077 cm)	1
P-3			3	✓	✓	✓		V. Low	V. Low	--	--
P-AAFA*			2	✓				Low	V. Low	0.110 in (0.280 cm)	5
CSA-1*		✓	5		✓	✓	✓	Mod.	Low	1.370 in (3.475 cm)	6
CSA-Latex		✓	5		✓	✓	✓	Low	V. Low	--	--
CSA-2	✓	✓	1	✓	✓	✓	✓	Mod.	V. Low	--	--
CSA-3		✓	0	✓	✓	✓	✓	Low	V. Low	--	--
CAC-1	✓	✓	1	✓			✓	V. Low	V. Low	--	--
CAC-Latex	✓		2	✓				V. Low	V. Low	--	--
CAC-2*	✓	✓	0	✓		✓	✓	Low	V. Low	1.230 in (3.125 cm)	3
CAC-3*			2	✓		--		Mod.	Mod.	1.300 in (3.300 cm)	4
PC Type III*	✓		3		✓	✓	✓	Mod.	Low	0.050 in (0.125 cm)	2

Note: Phase III materials denoted with asterisk (*). Properties denoted with "--" not tested for that specific material.

The summary and conclusions of the durability test program and the material's performance are listed as follows:

- Although not all materials met the required air content and spacing factors, the materials generally performed well according to ASTM C 672 and C 666. There is not always a correlation between a material's freeze-thaw performance and air content or makeup of that air.
- Several mixtures were not resistant to alkali-silica reaction or sulfate attack. It is important to note that CAC-1 and CSA-1 both exhibited some distress under each of these durability testing regimes.
- In general, styrene-butadiene latex creates a less permeable concrete matrix. Despite this, modified calcium aluminate cement and calcium sulfoaluminate cement worsen the effects of both alkali-silica reaction and sulfate attack.
- The materials are generally low in permeability according to ASTM C 12943.
- No conclusions could be made at the susceptibility of the materials to corrosion when placed as a repair and cyclically loaded. Corrosion was not initiated in any of the specimens.
- Carbonation depths are of a concern and are likely to cause corrosion if low reinforcement cover is specified.

Appendix A: Salt scaling images from ASTM C 672

Figure 66. Salt scaling (ASTM C 672) specimen for material P-1 after 0 cycles.

Figure 67. Salt scaling (ASTM C 672) specimen for material P-3 after 0 cycles.

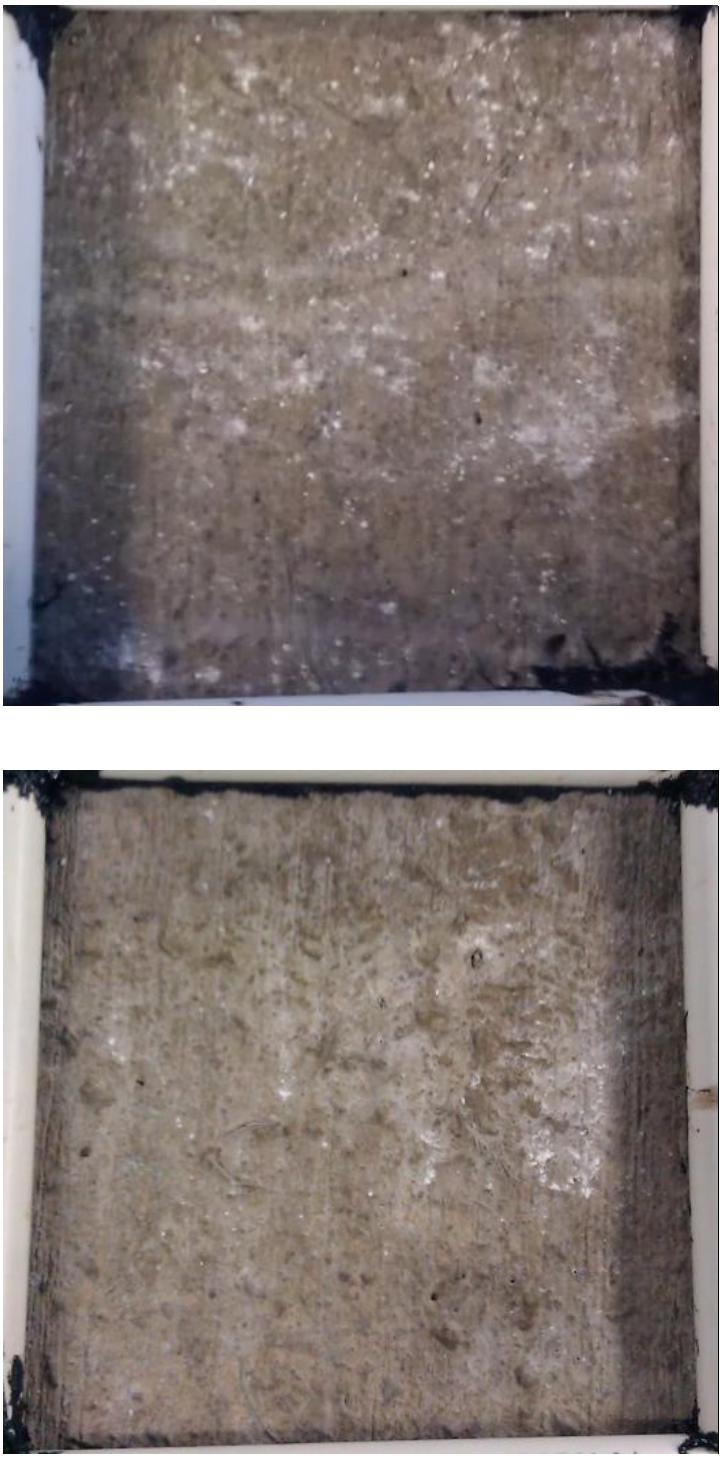

Figure 68. Salt scaling (ASTM C 672) specimen for material P-AAFA after 0 cycles.

Figure 69. Salt scaling (ASTM C 672) specimen for material CSA-1 after 0 cycles.

Figure 70. Salt scaling (ASTM C 672) specimen for material CSA-Latex after 0 cycles.

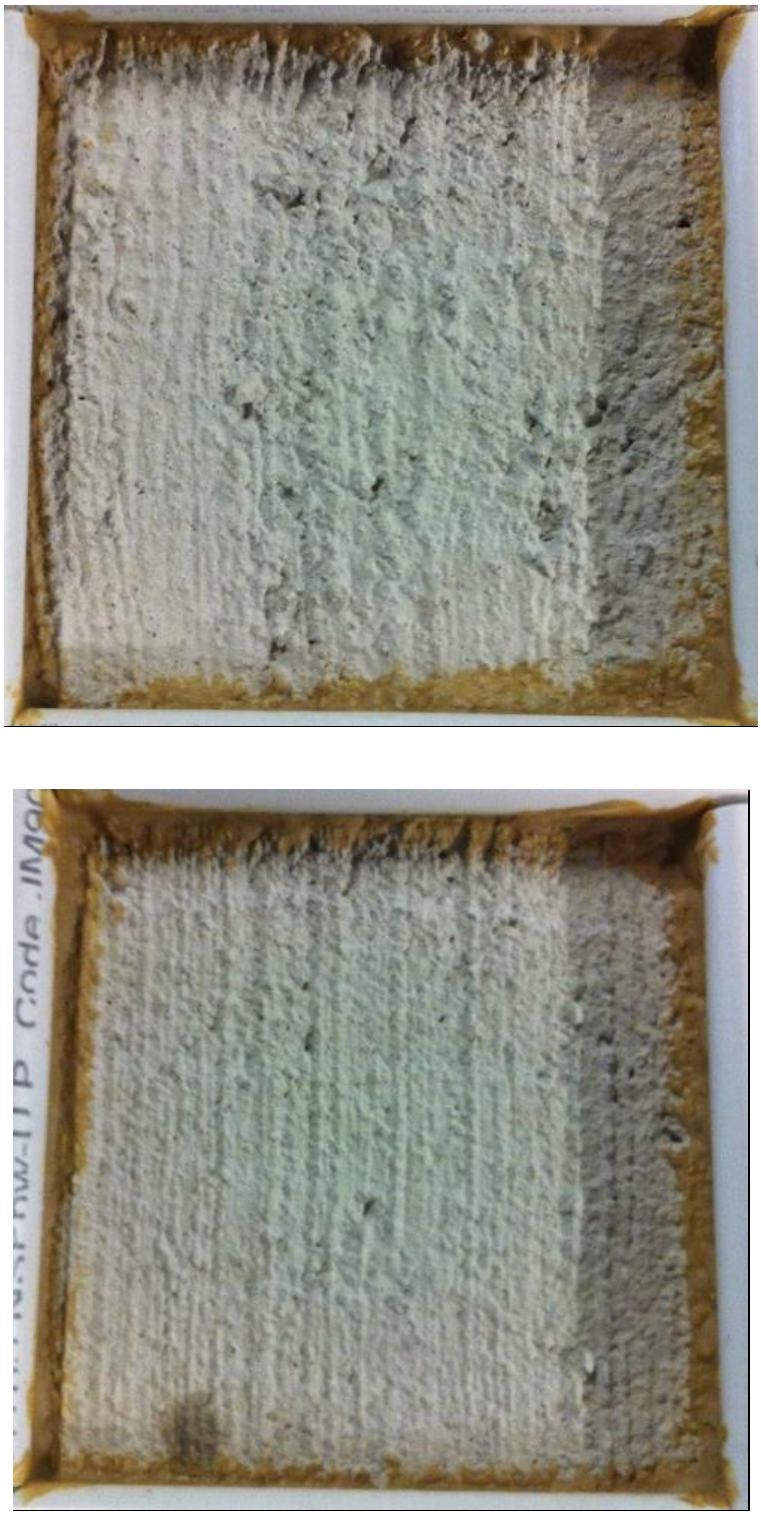

Figure 71. Salt scaling (ASTM C 672) specimen for material CSA-2 after 0 cycles.

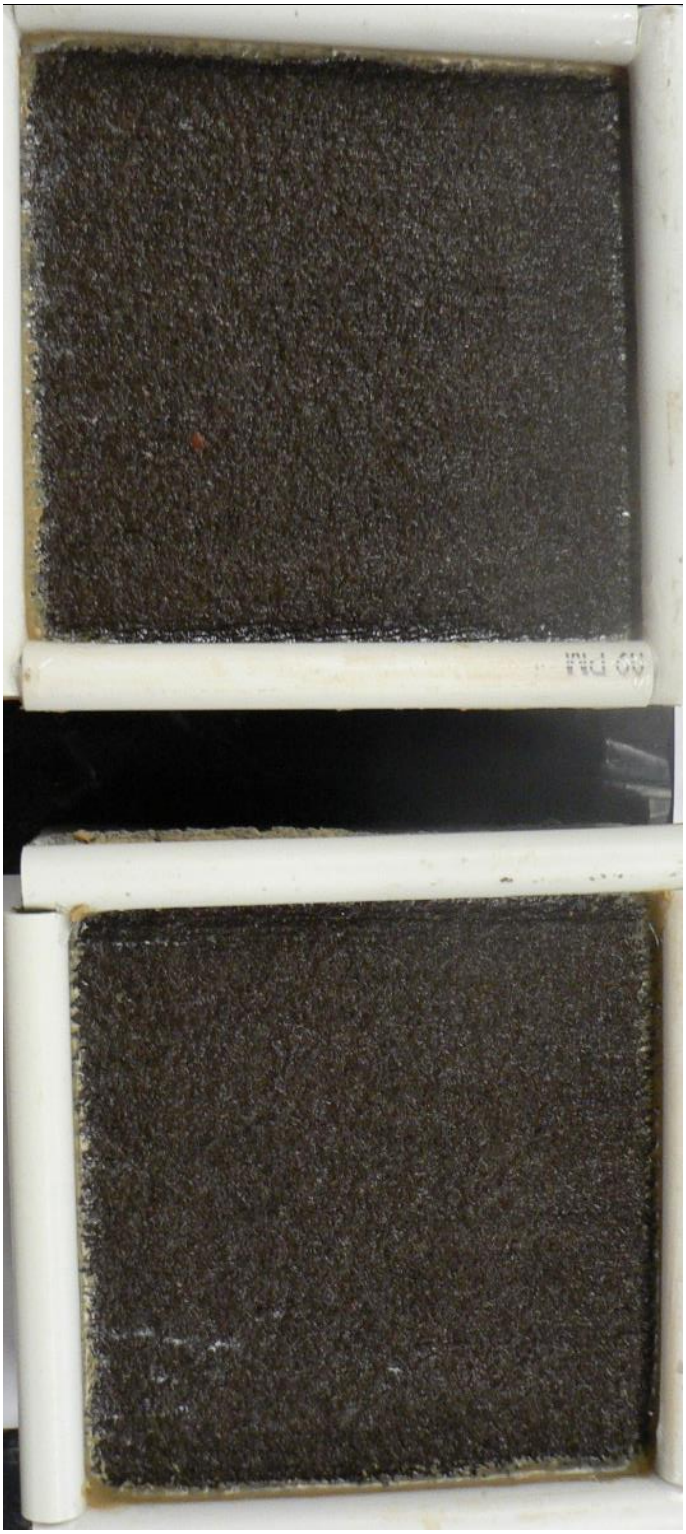

Figure 72. Salt scaling (ASTM C 672) specimen for material CAC-1 after 0 cycles.

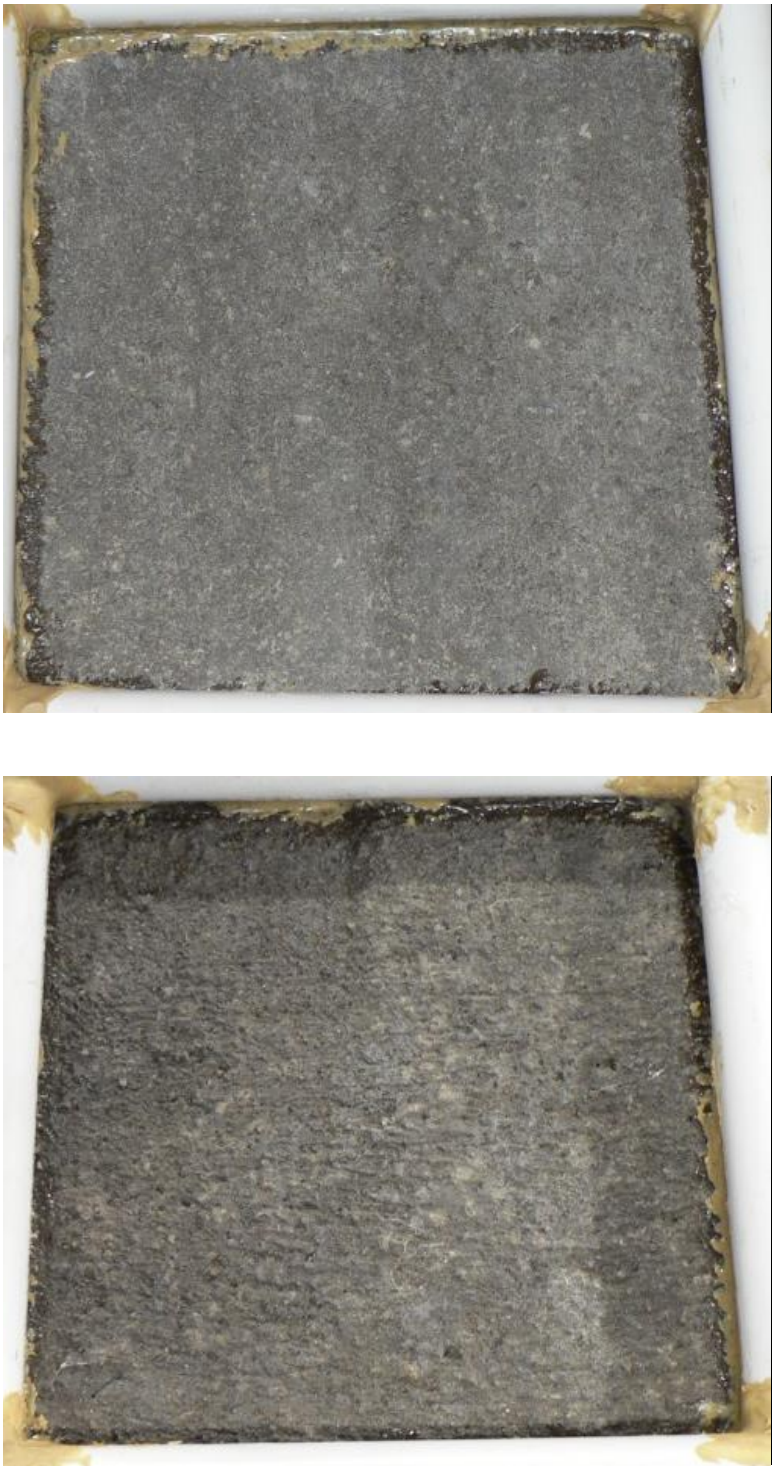

Figure 73. Salt scaling (ASTM C 672) specimen for material CAC-Latex after 0 cycles.

Figure 74. Salt scaling (ASTM C 672) specimen for material CSA-3 after 0 cycles.

Figure 75. Salt scaling (ASTM C 672) specimen for material CAC-3 after 0 cycles.

Figure 76. Salt scaling (ASTM C 672) specimen for material CAC-2 after 0 cycles.

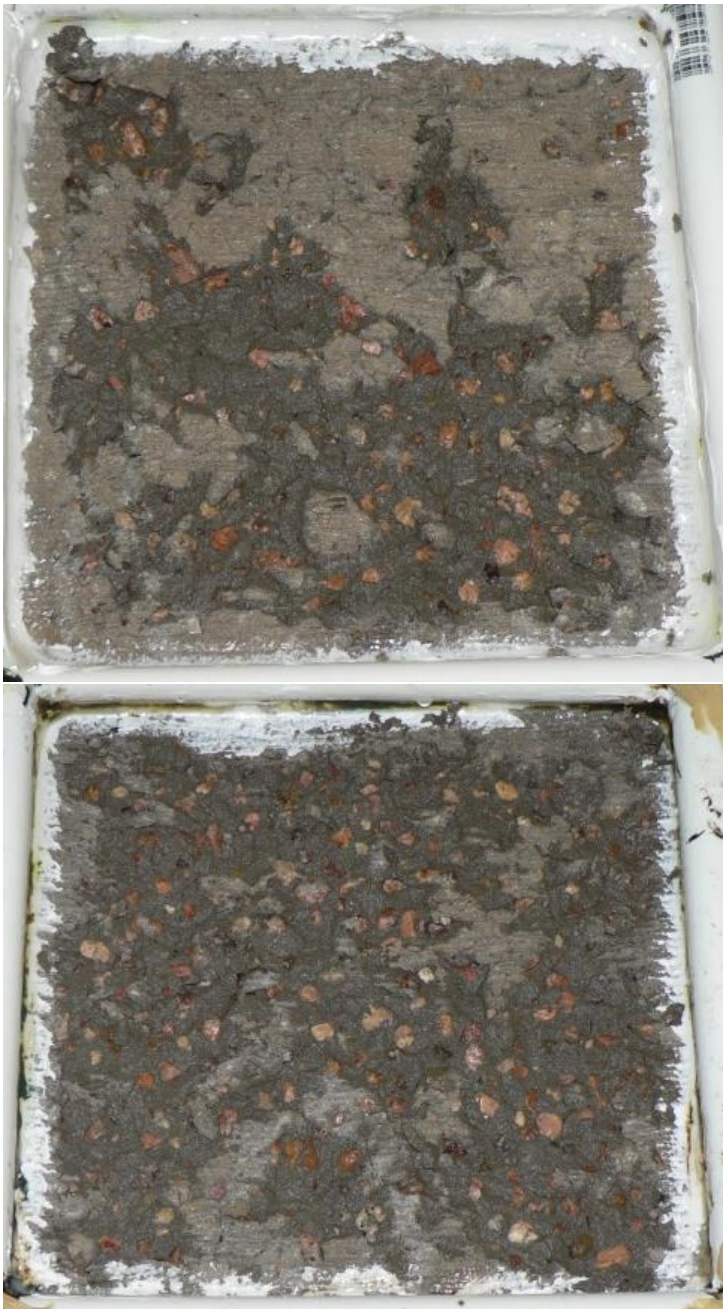

Figure 77. Salt scaling (ASTM C 672) specimen for material P-1 after 5 cycles.

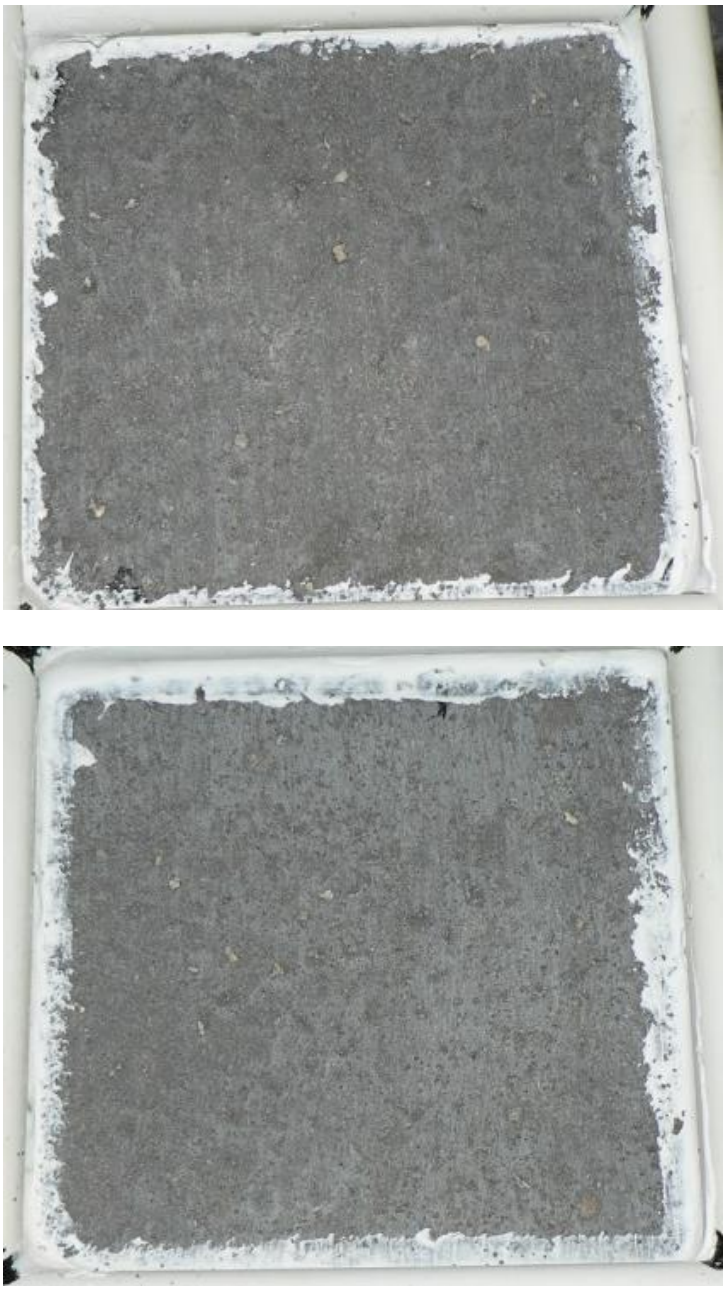

Figure 78. Salt scaling (ASTM C 672) specimen of material P-3 after 5 cycles.

Figure 79. Salt scaling (ASTM C 672) specimen of material CSA-1 after 5 cycles.

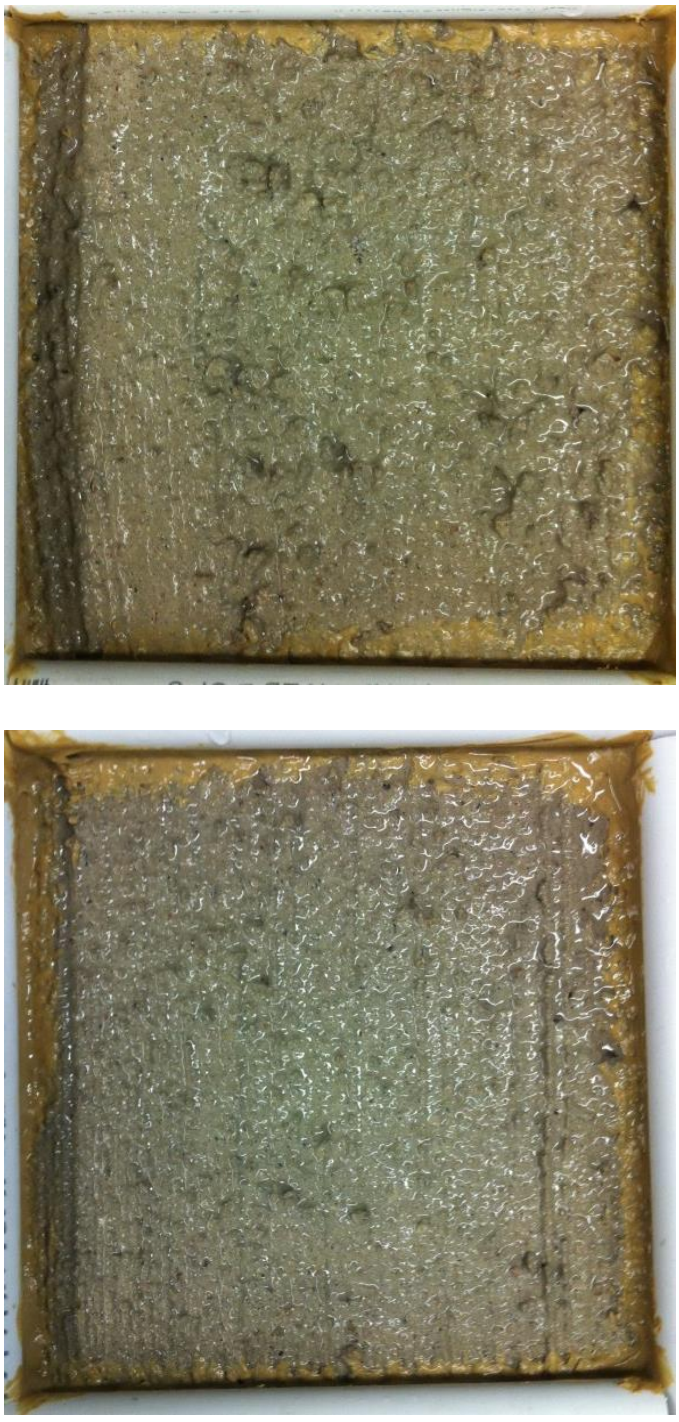

Figure 80. Salt scaling (ASTM C 672) specimen of material CSA-2 after 5 cycles.

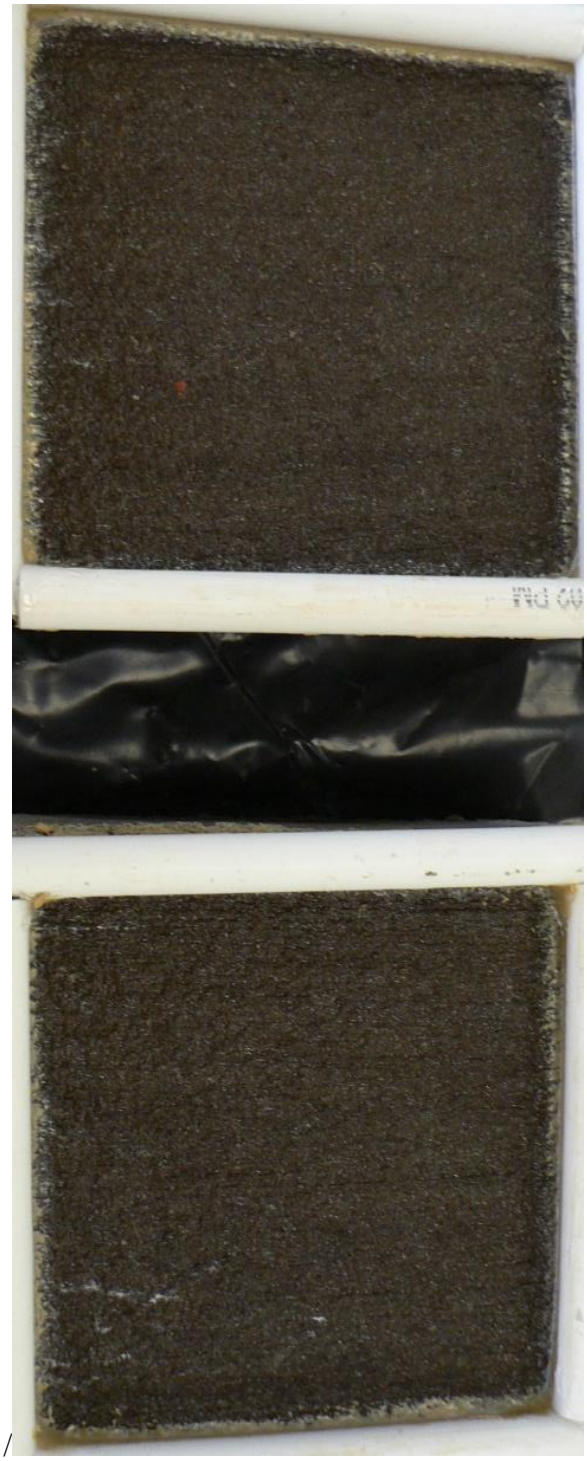

Figure 81. Salt scaling (ASTM C 672) specimen of material CAC-1 after 5 cycles.

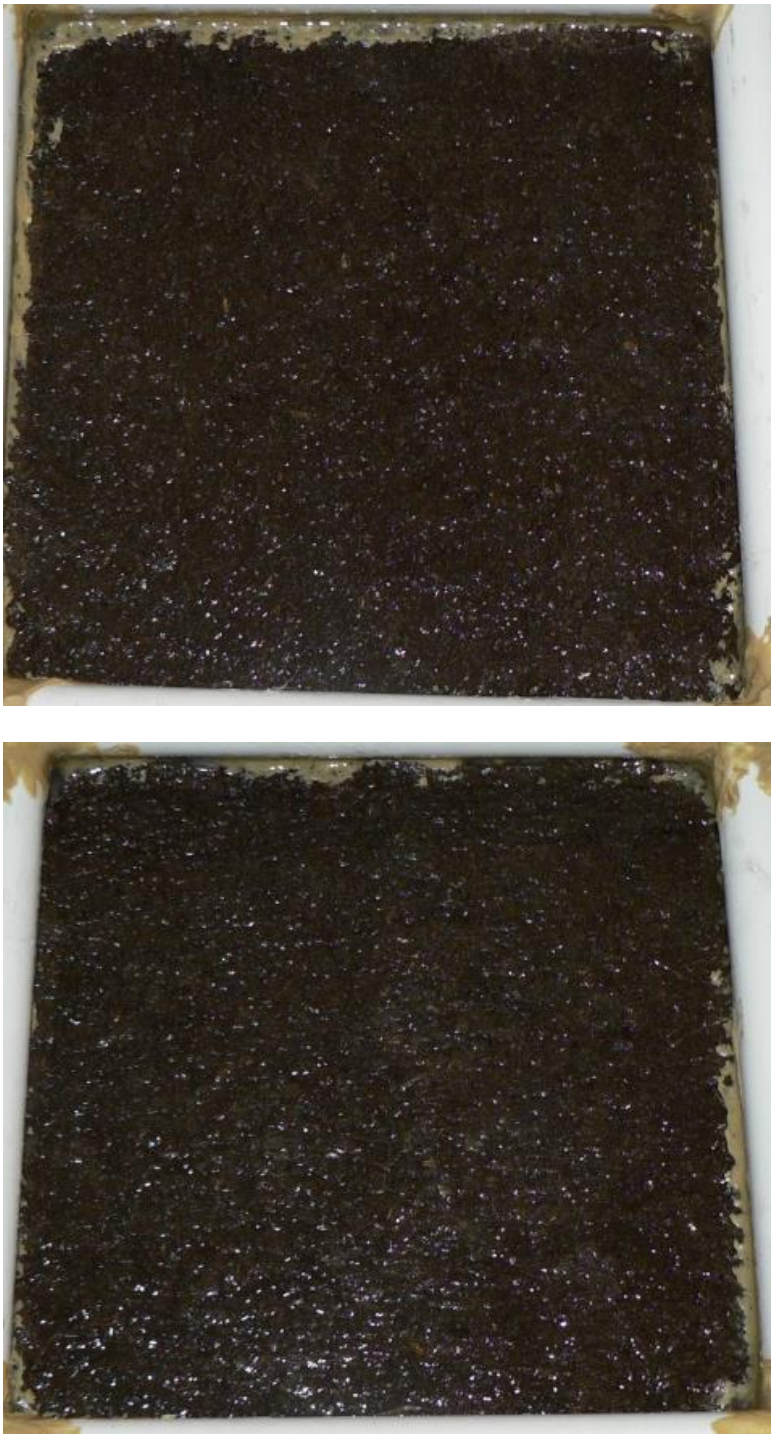

Figure 82. Salt scaling (ASTM C 672) specimen of material CAC-Latex after 5 cycles.

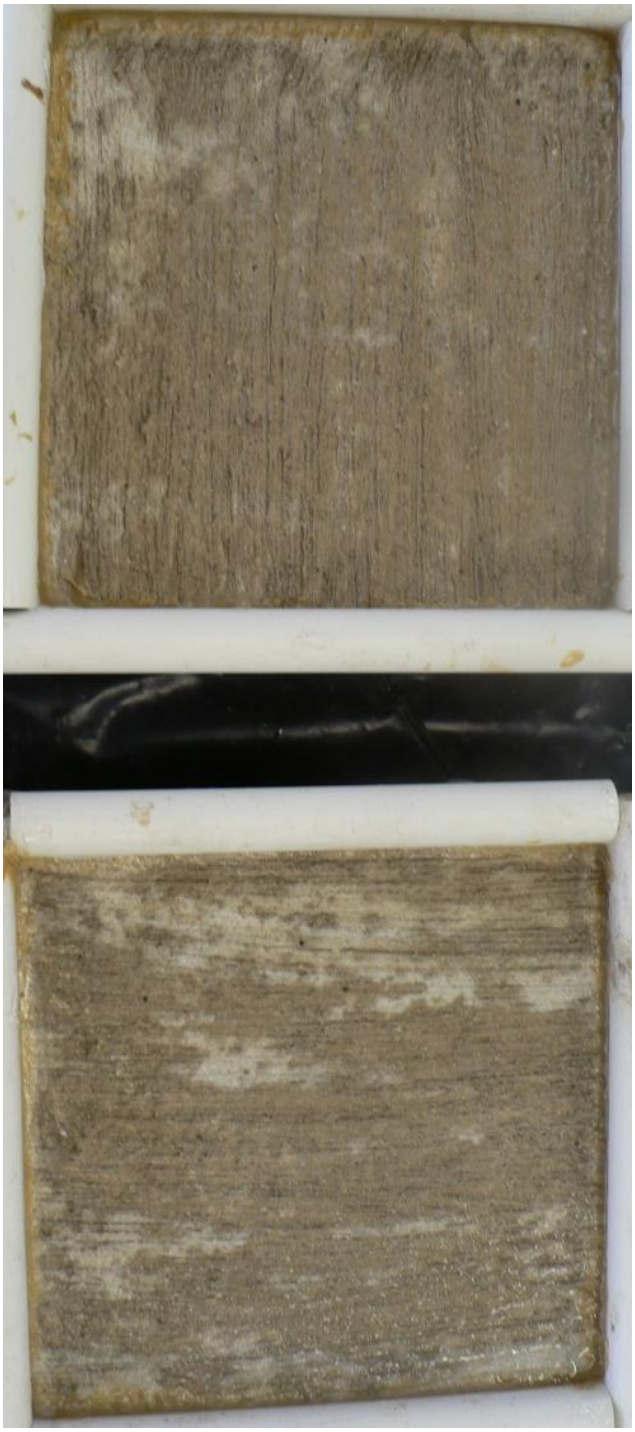

Figure 83. Salt scaling (ASTM C 672) specimen of material CSA-3 after 5 cycles.

Figure 84. Salt scaling (ASTM C 672) specimen of material CAC-3 after 5 cycles.

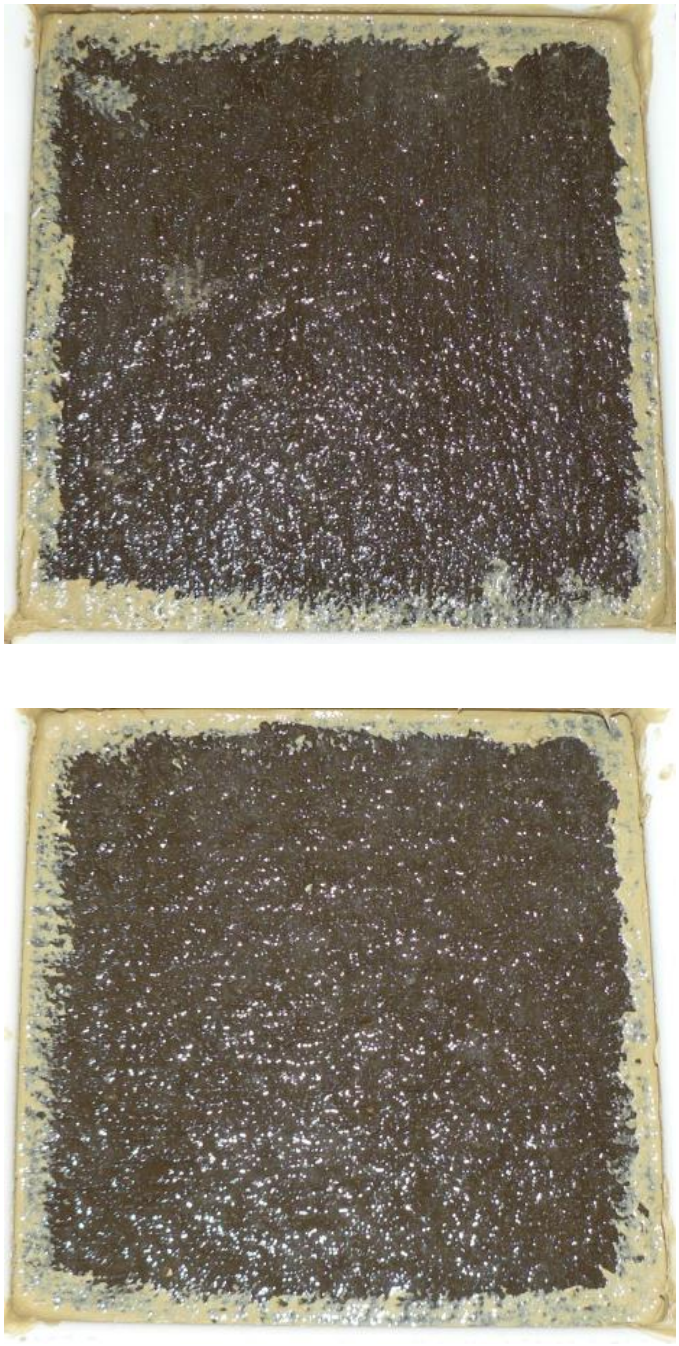

Figure 85. Salt scaling (ASTM C 672) specimen of material CAC-2 after 5 cycles.

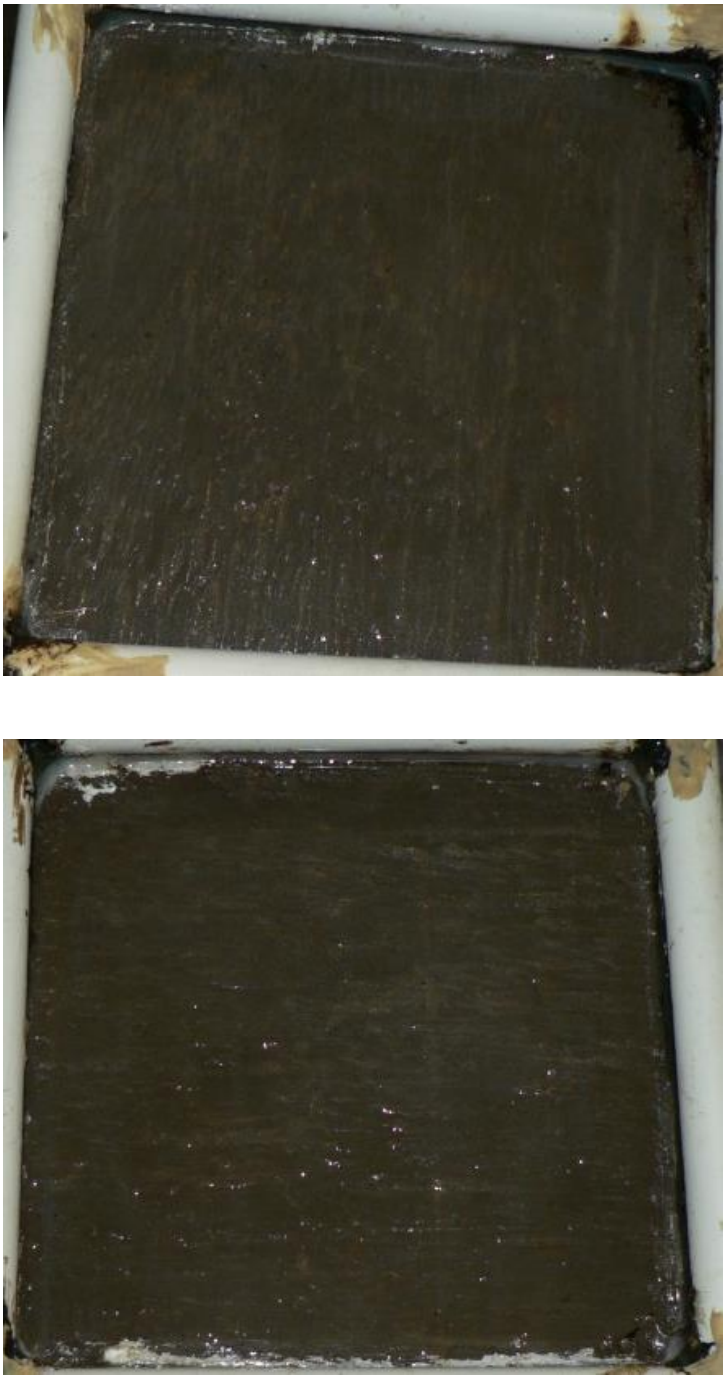

Figure 86. Salt scaling (ASTM C 672) specimen of material P-2 after 10 cycles.

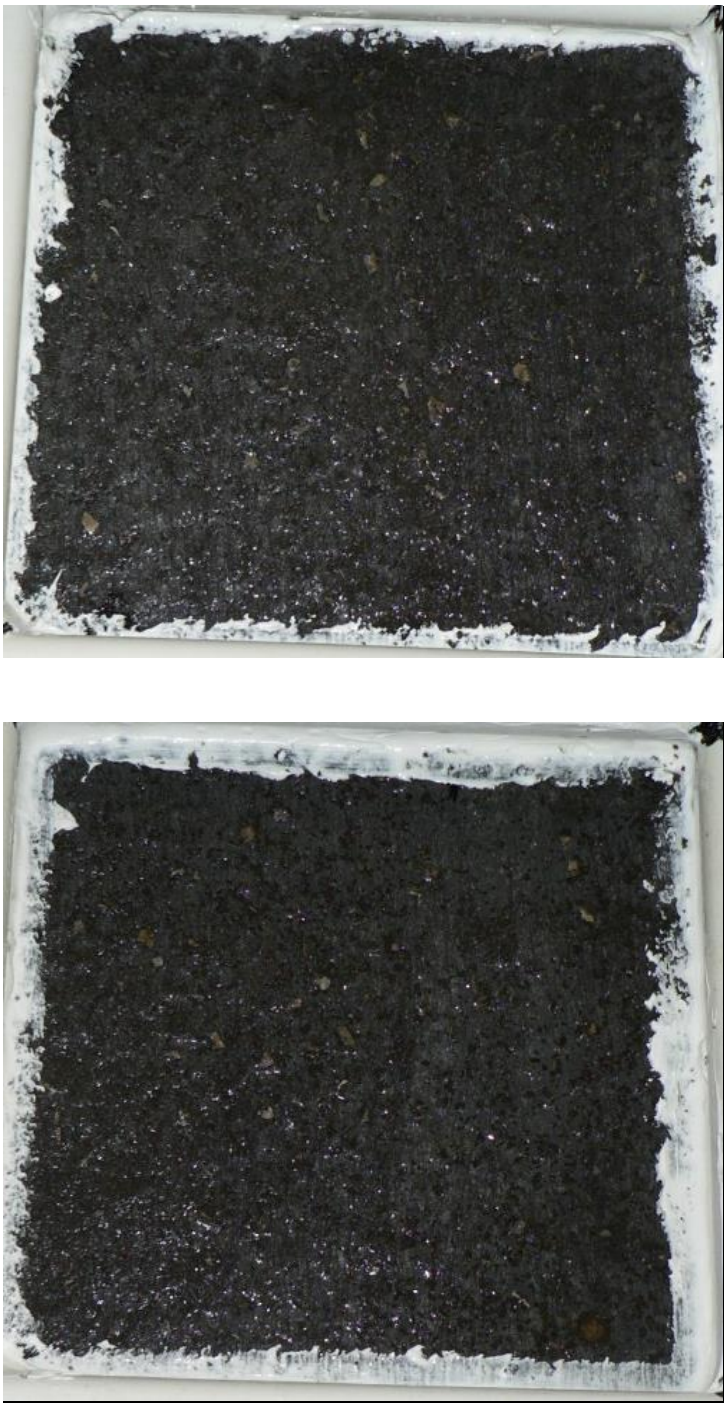

Figure 87. Salt scaling (ASTM C 672) specimen of material P-3 after 10 cycles.

Figure 88. Salt scaling (ASTM C 672) specimen of material P-AAFA after 10 cycles.

Figure 89. Salt scaling (ASTM C 672) specimen of material CSA-1 after 10 cycles.

Figure 90. Salt scaling (ASTM C 672) specimen of material CSA-Latex after 10 cycles.

Figure 91. Salt scaling (ASTM C 672) specimen of material CSA-2 after 10 cycles.

Figure 92. Salt scaling (ASTM C 672) specimen of material CAC-1 after 10 cycles.

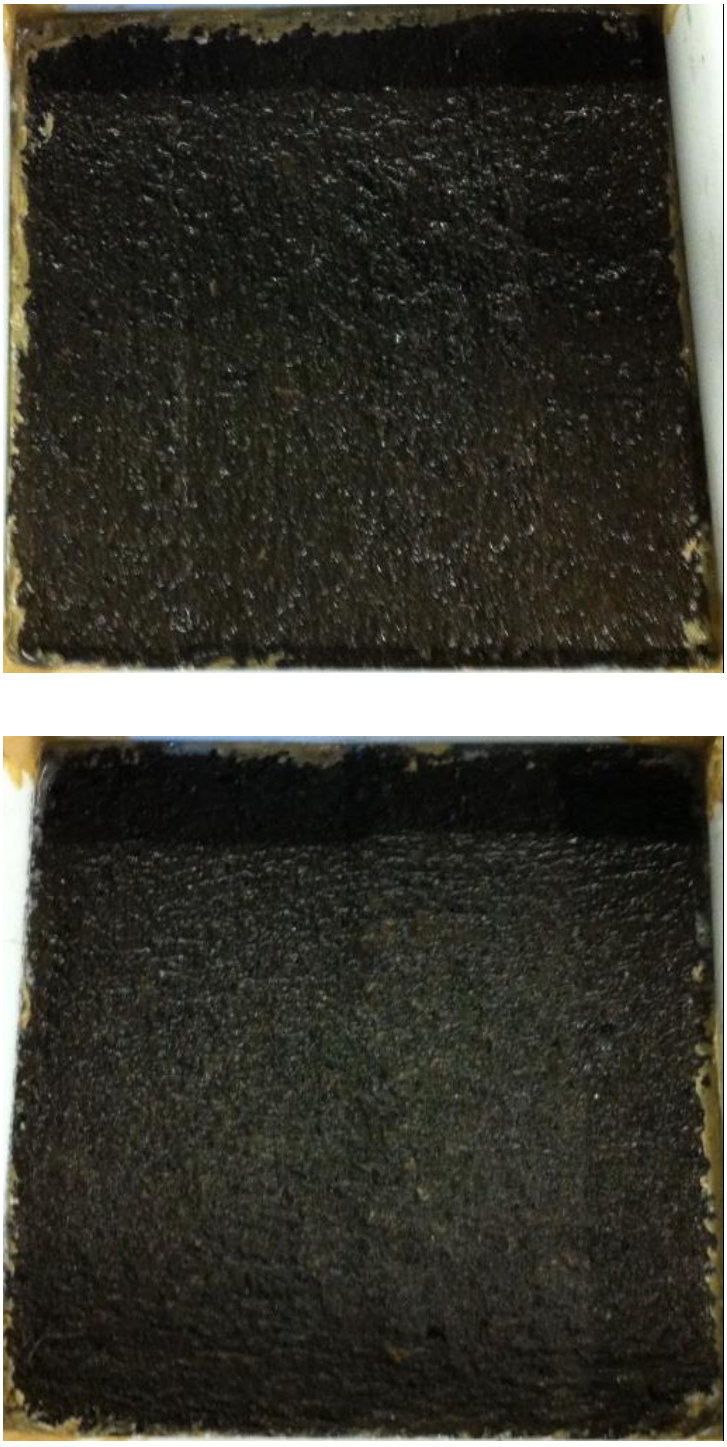

Figure 93. Salt scaling (ASTM C 672) specimen of material CAC-Latex after 10 cycles.

Figure 94. Salt scaling (ASTM C 672) specimen of material PC Type III after 10 cycles.

Figure 95. Salt scaling (ASTM C 672) specimen of material CSA-3 after 10 cycles.

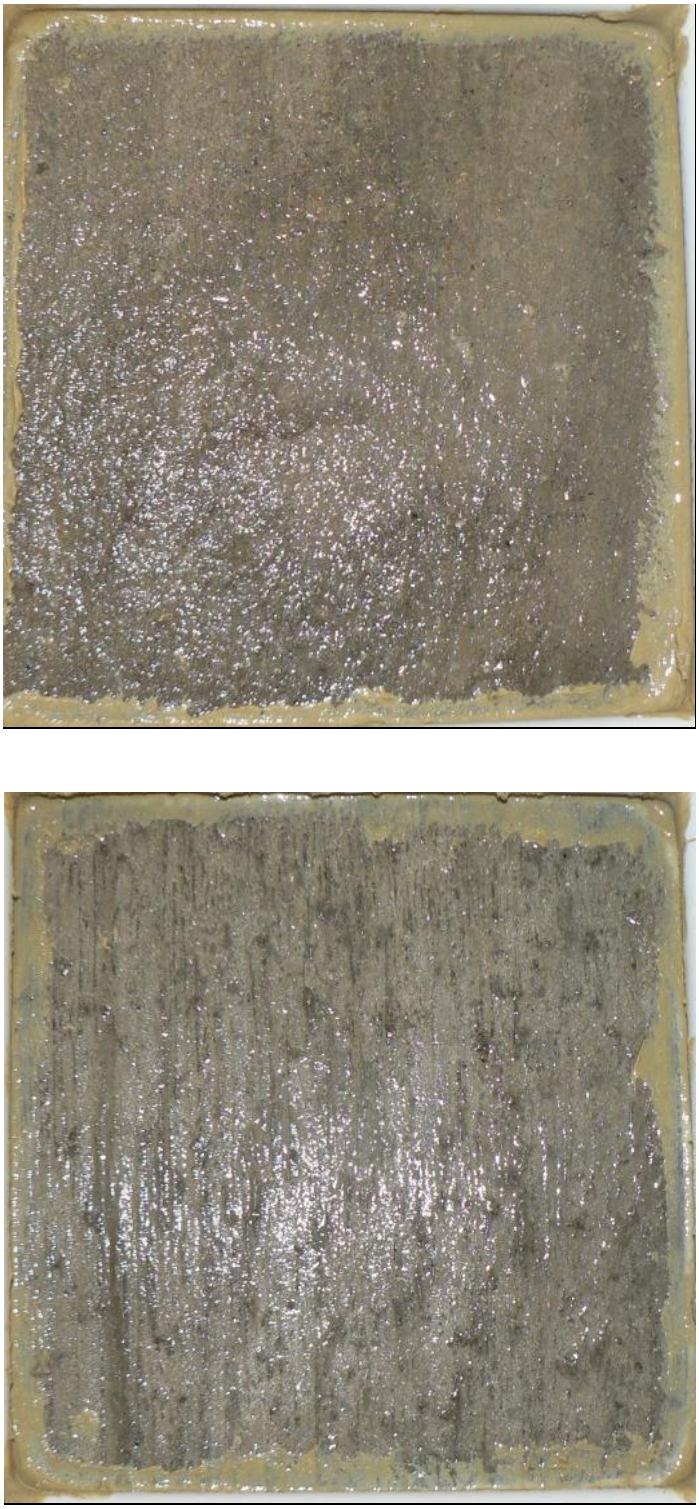

Figure 96. Salt scaling (ASTM C 672) specimen of material CAC-3 after 10 cycles.

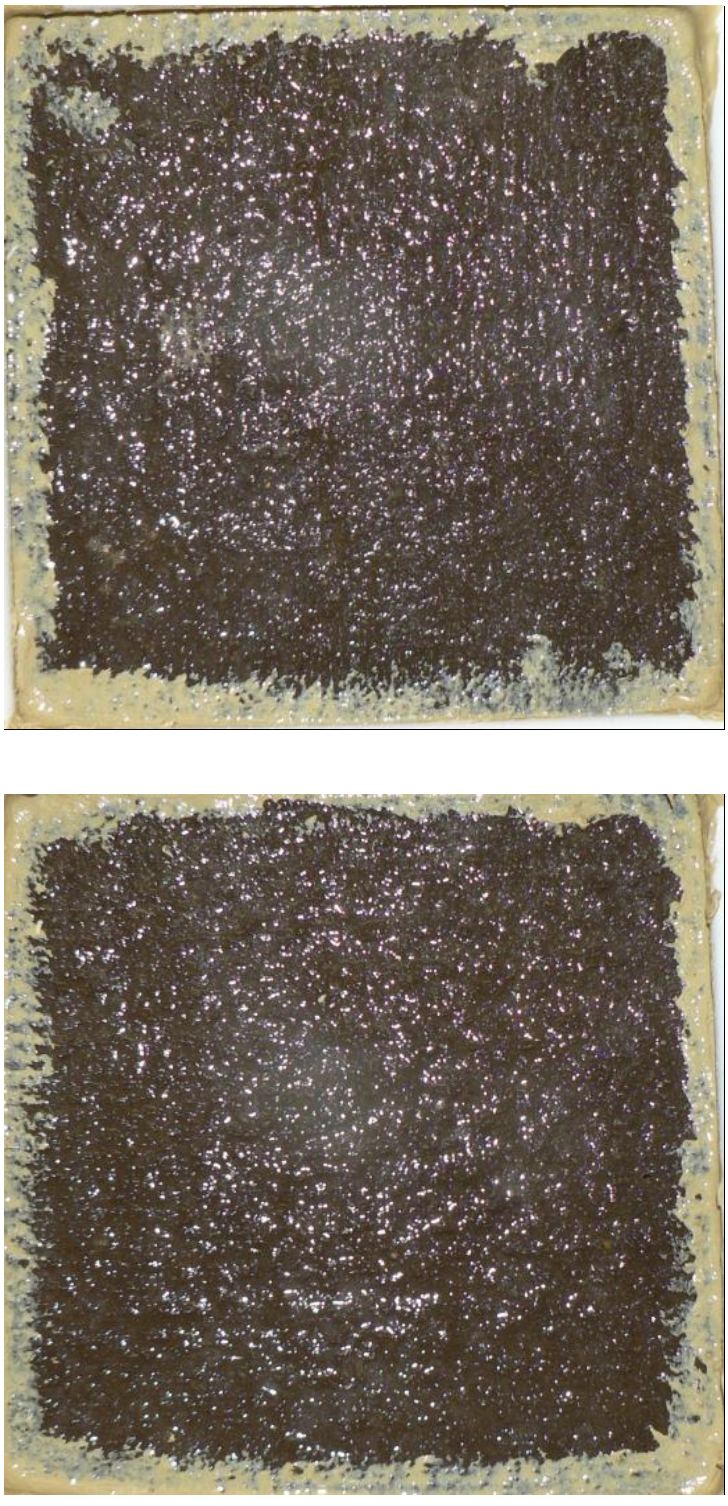

Figure 97. Salt scaling (ASTM C 672) specimen of material CAC-2 after 10 cycles.

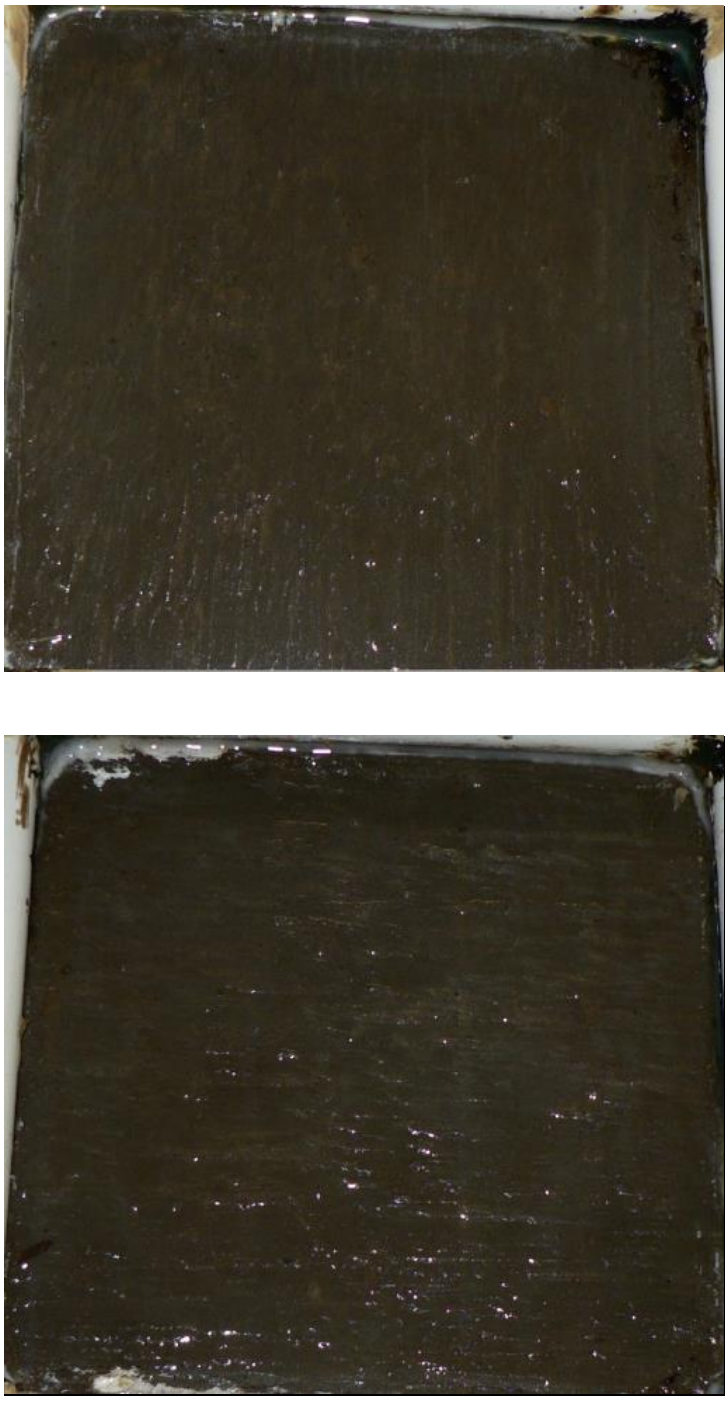

Figure 98. Salt scaling (ASTM C 672) specimen of material P-2 after 15 cycles.

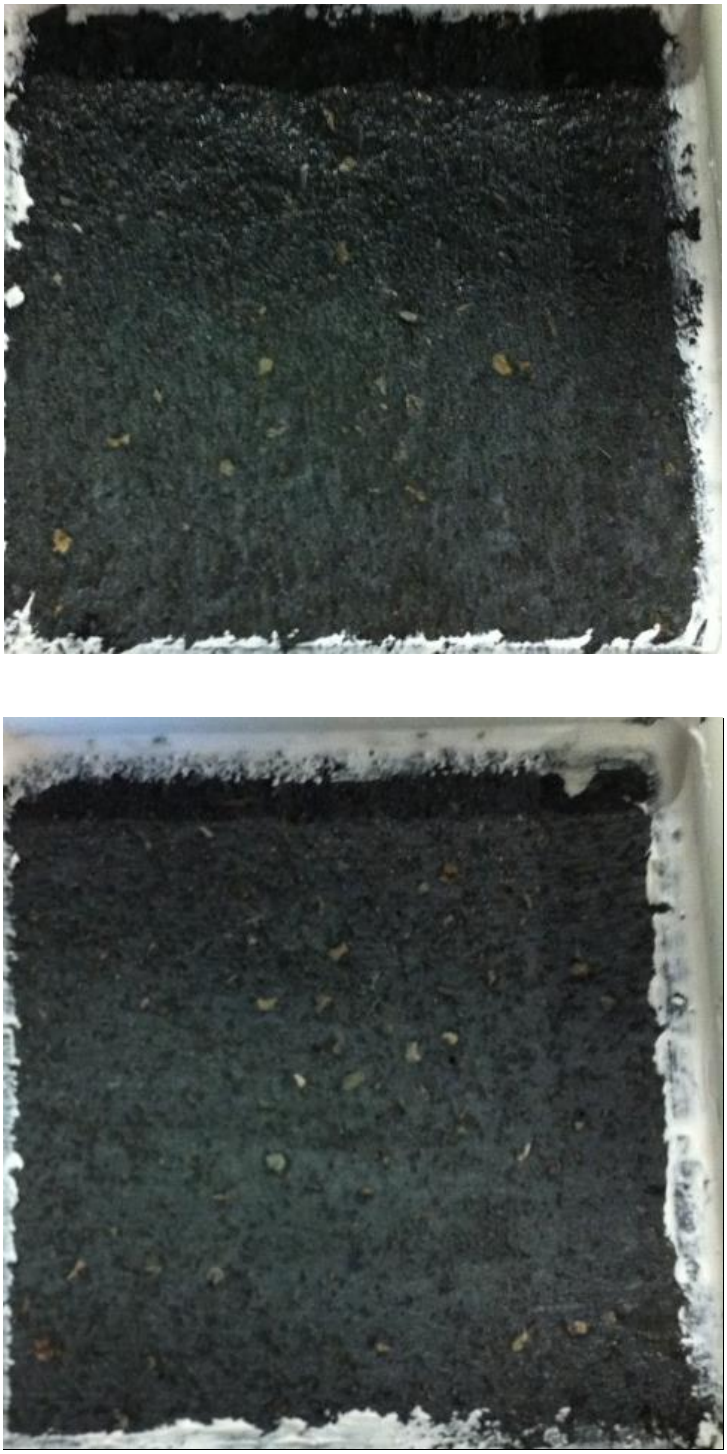

Figure 99. Salt scaling (ASTM C 672) specimen of material P-3 after 15 cycles.

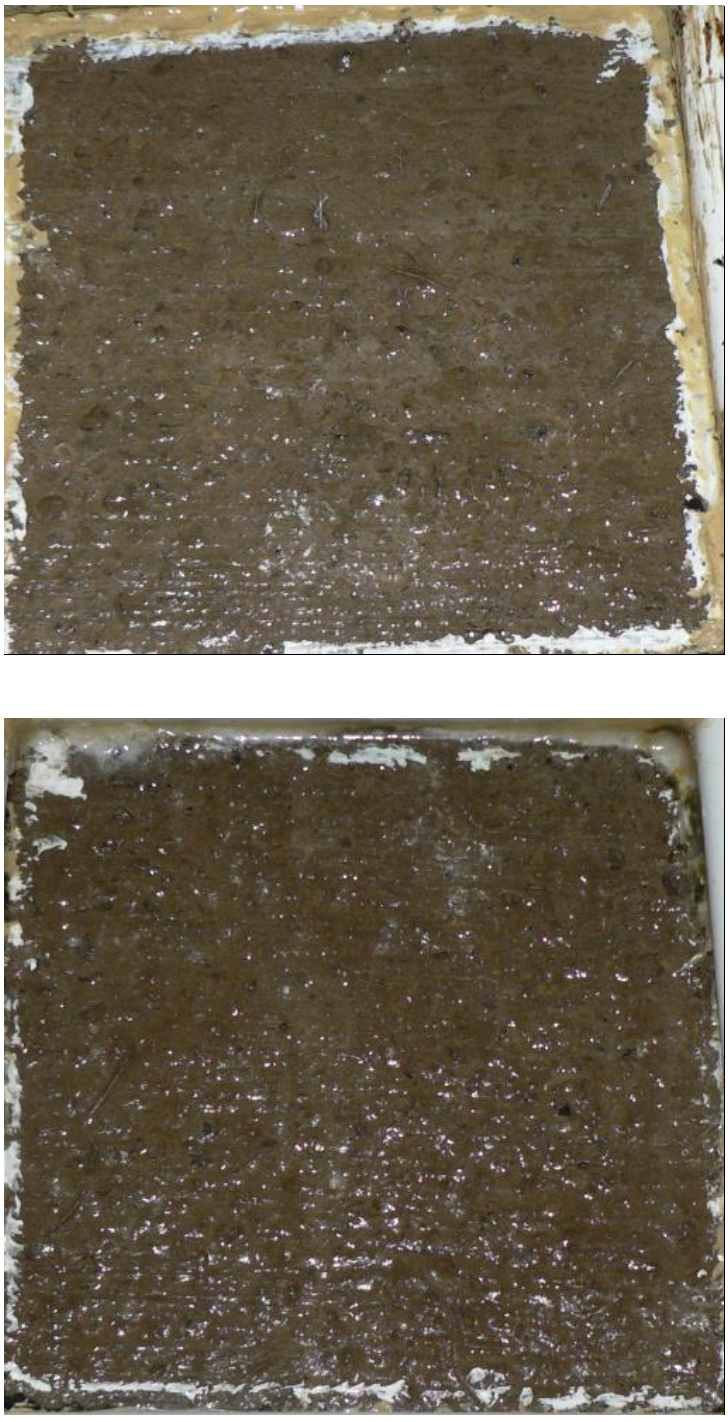

Figure 100. Salt scaling (ASTM C 672) specimen of material P-AAFA after 15 cycles.

Figure 101. Salt scaling (ASTM C 672) specimen of material CSA-1 after 15 cycles.

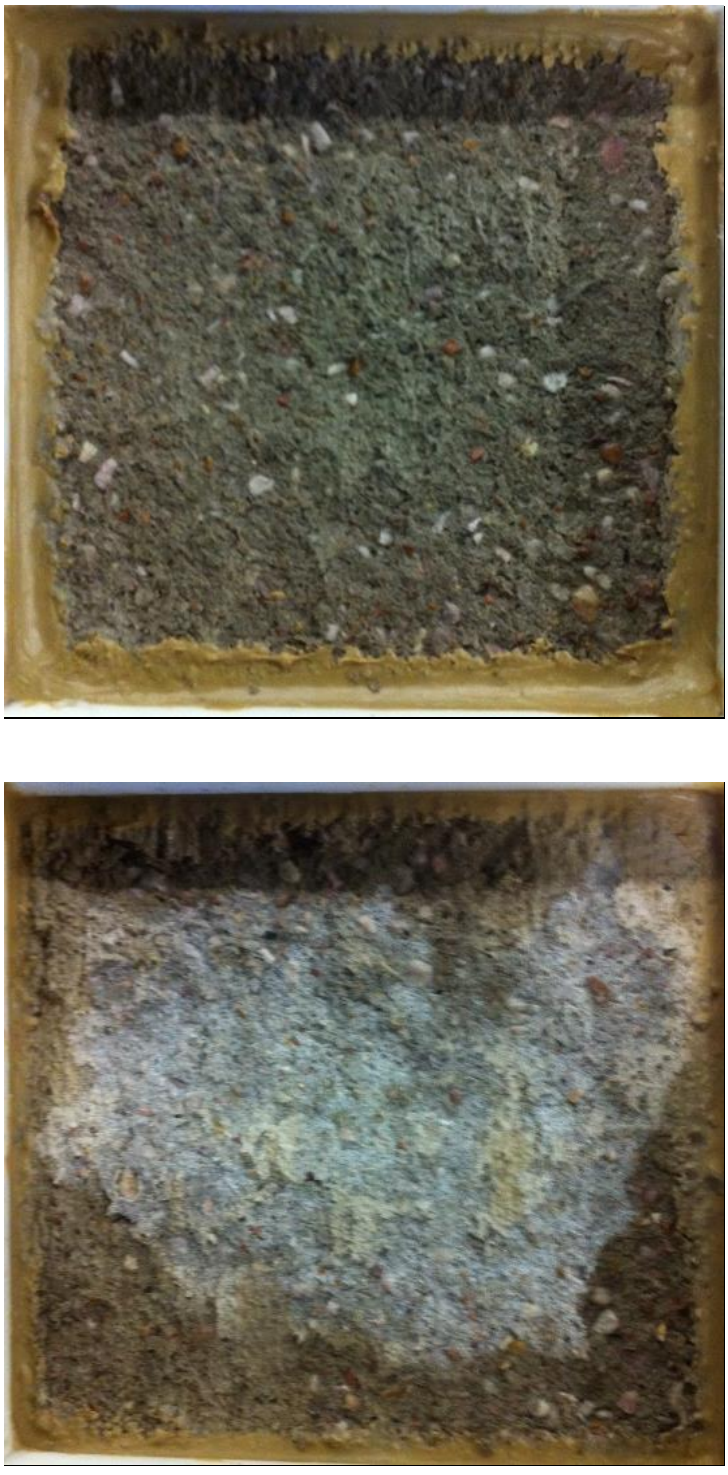

Figure 102. Salt scaling (ASTM C 672) specimen of material CSA-Latex after 15 cycles.

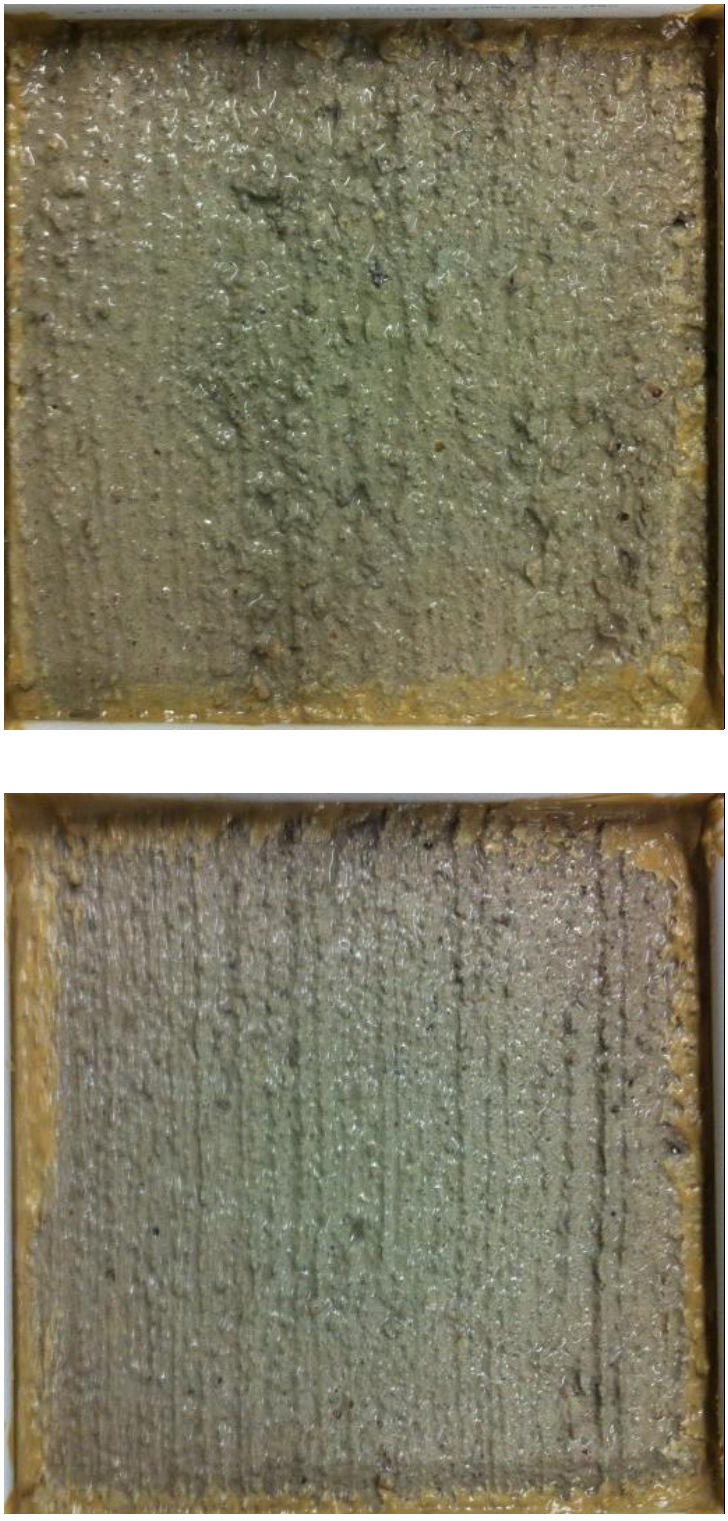

Figure 103. Salt scaling (ASTM C 672) specimen of material CSA-2 after 15 cycles.

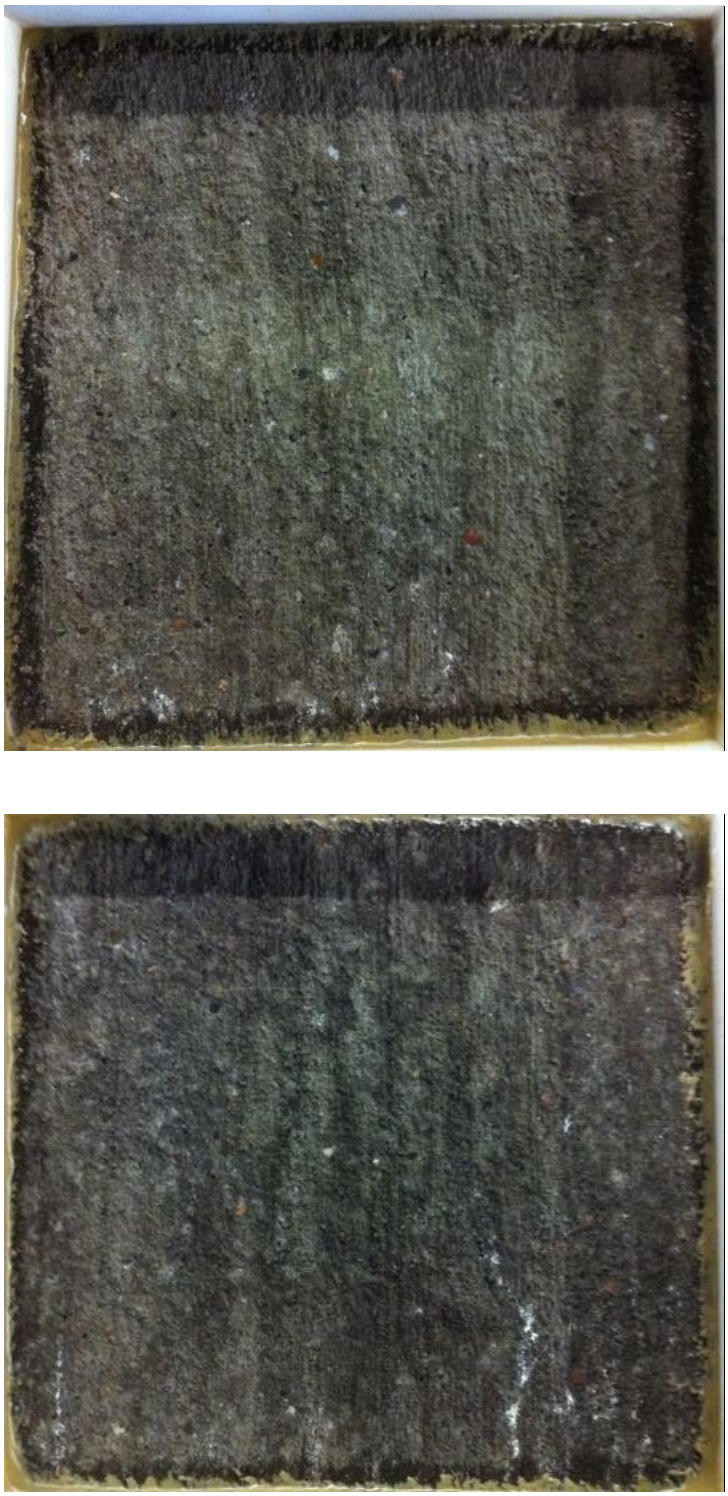

Figure 104. Salt scaling (ASTM C 672) specimen of material CAC-1 after 15 cycles.

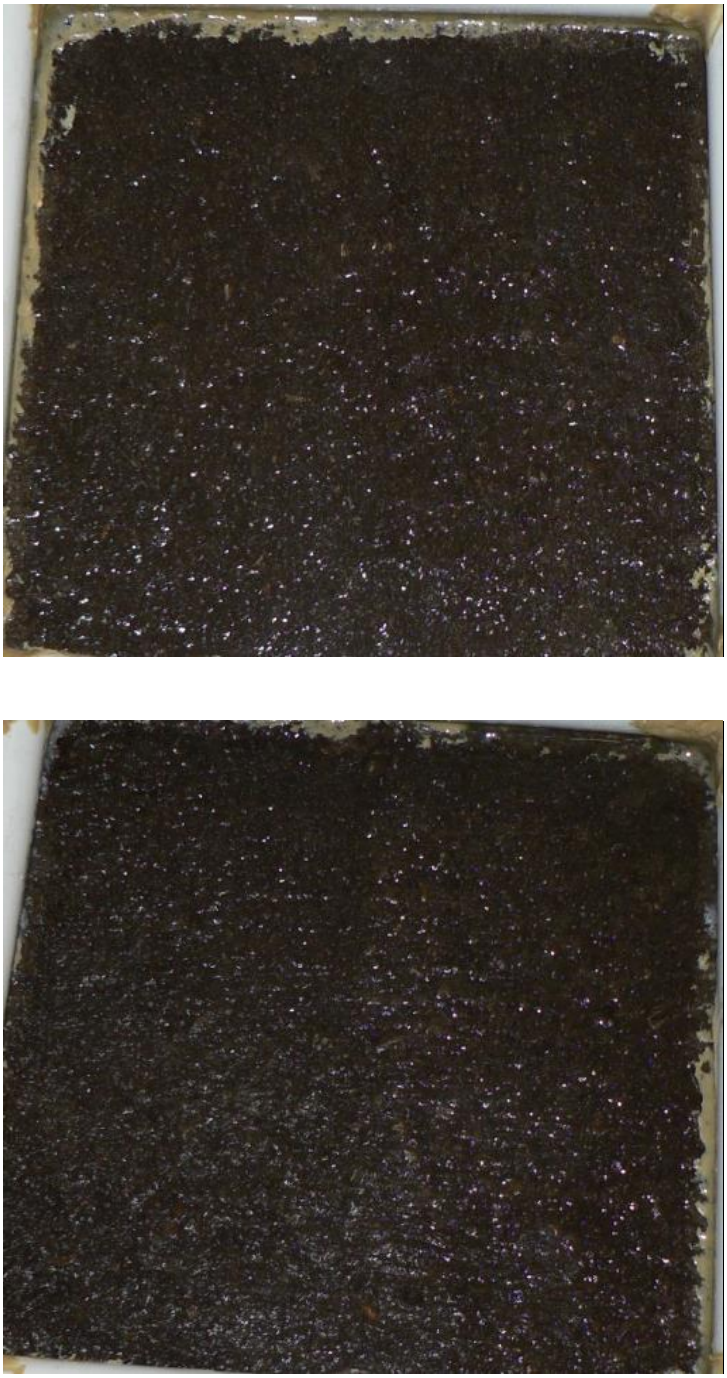

Figure 105. Salt scaling (ASTM C 672) specimen of material CAC-Latex after 15 cycles.

Figure 106. Salt scaling (ASTM C 672) specimen of material CSA-3 after 15 cycles.

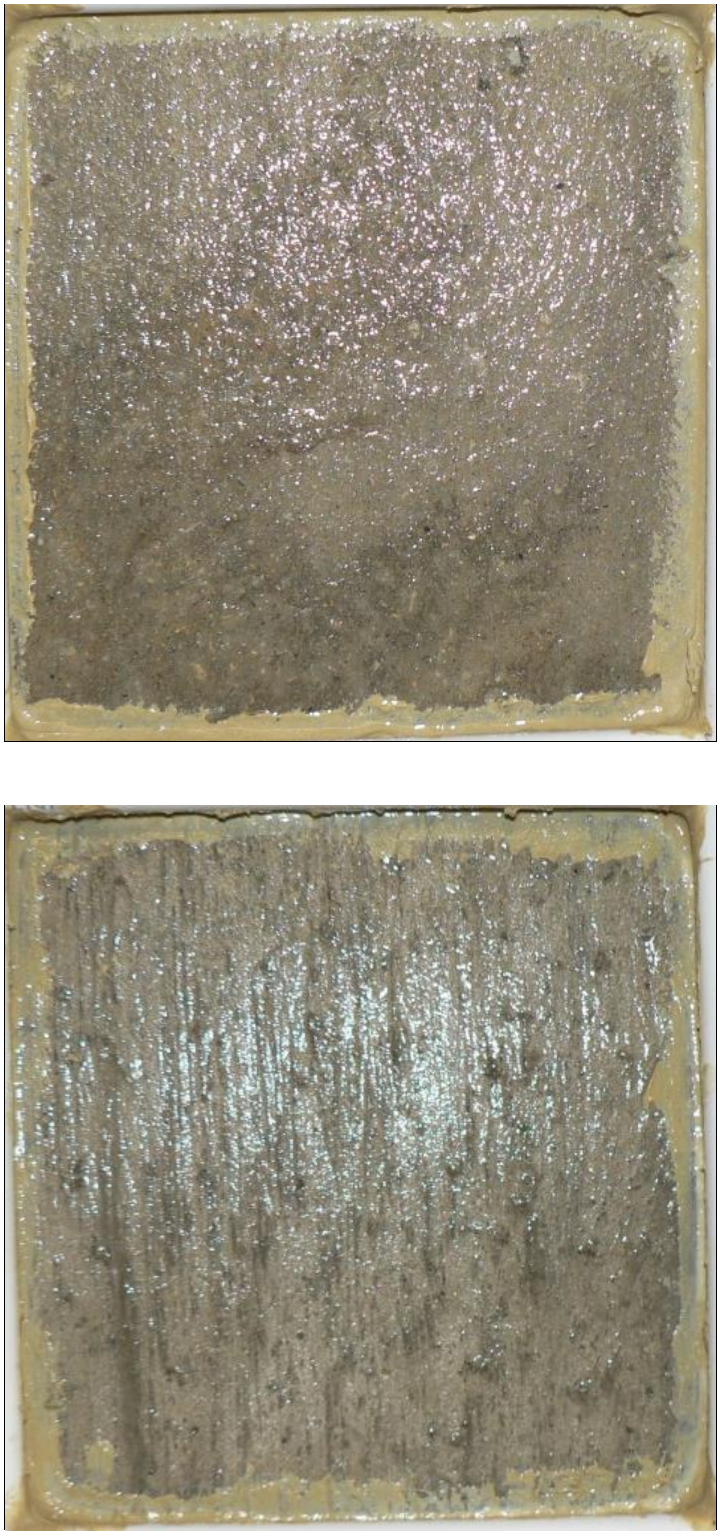

Figure 107. Salt scaling (ASTM C 672) specimen of material CAC-3 after 15 cycles.

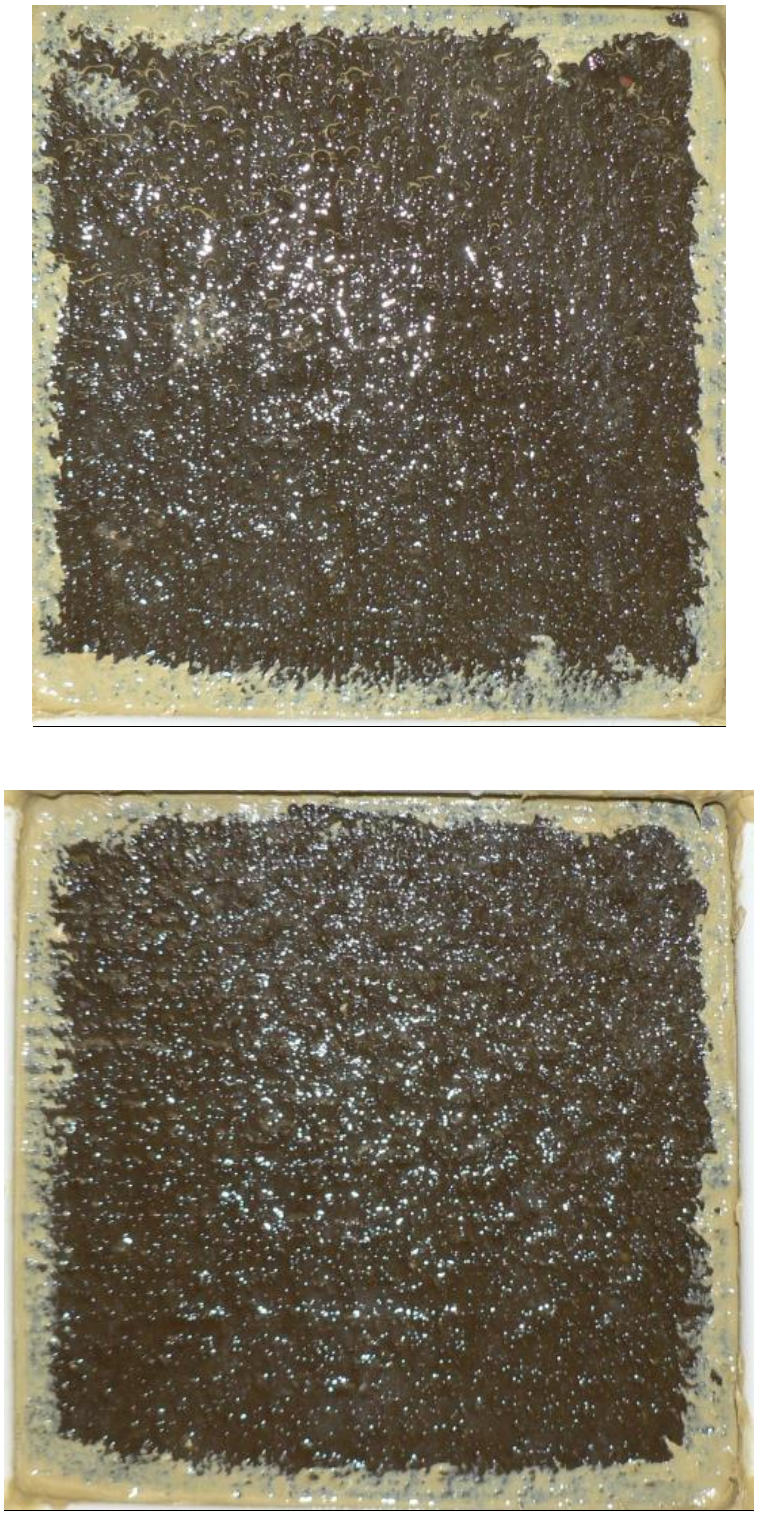

Figure 108. Salt scaling (ASTM C 672) specimen of material CAC-2 after 15 cycles.

Figure 109. Salt scaling (ASTM C 672) specimen of material P-2 after 25 cycles.

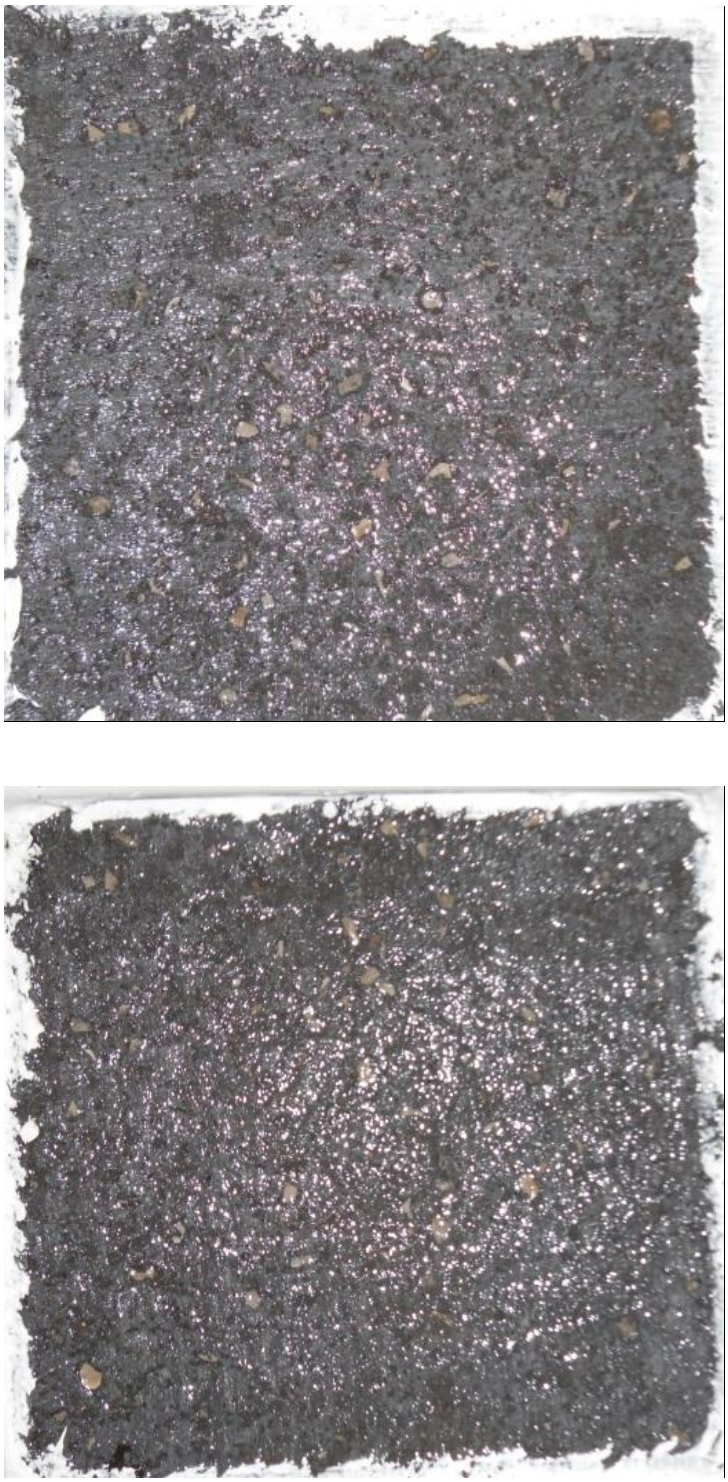

Figure 110. Salt scaling (ASTM C 672) specimen of material P-3 after 25 cycles.

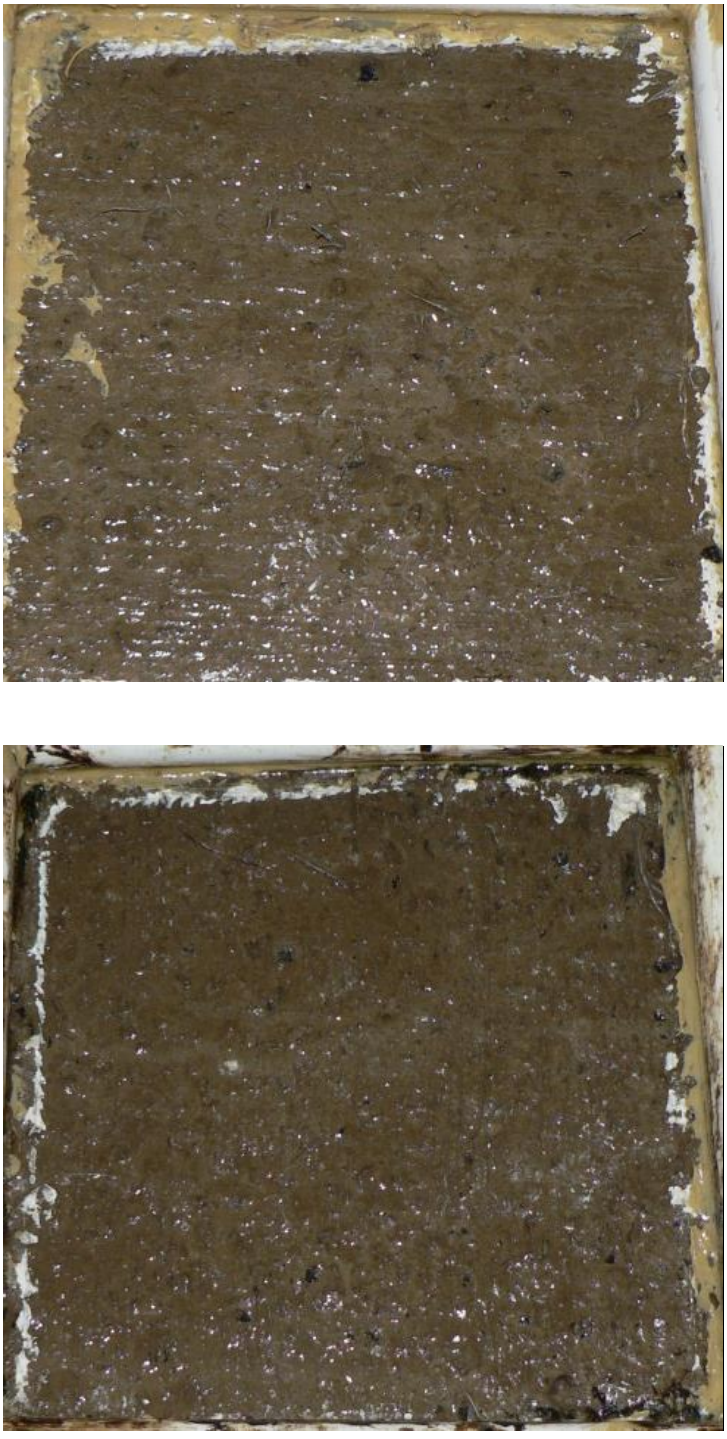

Figure 111. Salt scaling (ASTM C 672) specimen of material P-AAFA after 25 cycles.

Figure 112. Salt scaling (ASTM C 672) specimen of material CSA-1 after 25 cycles.

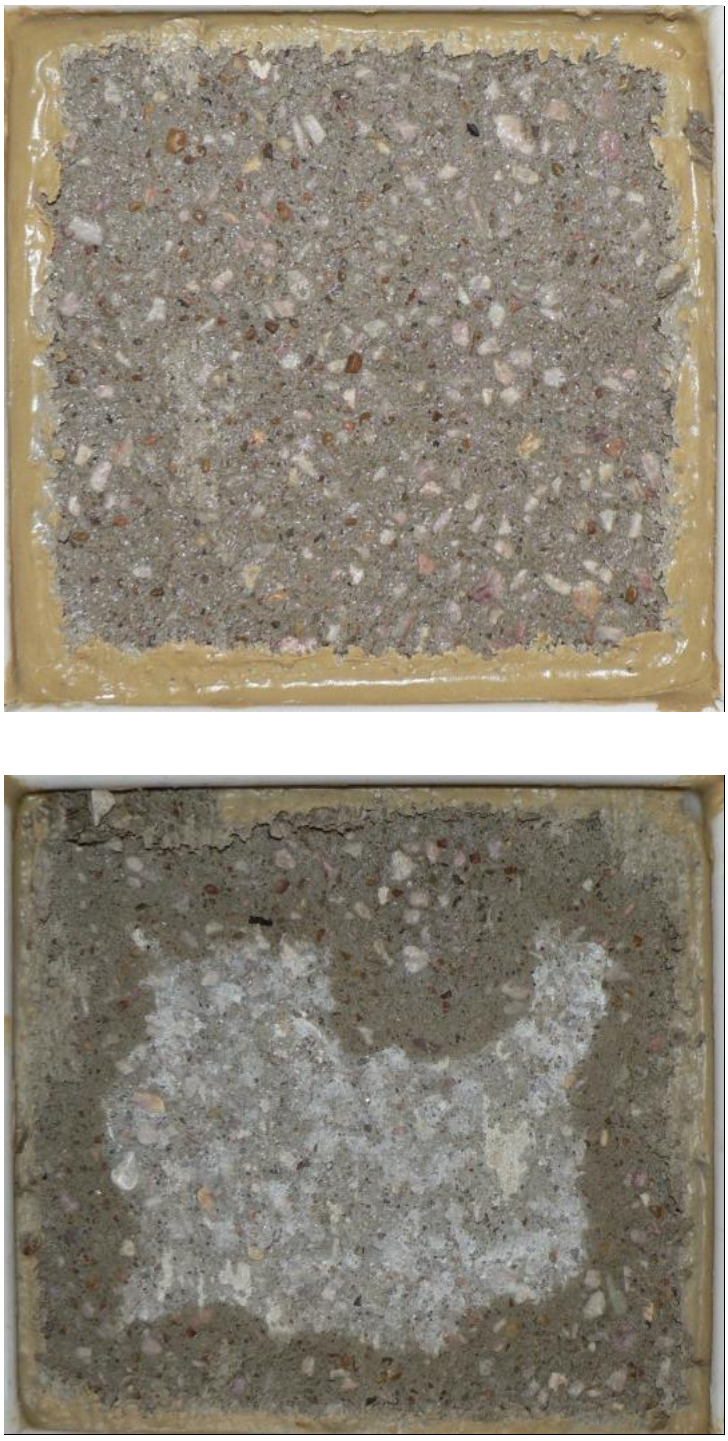

Figure 113. Salt scaling (ASTM C 672) specimen of material CSA-Latex after 25 cycles.

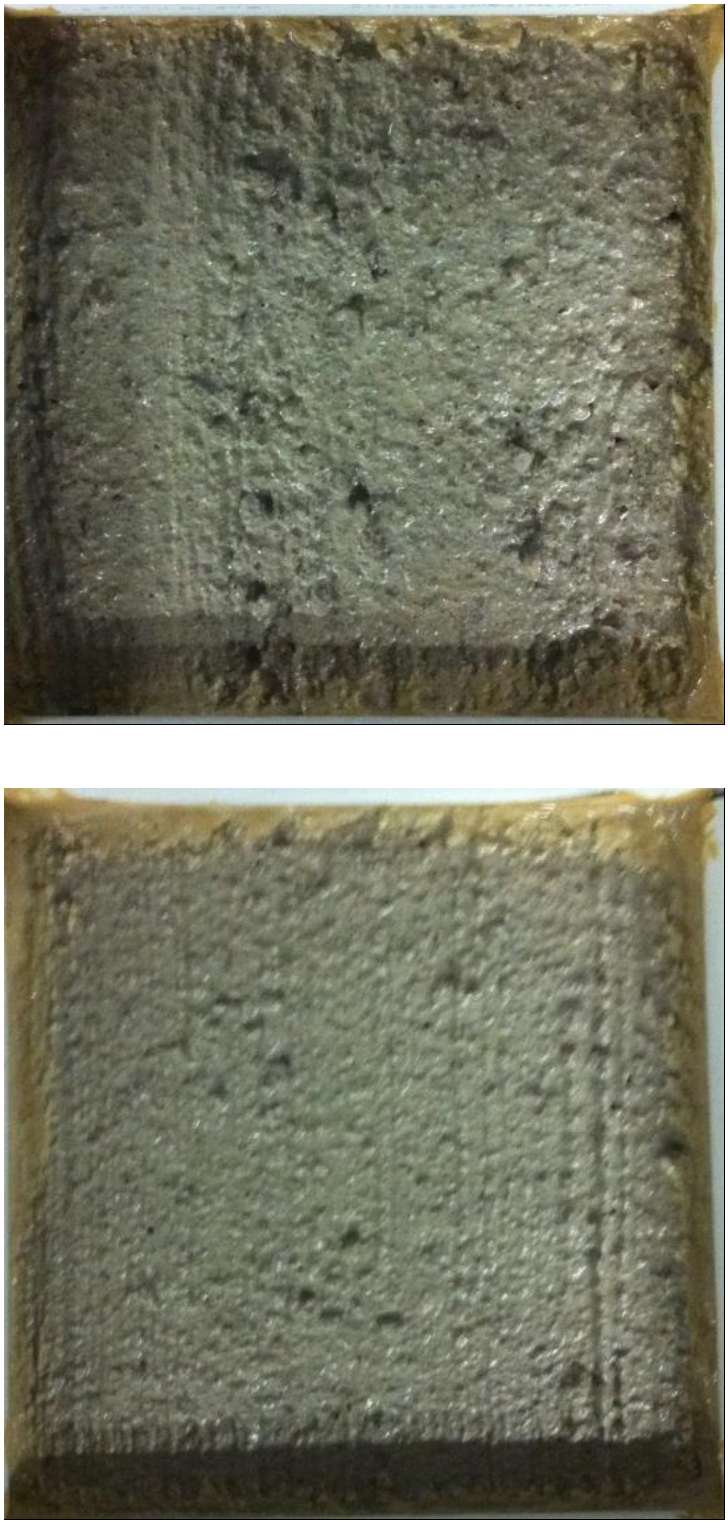

Figure 114. Salt scaling (ASTM C 672) specimen of material CSA-2 after 25 cycles.

Figure 115. Salt scaling (ASTM C 672) specimen of material CAC-1 after 25 cycles.

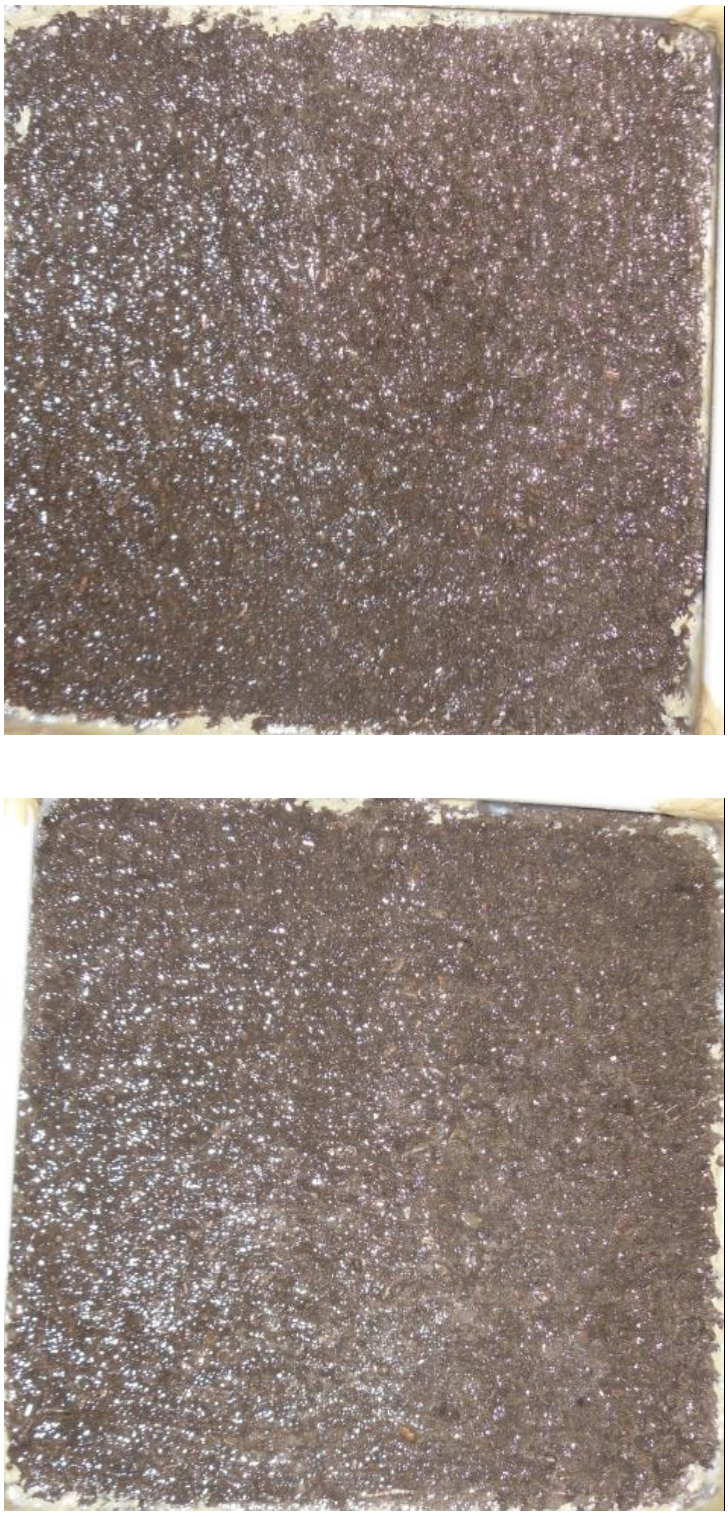

Figure 116. Salt scaling (ASTM C 672) specimen of material CAC-Latex after 25 cycles.

Figure 117. Salt scaling (ASTM C 672) specimen of material PC Type III after 25 cycles.

Figure 118. Salt scaling (ASTM C 672) specimen of material CSA-3 after 25 cycles.

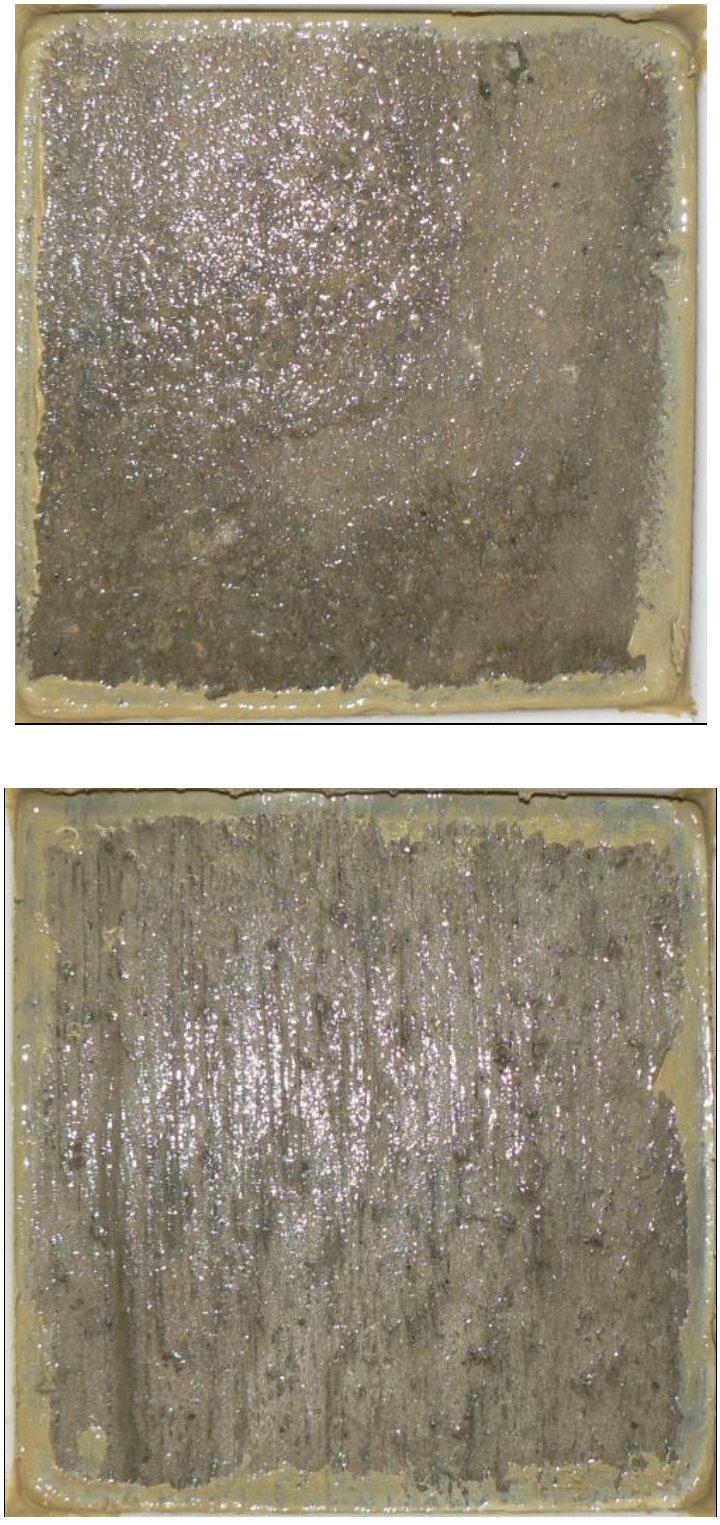

Figure 119. Salt scaling (ASTM C 672) specimen of material CAC-3 after 25 cycles.

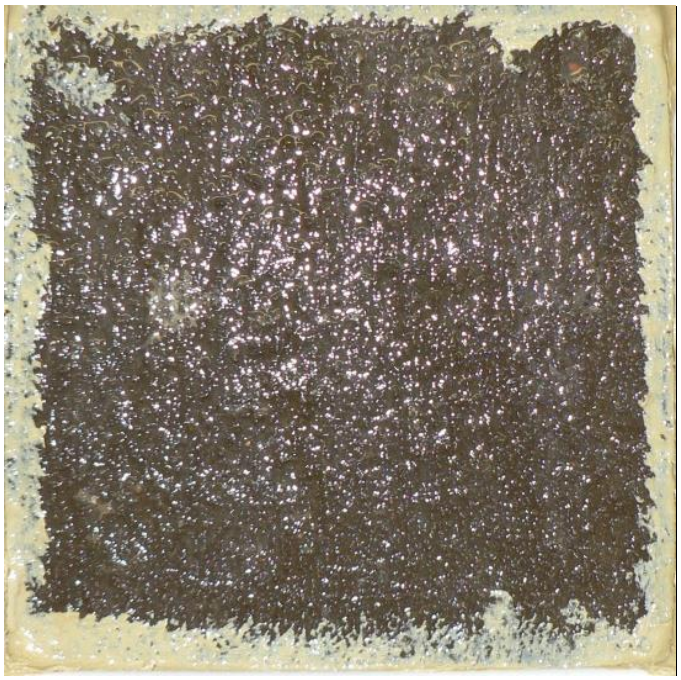

Figure 120. P-2 samples after 50 cycles according to ASTM C 672.

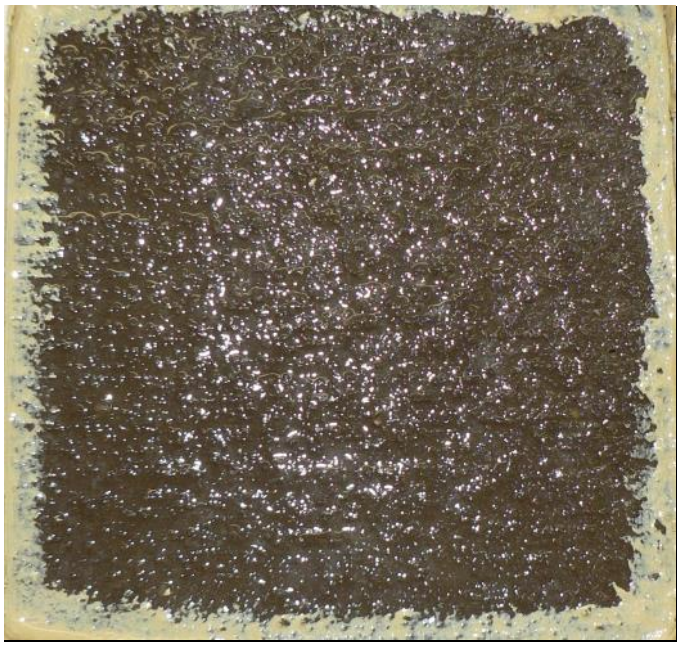

Figure 121. Salt scaling (ASTM C 672) specimen of material CAC-2 after 25 cycles.

Figure 122. P-2 samples after 50 cycles according to ASTM C 672.

Figure 123. P-3 samples after 50 cycles according to ASTM C 672.

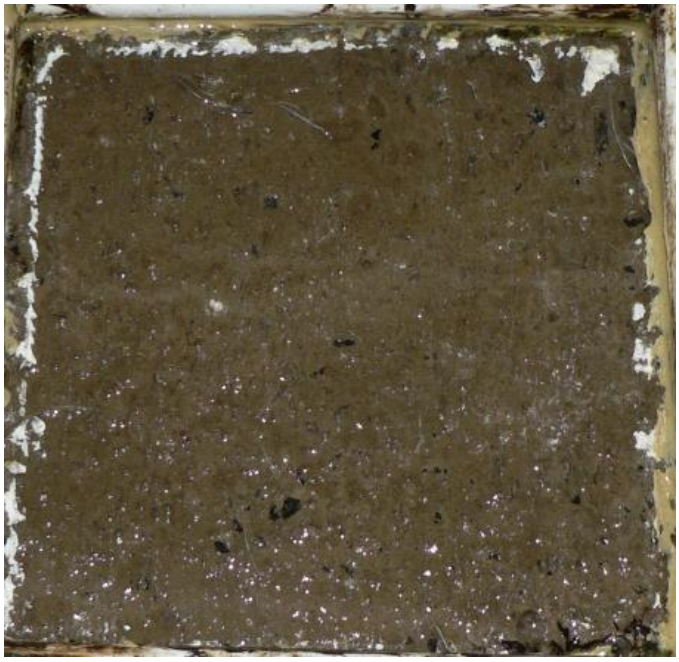

Figure 124. P-AAFA samples after 50 cycles according to ASTM C 672.

Figure 125. CSA-2 samples after 50 cycles according to ASTM C 672.

Figure 126. CSA-Latex samples after 50 cycles according to ASTM C 672.

Figure 127. CAC-1 samples after 50 cycles according to ASTM C 672.

Figure 128. CAC-Latex samples after 50 cycles according to ASTM C 672.

Figure 129. PC Type III samples after 50 cycles according to ASTM C 672.

Figure 130. CAC-3 samples after 50 cycles according to ASTM C 672.

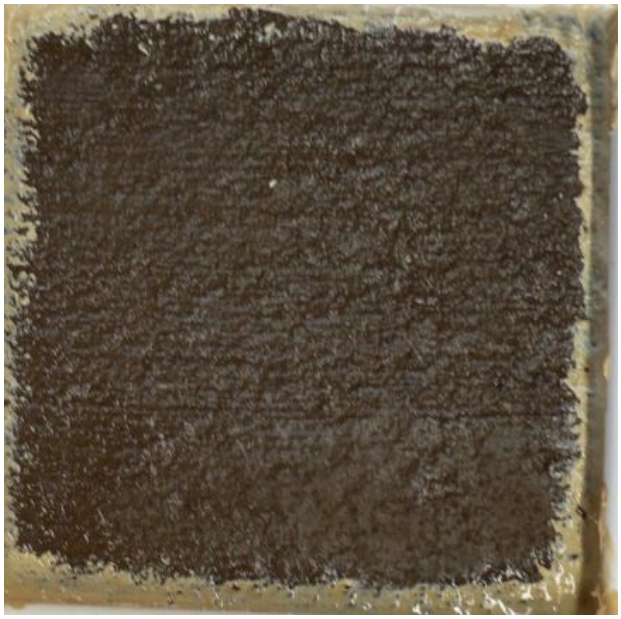

Figure 131. CAC-2 samples after 50 cycles according to ASTM C 672.

References

ACI 548.4 . (2011). *Specification for Latex-Modified Concrete Overlays.* The American Concrete Institute.

ASTM C 109. (2012). *Standard Test Method for Compressive Strength of Hydraulic Cement Mortars.* Conshohocken, PA: ASTM International.

ASTM C 1202. (2010). *Standard Test Method for Electrical Indication of Concrete's Ability to Resist Chlroride Ion Penetration.* Conshohocken, PA: ASTM International.

ASTM C 1293. (2008B). *Standard Test Method for Determination of Length Change of Concrete Due to Alkali-Silica Reaction.* Conshohocken, PA: ASTM International.

ASTM C 150. (2012). *Standard Specification for Portland Cement.* West Conshohocken, PA: ASTM International.

ASTM C 1556. (2011a). *Standard Test Method for Determining the Apparent Chloride Diffusion Coefficient of Cementitious Mixtures by Bulk Diffusion.* Conshohocken, PA: ASTM International.

ASTM C 457. (2009). *Standard Test Method for Microscopical Determination of Parameters of the Air-Void System in Hardened Concrete.* Conshohocken, PA: ASTM International.

ASTM C 618. (2011). *Standard Specification for Coal Fly Ash and Raw or Calcined Natural Pozzolan for Use in Concrete.* Conshohocken, PA: ASTM International.

ASTM C 666. (2008). *Standard Test Method for Resistance of Concrete to Rapid Freezing and Thawing.* Conshohocken,PA: ASTM International.

ASTM C 672. (2003). *Standard Test Method for Scaling Resistance of Concrete Surfaces Exposed to Deicing Chemicals.* Conshohoken, PA: ASTM International.

Carmmond, N. (1990). Long-term performance of high alumina cement concrete in sulphase-bearing environments. In R. Mangabhai, *Calcium Aluminate Cements.* Cambridge: Great Britain at the University Press.

CEN. (2007). *UNI CEN/TS 12390-10:2008 Testing of Hardened Concrete - Part 10: Determination Of The Relative Carbonation Resistance Of Concrete.* CEN.

Dornak, M. L. (2014). *Engineering Properties, Early-age Volume Change, and Heat Generation of Rapid, Cement-based Repair Materials.*

Farzam, H., Bollin, G., Howe, R. H., Marin, J., Erlin, B. J., Isabelle, H. L., et al. (2005). *Cement and Concrete Terminology.* ACI Committee 116.

Islam, M. (2004). *SHRP Product 2030: Standard Test Method for Chloride Content in Concrete.* Washington, D.C.: Strategic Highway Research Program (SHRP).

Ley, M. T. (2007). *The Effects of Fly Ash on the Ability to Entrain and Stabilize Air in.*

Maruya, T., Takeda, H., Horiguchi, K., Koyama, S., & Hsu, K.-L. (2007). Half-Cell Potential as an Indicator of Chloride-Induced Rebar Corrosion Initiation in RC. *Journal of Advanced Concrete Technology, 5(3)*.

Mindess, S., Young, J. F., & Darwin, D. (2003). *Concrete.* Upper Saddle River: Pearson Education, Inc.

Pesek, P. W. (2011). *Temperature, Stress, and Strength Development of Early-Age Bridge.*

Pradhan, B., & Bhattacharje, B. (2009). Half-Cell Potential as an Indicator of Chloride-Induced Rebar Corrosion Initiation in RC. *American Society of Civil Engineers*, 543-552.

Riding, K. A., Poole, J. L., Schindler, A. K., Juenger, M. C., & Folliard, K. J. (2008). Simplified Concrete Resistivity and Rapid Chloride Permeability Test Method. *ACI Materials Journal, 105(4)*, 390.

Shaker, F., El-Dieb, A., & Reda, M. (1997). Durability of Styrene-Butadiene Latex Modified Concrete. *Cement and Concrete Research 27(5)*, 711-720.

Valenza II, J. J., & Scherer, G. W. (2006). Mechanisms of Salt Scaling. *Journal of th eAmerican Ceramic Society, 89(4)*, 1161-1179.

Zuniga, J. R. (2013). *Development of Rapid, Cement-based Repair Materials for Transportation Structures.*